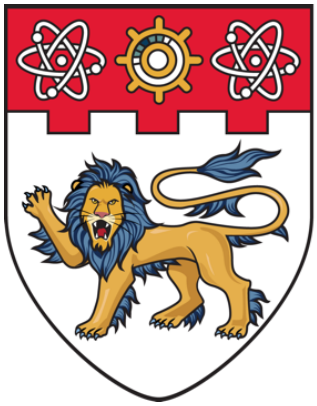

NANYANG TECHNOLOGICAL UNIVERSITY

SINGAPORE

Composite Membranes Comprising Nanoporous Materials for Carbon Dioxide Capture

GONG HEQING

School of Chemical and Biomedical Engineering

Composite Membranes Comprising Nanoporous Materials for Carbon Dioxide Capture

GONG HEQING

School of Chemical and Biomedical Engineering

A thesis submitted to the

Nanyang Technological University

In partial fulfillment of the requirement for the

degree of

Doctor of Philosophy

2017

Acknowledgements

First and foremost, I would like to express sincere thanks to my supervisor, Assistant Professor Bae Tae-Hyun for his guidance, encouragement and patience. During the four years, he has provided countless help and support on my research and study, from the design of projects, literature studies, practical lab operation, presentation and writing skills. Thanks again for Assistant Professor Bae, for bringing me into the exciting study of composite membranes for gas separation.

Besides, I would like to thank my TAC committee members: Professor Wang Rong, Associate Professor Chen Yuan and Associate Professor Liu Bin for the helpful advices for improving the quality of the thesis.

I would like to thank my co-workers: Dr. Yang Yanqin for providing the polymer samples, Mr Chuah Chongyang for helped to run characterization about membranes and porous materials and Dr. Siew Siang Lee for improving my writing and presentation skilles. In addition I would like to thank Dr. Tien Hoa Nguyen, Dr. Sunee Wongchitphimon, Dr. Wichitpan Rongwong, Dr. Goh Kunli, Dr. Jiun Hui Low, Dr. Lee Jaewoo, Ms Siow Kee Lim, Ms Dilhara Sethunga and Ms Li Wen for their kind suggestions during the group meeting. I benefit so much from their presentations.

I would like to express my deepest appreciation to my parents, who had always stood beside me and always willing to support all my decisions. It is sad to live so far away from you for the four years. However equipped with your encouragements, I can pursue my dreams step by step.

I would like to thank my best friends in Singapore: Mr Wang Peng, Mr Zhang Chaodong, Mr Jia Bowen. During the PhD study, I really enjoyed a really joyful time with you. Wish all your guys can have a bright future.

Last but not least, I would like to thank the financial support from the Nanyang Technological University and PUB.

Heqing Gong

20th May, 2017

TABLE OF CONTENTS

Acknowledgements I

Table of Contents III

List of Abbreviations IX

List of Figures XI

List of Tables XV

Summary 1

CHAPTER 1 Introduction 5

1.1 Importance of CO_2 separation 5

1.2 Current Technologies for Carbon Dioxide Capture 5

1.2.1 Conventional Techniques 6

1.2.2 Membrane Process 8

1.3 Type of Membranes 11

1.3.1 Polymeric Membranes 11

1.3.2 Inorganic Membranes 12

1.3.3 Composite Membranes 14

1.4 Aims and Objectives of Research 16

CHAPTER 2 Literature Review 18

2.1 Zeolite Molecular Sieve 18

2.1.1 Definition 18

2.1.2 Equilibrium Separation 19

2.1.3 Kinetic Separation 21

2.1.4 Chemical Treatment for Hierarchical Zeolites 24

2.1.5 Zeolite as Membrane Filler 26

2.1.6 Engineering the Interfacial Morphology of Zeolite-Based Composite Membrane 31

2.2 Metal Organic Framework 37

2.2.1 Definition 37

2.2.2 Synthesis Methods 38

2.2.3 Ligand Design and Post-synthetic Treatment 41

2.2.4 Working Stability 42

2.2.5 Metal Organic Framework as Membrane Filler 44

2.2.6 Crystal Size and Shape 46

CHAPTER 3 Solvothermal Deposition of Magnesium Oxides on LTA Zeolites For Compsite Membrane Fabrication 48

3.1 Introduction 48

3.2 Experimental Section 50

3.2.1 Materials 50

3.2.2 Synthesis of Zeolites 50

3.2.3 Solvothermal Treatment 51

3.2.4 Membrane Fabrication 53

3.2.5 Characterization 54

3.2.6 Gas Adsorption Analysis 55

3.2.7 Permeation Tests 56

3.3 Results and Discussion 56

3.3.1 Zeolite Synthesis and Surface Treatment 56

3.3.2 Morphology of Surface Treated Zeolites 64

3.3.3 Characterization of Surface Treated Zeolites 66

3.3.4 Characterization of Composite Membranes 70

3.3.5 Permeation Tests 71

3.4 Conclusion 73

3.5 Declaration 75

CHAPTER 4 Amine Grafting LTA Zeolites for Composite Membrane Fabrication 76

4.1 Introduction 76

4.2 Experimental Section 77

4.2.1 Materials 77

4.2.2 Synthesis of Mesoporous LTA Zeolite 78

4.2.3 Post-Synthetic Amine Grafting and Membrane Fabrication 78

4.2.4 Characterization 80

4.2.5 Permeation Tests 81

4.3 Results and Discussion 82

4.3.1 Synthesis of Mesoporous LTA Zeolite and Amine Grafting 82

4.3.2 Characterization of Zeolite 83

4.3.3 Characterization of Composite Membranes 87

4.3.4 Permeation Tests 88

4.4 Conclusions 90

4.5 Declaration 91

CHAPTER 5 Submicron Crystals of Metal-Organic Framework and Their Applications in Carbon Capture 92

5.1 Introduction 92

5.2 Experimental Section 94

5.2.1 Materials 94

5.2.2 Synthesis of Submicron $Zn(pyrz)_2(SiF_6)$ Crystals 94

5.2.3 Fabrication of Crosslinked Polyethylene Oxide (XLPEO)Membran 95

5.2.4 Characterizations of $Zn(pyrz)_2(SiF_6)$ Crystals and Membranes 96

5.2.5 Mixture Gas Permeation Tests 97

5.2.6 Prediction of Membrane Performance with the Maxwell Model 98

5.3 Results and Discussion 98

5.3.1 Synthesis of $Zn(pyrz)_2(SiF_6)$ Metal-Organic Framework Crystals 98

5.3.2 Gas Adsorption Properties of $Zn(pyrz)_2(SiF_6)$ Crystals 101

5.3.3 Fabrications of Composite Membranes 103

5.3.4 Gas Permeation Properties of Composite Membranes 105

5.3.5 Prediction of Performance of Hypothetical Membranes Comprising $Zn(pyrz)_2(SiF_6)$ Crystals 108

5.4 Conclusions 110

5.5 Declaration 111

Chapter 6 High Performance Composite Membranes Comprising $Zn(pyrz)_2(SiF_6)$ Nanocrystals for CO_2/CH_4 Separation 112

6.1 Introduction 112

6.2 Experimental Section 113

6.2.1 Materials 113

6.2.2 Synthesis of Submicron $Zn(pyrz)_2(SiF_6)$ Crystals 114

6.2.3 Synthesis of 6FDA-TMPDA Polyimide 114

6.2.4 Fabrication of Membranes 115

6.2.5 Characterization 116

6.2.6 Mixture Gas Permeation Tests 117

6.2.7 Gas Adsorption Analysis 118

6.2.8 Density of the Membranes 118

6.3 Results and Discussion 120

6.3.1 Synthesis of $Zn(pyrz)_2(SiF_6)$ Nanocrystals 120

6.3.2 Gas Adsorption Properties of $Zn(pyrz)_2(SiF_6)$ Nanocrystals 122

6.3.3 Fabrications of Composite Membranes 123

6.3.4 Gas Permeation Properties 129

6.4 Conclusions 138

6.5 Declaration 139

CHAPTER 7 Conclusions and Future Work 140

7.1 Conclusions 140

7.2 Recommendations for Future Work and Expectations..... 142

Reference..... 146

List of Publication..... 173

List of Abbreviations

LTA	Linde Type A
CHA	Chabazite
FAU	Faujasite
ZSM	Zeolite Socony Mobil
SAPO	Silico-Alumino-Phosphate
MFI	Mordenite Framework Inverted
MWW	M-tWenty-tWo
BEA	Beta Type
LTL	Linde Type L
DDR	Deca-dodecasil 3R
ETS	Engelhard titanosilicate
APTES	(3-Aminopropyl)triethoxysilane
APDMES	(3-aminopropyl)-dimethyl-ethoxysilane
APMDES	3-aminopropylmethyldiethoxysilane
TPOAC	[3-(trimethoxysilyl)propyl]octadecyldimethylammonium chloride
APTMS	(3-Aminopropyl)trimethoxysilane
1D	One Dimensional
2D	Two Dimensional
3D	Three Dimensional
PES	Polyethersulfone
PSF	Polysulfone
PVDF	Poly(vinylidene difluoride)
PVAc	Poly(vinyl acetate)
PI	Polyimide
XLPEO	Cross-linked polyethylene oxide

PEGMEA	Poly(ethylene glycol) methyl ether acrylate
AIBN	Azobisisobutyronitrile
PEGDA	Poly(ethylene glycol) diacrylate
PDMS	Poly(dimethylsiloxane)
PEI	Poly(ether imide)
PC	Polycarbonate
BET	Brunauer, Emmett and Teller
SEM	Scanning electron microscopy
TGA	Thermogravimetric analysis
DSC	Differential scanning calorimetry
EDX	Energy dispersive X-ray spectrometer
XRD	X-ray diffraction
DLS	Dynamic light scattering
6FDA	(2,2′ bis(3,4′-dicarboxyphenyl)hexafluoropropane dianhydride)
TMPDA	N,N,N′,N′-Tetramethyl-1,3-propanediamine
ODA	4,4'-oxydianiline
DAT	diallyl terephthalate
DAM	Diaminomesitylene
MOF	Metal Organic Framework
ZIF	Zeolitic imidazolate framework
CTABr	Cetyltrimethylammonium bromide
GPU	Gas Permeation unit
RTIL	Room temperature ionic liquid
MMM	Mixed Matrix Membrane
DCM	Dichloromethane
NMP	N-Methyl-2-Pyrrolidone
GC	Gas chromatography

List of Figures

Figure 1-1 Illustration diagrams of amine absorption process for carbon dioxide separation. (Resource: CO_2 capture-separation technologies, Retrieved 16th, November, 2017 from http://eurogrant.ucoz.ru/resour/resour61-2.html)..... 7

Figure 1-2 Illustration diagrams of physical adsorption process for carbon dioxide separation[8]….....8

Figure 1-3 Illustration diagrams of spiral membrane for carbon dioxide separation[8]….....9

Figure 1-4 Robeson upper bounds for CO_2/CH_4 separation. Prior and current upper bounds were established in 1991 and 2008, respectively [17]….....12

Figure 1-5 Performance of microporous membranes in the Robeson plots; (a) CO_2/CH_4 and (b) CO_2/N_2 [25]….....14

Figure 1-6 Possible interfacial defects for the composite membranes and their influence towards the membrane performance[27].....15

Figure 2-1 Potential energy as a function of angle out of plane of the 8-membered ring windows for the ideal geometry of CO_2 and CH_4 showing 8-ring zeolite is more likely to attract and store the CO_2 [50]….....22

Figure 2- 2 Schematic Illustration of the hierarchical zeolites (Resource retrieved 16th, November, 2017 from http://news.engr.uconn.edu/dr-ioulia-valla-awarded-nsf-grant.php).....25

Figure 2- 3 The modification of zeoite surfaces with silane agents [90]….....33

Figure 2-4 SEM images of cross sections of composite membranes composed of pure-silica-MFI and Ultem. (a) 5 μm untreated MFI, (b) 300 nm untreated MFI showing extensive voids between bare zeolites and polymers which can not be observed in (c) 5 μm solvothermally treated MFI, and (d) 300 nm solvothermally treated MFI [85]….....36

Figure 2-5 Representations of ZIF crystal structures [123]….....43

Figure 3-1 FESEM image of bare LTA zeolite particles prior to surface treatment (before ion exchange with $MgCl_2$)….....57

Figure 3-2 FESEM images of surface treated 5A zeolites (ST-5A) with different concentration of Mg ions in substrates and reaction pH: (a) 0.1 mol/L Mg, pH = 9.5, (b) 0.2 mol/L Mg, pH = 9.5, (c) 0.4 mol/L Mg, pH = 9.5, (d) 0.1 mol/L Mg, pH = 11.0 showing higher pH and Mg concentration will lead to a rougher external surface….....58

Figure 3-3 Powder X-ray diffraction patterns of bare 5A and ST-5A which were synthesized under different reaction conditions….....59

Figure 3-4 EDX spectrum of the surface modified LTA….....60

Figure 3-5 DSC Curve of the surface modified LTA zeolite….....61
Figure 3-6 N_2 physisorption isotherms of bare 5A and surface treated 5A zeolites which were synthesized under different reaction conditions….....63
Figure 3-7 Pure components CO_2 and CH_4 adsorption isotherms of bare 5A and ST1-5A measured at 40 ℃, along with corresponding Langmuir fits (solid lines)….....65
Figure 3-8 Cross section FESEM images of mixed-matrix membranes to show the enhanced polymer-zeolites interfacial morphology: (a) low magnification Matrimid®/bare 5A, (b) high magnification Matrimid®/bare 5A, (c) low magnification Matrimid®/ST1-5A, and (d) high magnification Matrimid®/ ST1-5A….....67
Figure 3-9 Stress-strain curves for Matrimid® membrane, Matrimid®-bare 5A mixed-matrix membranes, Matrimid®-surface treated 5A mixed-matrix membranes….....68
Figure 3-10 Pure component CO_2 adsorption by Matrimid®/20 wt% bare 5A and Matrimid®/20 wt% ST1-5A mixed-matrix membrane measured at 40 ℃….....71

Figure 4-1 (a) A scheme of amine-appended hierarchical Ca-A and (b) SEM image, (c) N_2 physisorption at 77 K and (d) XRD pattern of hierarchical mesoporous Ca-A before amine-grafting….....82

Figure 4-2 TGA curve of amine-functionalized hierarchical mesoporous Ca-A zeolite. (NH_2-mesoporous Ca-A)….....84

Figure 4-3 Pore size distribution of hierarchical mesoporous Ca-A zeolite before and after amine grafting….....85

Figure 4-4 CO_2 and CH_4 adsorption isotherms of mesoporous Ca-A measured at 25 ℃….....86

Figure 4-5 SEM images of a series of composite membranes. (a) and (b) low and high magnification of Matrimid®/20% wt bare mesoporous Ca-A; (c) and (d) low and high magnification of Matrimid®/20% wt NH_2-mesoporous Ca-A; (e) and (f) low and high magnification of XLPEO/NH_2-mesoporous Ca-A showing NH_2-decorated zeolite had a much better adhesion with the Matrimid® than the zeolite….....88

Figure 4-6 Mixed-gas permeation properties of membranes at 25 ℃ and 1 bar total feed pressure with a 1:1 CO_2/CH_4 mixture. The filler loading was 20 wt% for

all mixed-matrix membranes. The solid line is the upper bound limit for polymer membranes established in 2008….....90

Figure 5-1 FESEM images of $Zn(pyrz)_2(SiF_6)$ crystals synthesized by (a) the conventional and (b) the sonochemical approaches….....99

Figure 5-2 Powder X-ray diffraction patterns of $Zn(pyrz)_2(SiF_6)$ crystals….....100

Figure 5-3 TGA curves of $Zn(pyrz)_2(SiF_6)$ crystals….....101

Figure 5-4 Pure component CO_2, CH_4, and N_2 adsorptions on $Zn(pyrz)_2(SiF_6)$ submicron crystals measured at 25 ℃….....102

Figure 5-5 FESEM images of cross-sections of composite membranes containing $Zn(pyrz)_2(SiF_6)$ crystals. (a) and (b) 10 wt % bulk $Zn(pyrz)_2(SiF_6)$ crystals in XLPEO; (c) and (d) 10 wt % submicron crystals in XLPEO; (e) and (f) 20 wt % submicron crystals in XLPEO demonstrating both the submicron and bulk crystals can have a desirable interfacial morphology with the XLPEO, while the submicron crystal's distribution in membrane is better than the bulk crystals…103

Figure 5-6 Robeson plots of (a) CO_2/CH_4 (50/50) and (b) CO_2/N_2 (20/80) mixture gas permeation data presented in Table 5-1 and 2. The solid lines represent the upper bound limit for polymeric membranes established in 2008[17]….....108

Figure 5-7 Predicted CO_2/CH_4 permeation properties of hypotheticals composite membranes synthesized by incorporating 20 wt% $Zn(pyrz)_2(SiF_6)$ submicron crystals into various 6FDA polyimides. Solid and empty symbols represent predicted composite membranes and pure polymer membranes respectively. The calculations were carried out using the Maxwell model describe indicating the as-made composite membranes will show extraordinary CO_2 separation performance if combine the $Zn(pyrz)_2(SiF_6)$ submicron crystals together with high performance 6FDA-based polymers[179, 180]….....110

Figure 6-1 (a) Particle size distribution, (b) SEM image, (c) powder X-ray diffraction pattern, and (d) TGA curve of $Zn(pyrz)_2(SiF_6)$ nanocrystals….....121

Figure 6-2 CO_2 and CH_4 adsorption of $Zn(pyrz)_2(SiF_6)$ nanocrystals at 25 ℃..123

Figure 6-3 Photographic images of the as-made cast solutions after **(a)** 1 hour **(b)** 2 hours **(c)** 4 hours **(d)** 8 hours **(e)** 16 hours and **(f)** 24 hours. The as-made cast solution was based on 20 wt% $Zn(pyrz)_2(SiF_6)$ nanocrystal in DCM containing 15 wt% 6FDA-TMPDA.....124

Figure 6-4 FESEM images of the cross-section of 6FDA-TMPDA mixed-matrix membrane containing **(a, b)** 10 wt% $Zn(pyrz)_2(SiF_6)$ nanocrystals and **(c, d)** 20 wt% $Zn(pyrz)_2(SiF_6)$ nanocrystals at **(a, c)** high magnification and **(b, d)** low magnification.....126

Figure 6-5 EDX mapping of **(a)** 20 wt% $Zn(pyrz)_2(SiF_6)$ nanocrystals in 6FDA-TMPDA membrane with the corresponding elemental distribution of Si **(b)**.....126

Figure 6-6 EDX mapping of **(a)** 20 wt% sub-micron $Zn(pyrz)_2(SiF_6)$ crystals in XLPEO membrane with the corresponding elemental distribution of Si **(b)**.....127

Figure 6-7 Pure component (a) CO_2 and (b) CH_4 adsorption properties of 20wt% $Zn(pyrz)_2(SiF_6)$/6FDA-TMPDA and pure 6FDA-TMPDA membranes at 25 ℃.....128

Figure 6-8 (a) Permselectivity, sorption selectivity and diffusion selectivity of membranes and (b) CO_2/CH_4 separation performance of membranes together with literature data for mixed-matrix membrane made up of 6FDA-based polymers; The exact data points are presented in **Table 6-4**. The black solid line represents the Robeson upper bound limit for polymeric membrane established in 2008. [191].....133

Figure 6-9 CO_2/CH_4 separation of our membranes together with the literature data for high permeable polymers. The exact number are summarized in table 6-5 and 6-6. The black solid line represents the upper bound limit for polymeric membrane constructed in 2008 [17].....136

List of Tables

Table 1-1 Summary of carbon dioxide separation processes.....10

Table 2-1 Experimentally measured diffusion rates of CO_2 and CH_4 in zeolites……..……21

Table 2-2 Main characteristics of common zeolite fillers 24

Table 2-3 CO_2 separation performance of zeolite-based mixed matrix membranes 31

Table 2-4 MOF particle size from various synthesize methods. 40

Table 2-5 CO_2 separation performance of zeolite-based mixed matrix membranes 46

Table 3-1 Reaction conditions for surface treatment of zeolites.....53

Table 3-2 EDX elemental analysis of Mg-containing zeolite (after ion-exchange with $MgCl_2$).....62

Table 3-3 Properties of bare and surface treated 5A zeolites calculated from N_2 physisoprtion at 77 K….....64

Table 3-4 Fitting parameters for Langmuir model, Henry's coefficients, and sorption selectivities….....65

Table 3-5 Mechanical strength of mixed-matrix membranes….....70

Table 3-6 Mixed-gas permeation properties of membranes at 40 ℃ and 1 bar total feed pressure with a 1:1 CO_2/CH_4 mixture….....72

Table 3-7 CO_2 solubility, diffusivity and permeability data for Matrimid® and Matrimid®/20wt% ST1-5A….....73

Table 4-1 Physical properties of mesoporous Ca-A and NH_2-mesoporous Ca-A.....87

Table 4-2 Mixed-gas permeation properties of membranes at 40 ℃ and 1 bar total feed pressure with a 1:1 CO_2/CH_4 mixture ……..89

Table 5-1 CO_2/CH_4 (50/50) mixture gas permeation properties of membranes measured at 25 ℃ and 1 bar of upstream pressure….....106

Table 5-2 CO_2/N_2 (20/80) mixture gas permeation properties of membranes measured at 25 ℃ and 1 bar of upstream pressure….....107

Table 6-1 Mixture gas (CO_2/CH_4, 50/50) permeation properties of membranes measured at 1 bar upstream pressure and 25 ℃….....130
Table 6-2 Comparison between the density of polymeric membrane and mixed-matrix membrane.....131
Table 6-3 CO_2 and CH_4 solubility and diffusivity data for pure 6FDA-TMPDA and 20 wt% $Zn(pyrz)_2(SiF_6)$/6FDA-TMPDA membranes….....133
Table 6-4 Comparison of mixed-matrix membrane performance reported in **Figure 6-8 (b)…**.....135
Table 6-5 Performance of TR-polymer reported in **Figure 6-9**.....137
Table 6-6 Performance of PIM-polymer reported in **Figure 6-9**.....138

Summary

Composite Membranes Comprising Nanoporous Materials for Carbon Dioxide Capture

Membrane-based gas separation provides various advantages over conventional gas separation techniques such as desirable energy efficiency, small footprint and ease of operations. However, conventional polymeric membranes in which mass transport is governed by solution-diffusion have shown the limited performance although their excellent processability is highly desirable for the fabrication of membrane in large scales. In this regard, incorporating microporous materials that can selectively transport the targeted molecules into polymer membranes has been proposed as an attractive option to fabricate membranes with large membrane areas and high separation performance. In this thesis, composite membranes containing various nanoporous materials are reported. The membranes were designed to be applied in CO_2 separation which is highly important in clean energy production and greenhouse gas control.

At first, the CO_2 separation performance of commercial polyimide membrane was enhanced by incorporating engineered Ca-A zeolite. In order to improve filler/polymer adhesion, LTA zeolites with highly roughened surfaces were made by the ion-exchange-induced growth of $Mg(OH)_2$ nanostructures on

the zeolite surfaces. The morphology of LTA crystals was tuned by the systematic modification of reaction parameters such as the pH of the reaction medium and the amount of magnesium loaded in the substrates. After converting surface-modified LTA to Ca-A, which has been known as a good candidate for selective CO_2 uptake and transport, by replacing extra-framework cations remaining in LTA with Ca^{2+}, a series of mixed-matrix membrane incorporating Matrimid® and Ca-A was fabricated. Owing to improved zeolite/polymer adhesion property along with the selective transport of CO_2 by the fillers, mixed-matrix membranes containing surface modified Ca-A showed enhanced CO_2/CH_4 separation properties, which are measured by a binary mixture permeation testing. In light of that, a dramatically increase in CO_2 permeability (ca. 120 %) was observed for Matrimid®/20 wt% Ca-A membrane which also showed an improved CO_2/CH_4 selectivity. In contrast, untreated Ca-A decreased CO_2/CH_4 selectivity of Matrimid® membrane due to defects formed at zeolite/polymer interfaces.

Secondly, amine-appended hierarchical Ca-A zeolite possessing an outstanding CO_2 capture property was synthesized and incorporated into polyethylene oxide and Matrimid®, to design mixed-matrix membranes with high CO_2/CH_4 selectivity. Binary mixture permeation testing revealed that amine-appended mesoporous Ca-A is highly effective in improving CO_2/CH_4 selectivity of polymeric membranes. Furthermore, the formation of filler/polymer interfacial defects, which is typically found in glassy

polymer-zeolite pairs, was inhibited owing to the interaction between the amine groups on the external surface of zeolites and polymer chains.

Thirdly, metal-organic frameworks, an emerging class of nanoporous material, were employed as the filler materials for composite membranes. Among them the $Zn(pyrz)_2(SiF_6)$ (or SIFSIX-3-Zn) which is known to have strong affinity to CO_2 was chosen as a promising candidate. However, crystals harvested from traditional synthesis method are too large to be used in membrane fabrication. In order to utilize this filler, therefore, a facile sonochemical method was employed to synthesize uniform submicron-sized SIFSIX-3-Zn crystals. Then, high-quality mixed-matrix membranes free of filler/polymer interfacial voids were successfully fabricated by employing cross-linked polyethylene oxide (XLPEO) as a polymer matrix. CO_2/CH_4 and CO_2/N_2 mixture gas permeation tests revealed that the separation properties of mixed-matrix membranes, especially selectivities, were significantly improved compared to those of pure polymeric membrane owing to the selective CO_2 uptake and transport in $Zn(pyrz)_2(SiF_6)$ crystals.

Although the $Zn(pyrz)_2(SiF_6)$ was proved to be an effective filler for designing CO_2-selective membrane, the overall CO_2 separation performace was limited the moderate performance of XLPEO, which is also suffering from poor mechanical stability. A theoretical analysis with Maxwell model revealed that 6FDA-TMPDA polyimide is a promising candidate to design high-performance

membranes surpassing the upper-bound limit for polymer membranes. In addition, to maximize the effect of the filler, the nanoscrystal form of $Zn(pyrz)_2(SiF_6)$ was synthesized by a modified sonochemical method. The FESEM and EDX analysis showed that the nanocrystal fillers were unformly distributed in the polymer matrix. Binary CO_2/CH_4 mixture gas permeation tests revealed that both CO_2 permeability and CO_2/CH_4 selectivity of mixed-matrix membranes, especially for the membrane with 20 wt% filler loading, were significantly improved compared to those of pure polymeric membrane due to the selective CO_2 uptake and transport by $Zn(pyrz)_2(SiF_6)$ crystals. As a result, a performance surpassed the upper bound limt for polymeric membranes was achived.

Chapter 1

Introduction

1.1 Importance of CO_2 Separation

Global industrialization and urbanization have resulted in a large demand for energy. Based on a report published by the US Energy Information Administration [1], at present, more than 65% of electricity is produced by burning carbon-based fuels, creating over 5 billion tons of CO_2 per year. The rising level of atmospheric CO_2 has become one of the major concerns facing society due to its global warming effect and biological hazard [2-4]. The way we manage CO_2 may determine the health and welfare of our society in the next 50-100 years. This concern has motivated countless studies on energy-efficient carbon separation techniques.

1.2. Current Technologies for Carbon Dioxide Capture

CO_2 can be separated and concentrated from mixture gas based on its boiling point, kinetic diameter, polarizability, quadruple moment and chemical properties. The ideal technique should be energy efficient (current carbon capture techniques will increase the cost of electricity by 50%) and also environmental friendly[5]. Membrane separation technique is known to be a promising option that can fulfil these requirements.

1.2.1 Conventional Techniques

Chemical absorption process (amine scrubbing) has been the most widely used technique for carbon capture due to their high selectivity (98% for monoethanolamine) and desirable separation performance even at low CO_2 concentrations. In this technology, CO_2 is captured from a flue gas or natural gas by aqueous amine solutions in which chemical reactions occur between CO_2 and amine groups, namely mono-amine, di-amines, tri-amines and di-isopropanol amines. The amine solutions are typically in packed and plated columns that require a large space and high installation cost. After the absorption of CO_2, the media must be regenerated by applying thermal energy [6] and thus this process is typically considered energy-intensive. The consumed energy is approximately 0.31-0.37 kWh/kg CO_2, including approximately 0.16 kWh/kg of CO_2 liquefaction energy [7]. Overall, the high installation and regeneration costs can be a limiting factor for this technology, and the long-term stability of the amine solution, which is highly corrosive, is also questionable.

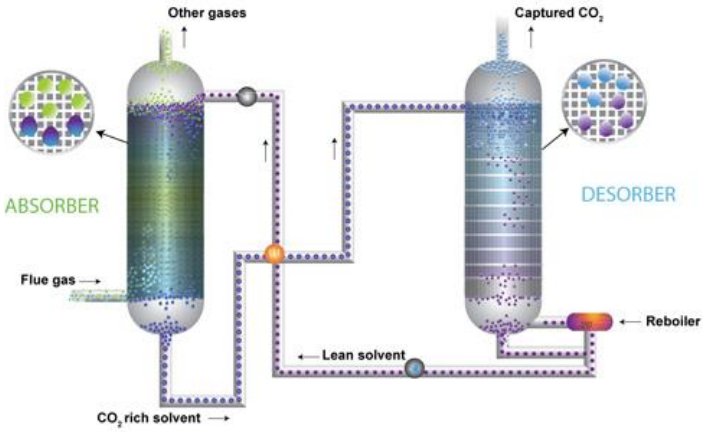

Figure 1-1 Illustration diagrams of amine absorption process for carbon dioxide separation. (Resource: CO_2 capture-separation technologies, Retrieved 16th, November, 2017 from http://eurogrant.ucoz.ru/resour/resour61-2.html)

Physical adsorption is based on the affinity between CO_2 molecules and microporous adsorbents, including zeolites, activated carbon, mesoporous silica and metal-organic frameworks (MOFs). When mixture gases pass through a packed bed filled with adsorbents, CO_2 will be captured by the adsorbents and other gases will pass through freely. Based on the methods for the regeneration of media, the processes can be classified into pressure swing adsorption (PSA), temperature swing adsorption (TSA) and pressure and temperature swing adsorption (PTSA). Adsorptive carbon capture typically consumes less amount of energy than amine scrubbing because the heat capacity of solid adsorbents is typically lower than that of aqueous amine solution. The performance and cost of the process depends largely on the pore volume, pore size and affinity to CO_2

or binding energy of the absorbents. Thus, emerging microporous materials, such as MOFs and COFs (covalent organic frameworks) possessing large surface areas and tunable functionality, may have promising potential for this application.

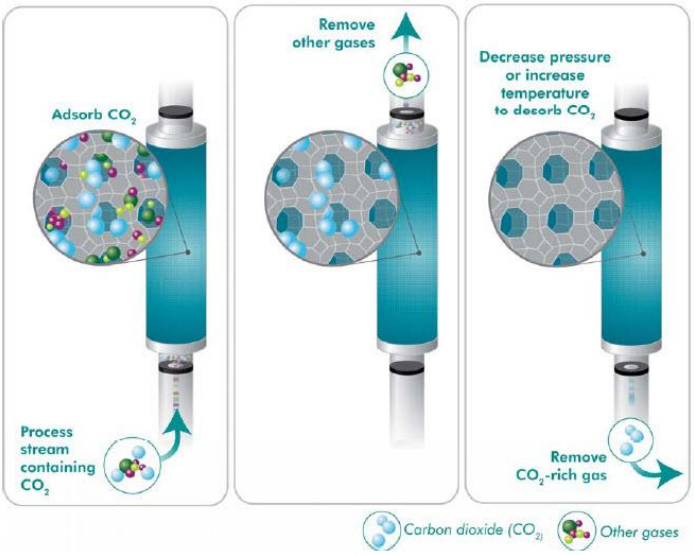

Figure 1-2 Illustration diagrams of physical adsorption process for carbon dioxide separation[8].

The cryogenic process involves the cooling of mixture gases to their boiling point at which the phase change occurs. The main advantages of this process are its high separation efficiency and strong reliability. However, the large energy consumption required for the phase change of the gases is a major drawback of this process [9].

1.2.2 Membrane Process

Membrane technology, which does not involves a phase change, is considered as an energy-efficient separation method. The separation mechanism

is based on the differences in the permeation rates of gas molecules through membrane materials. A partial pressure difference across the membrane acts as the driving force for mass transport, which is governed by both the diffusivity of gas and the affinity between gas and membrane material. A desirable membrane should have high gas permeability together with a decent selectivity. Gas permeability is the index for describing the speed at which a gas can transport through the membranes. A higher permeability can lead to a smaller membrane area, which can efficiently reduce the membrane cost and the footprint of overall system. Gas selectivity, which is dependent on the property of membrane material, can determine the purity of the product gas.

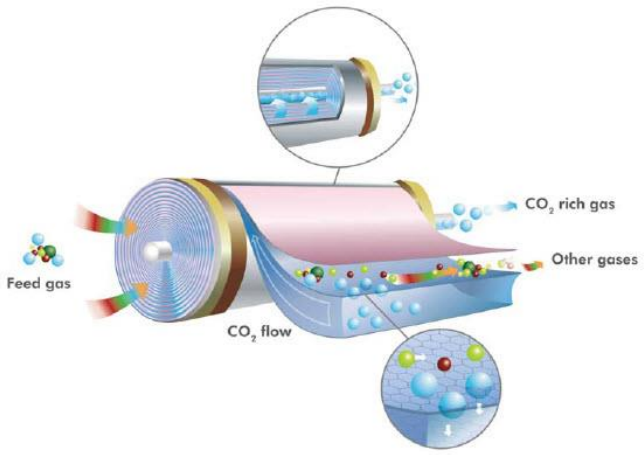

Figure 1-3 Illustration diagrams of spiral membrane for carbon dioxide separation[8].

Several types of gas separation membranes can be used for CO_2 capture, including polymer membranes, inorganic membranes and composite membranes. The energy consumption of membrane-based carbon capture was reported to be even lower than 0.072 kWh/kg CO_2 with the membrane exhibiting a desirable performance [7]. Merkal et.al reported for

commercialization, carbon dioxide separation membrane should demonstrated at least 1000 GPU with a CO_2/N_2 mixture selectivity around 50 to make whole process economical-viable[10, 11].

Method Parameters	Chemical Absorption[a] (Amine Scrubbing)	Physical adsorption	Cryogenic Distillation	Gas Separation Membrane
Working principle	• Chemical Reaction between amine groups and CO_2.	• Physical interactions between CO_2 and microporous adsorbents. • Adsorption at high pressure and/or low temperature and desorption at low pressure and/or high temperature	• Cooling of mixture gases to their boiling point at which the phase change occurs	• Differences in the permeation rates of gas molecules through membrane materials
Pros	• High removal efficiency even at low pressure. • High selectivity • Operation at ambient condition is feasible	• Selection of high specific surface areas of adsorbents can maximize adsorption capability of CO_2 • High enrichment of CH_4 can be generated	• High separation factor. • Large quantities of biogas can be processed • Process is high reliable. • Other impurities can be removed effectively by selecting suitable temperature and pressure	• Small plant footprint • Low operational and installation costs • Process can operate continuously.
Cons	• High energy consumption to desorb CO_2 from the solution. • Long time stability is questionable. • Large working space and high installation cost. • Amine solutions is not environmental-friendly.	• Presence of impurity such as H_2O leads to competitive adsorption and reduce the uptake ability of CO_2. • Stability of the adsorbents is highly important, especially in humid conditions. • Need to activate multiple times before working.	• Large amount of process equipment • Harsh operating conditions.	• Membrane wetting increases the mass transfer resistance across the membrane • Hydrophobic surface tends to reduce fouling resistance.

Table 1-1 Summary of carbon dioxide separation processes

1.3 Types of Membranes

1.3.1 Polymeric Membranes

Polymers are the most widely used material in commercial membranes due to their desirable processability, mechanical strength and low cost. Gas transport in polymeric membranes follows the solution-diffusion mechanism, in which gas molecules first dissolve in the polymer surfaces and then diffuse through the membranes. Thus, the permeability flux of the target gas depends on both the solubility and the diffusivity in the membranes:

$$P = S \times D$$

where P is the permeability, S is the solubility, and D is the diffusivity.

The selectivity (S) is defined as the ratio of the permeability, which can be expressed as follows:

$$S = P_A/P_B = (S_A \times D_A) / (S_B \times D_B)$$

where P_A and P_B are the permeabilities of component A and B, respectively.

According to this theory, a membrane possessing a high free volume typically shows a high permeability. A high free volume in membrane, however, generally gives a poor selectivity. This trade-off between permeability and selectivity for polymeric membranes was first established by L.M. Robeson and has been accepted as a general trend [12]. In past few decades, the membrane

community has explored a large number of polymer materials, some of which have shown promising results, particularly for the thermally rearranged (TR) polymers and polymers of intrinsic microporosity (PIMs) [13-16]. However, the trade-off is still valid for the majority of polymers which can be seen in Figure 1-1.

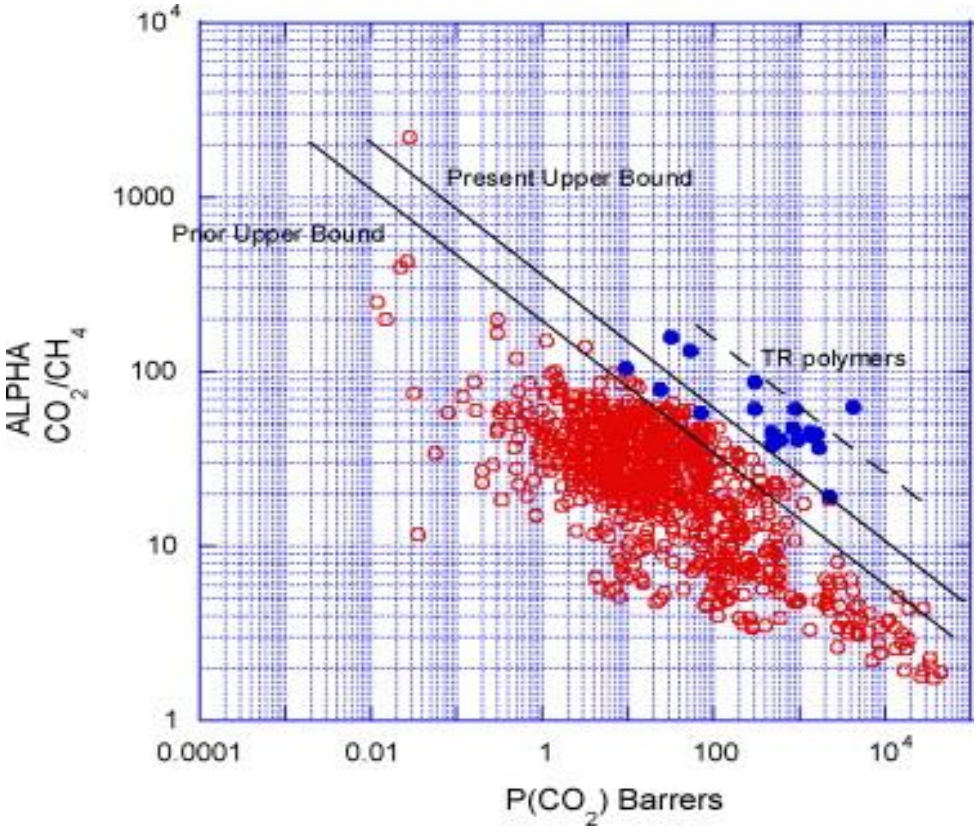

Figure 1-4 Robeson upper bounds for CO_2/CH_4 separation. Prior and current upper bounds were established in 1991 and 2008, respectively [17].

1.3.2 Inorganic Membranes

Inorganic membranes, such as zeolites, metal organic frameworks and carbon nanomaterials, were introduced as an alternative to polymeric

membranes. Unlike polymeric membranes, the uniform and well-defined pore channels of the inorganic materials can exhibit a sharp size and/or shape discrimination for the target gas molecules. Due to such molecular sieving mechanism, various laboratory-scale zeolite membranes, such as DDR, CHA, MFI, and FAU, have demonstrated both superior permeability and selectivity for CO_2 separation [18-22]. Emerging materials, such as MOF membranes and graphene-based membranes have also shown great potentials in this field, with performances located above the Robeson upper bound (Figure 1-2) [12, 17]. Moreover, inorganic materials tend to exhibit higher thermal and chemical stability than pure polymers that are suffering from plasticization in high pressure CO_2 separations. Although there are a few successful commercial examples of inorganic membranes, such as LTA zeolite membranes that employed in some liquid-phase separations, the poor scalability and the intrinsic brittleness of materials are still major drawbacks hindering their applications in industrial gas separation processes, which are less tolerant of defects as compared to liquid phase operation [23, 24]. In addition, their high production cost has also limited the translation from laboratory research to industrial application.

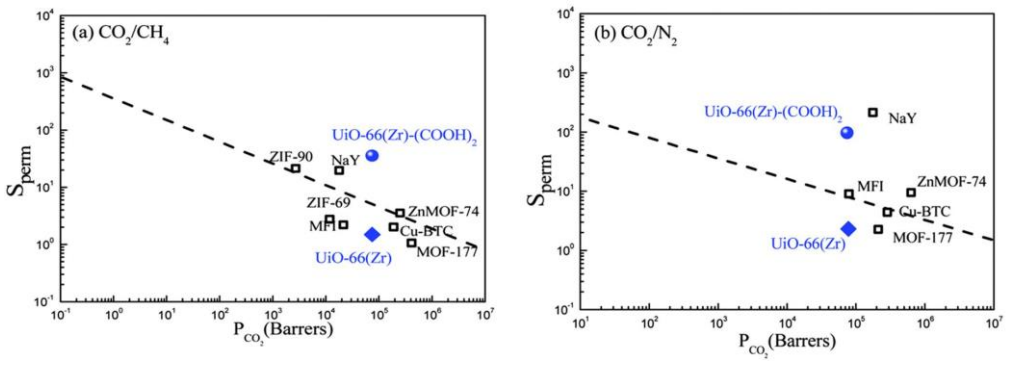

Figure 1-5 Performance of microporous membranes in the Robeson plots; (a) CO_2/CH_4 and (b) CO_2/N_2 [25].

1.3.3 Composite Membranes

In 1973, D. Paul and D. Kemp first introduced the concept of composite membranes which is compose of continuous polymer phase and inorganic fillers [26]. They found the Ca-A zeolite in poly(dimethylsiloxane) (PDMS) membranes can tailor the diffusions of gas molecules. This concept has been widely used over the past 40 years, as it combines the advantages of both phases low cost, good processibility and ideal mechanical properties of polymers and desirable separation performance of fillers.

In order to select the suitable filler and polymers, the separation performance of the composite membranes can be predicted with several mathematic models. The most famous one is the Maxwell model which is described as follows:

$$P_{MMM} = P_p[\frac{P_s + 2P_p - 2\varphi_s(P_p - P_s)}{P_s + 2P_p + \varphi_s(P_p - P_s)}]$$

where P_{MMM}, P_p, and P_s denote the permeabilities of the mixed matrix membranes, polymers and sieves, respectively, and φ_s denotes the volume fraction of the sieve.

The model suggests that performance of composite membranes is simply dependent on the properties of both phases and the volume fraction of fillers. However, the model often fails to predict the performance of composite membrane due to the undesirable interfacial morphology which is summarized in Figure 1-3. The model is based on a hypothesis that fillers and polymers have a perfect interfacial interactions, thus it may fail if the defects in membranes can not be ignored.

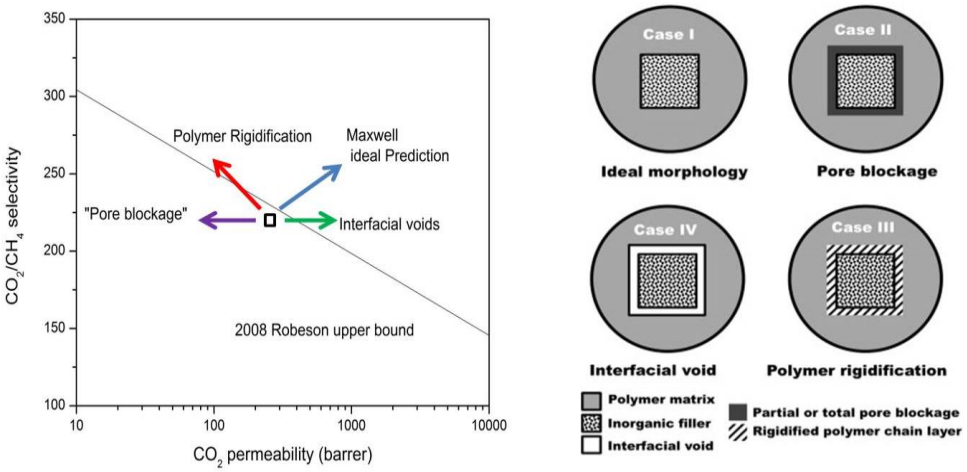

Figure 1-6 Possible interfacial defects for the composite membranes and their influence towards the membrane performance[27]

Thus far, vast amounts of efforts have been made to realize high separation performance via judicious selection of filler-polymer pair, modifying the surfaces of fillers to improve the polymer/filler adhesion, and optimizing the filler loading to overcome the Robeson upper bound limit [28, 29].

1.4 Aims and Objectives of Research

Membrane-based carbon capture is an energy-efficient alternative to current amine-scrubbing. Among various membrane types, composite membranes have been considered as a technically viable option to produce high-performance gas separation membrane in large scales. In this work, various composite membranes containing functional nanoporous materials such as zeolites and MOFs were fabricated for potential application in industrially important CO_2 separations such as CO_2/N_2 and CO_2/CH_4 separations. These separations are applicable in post-combustion carbon capture, biogas upgrading and natural gas treatment.

This thesis mainly focuses on:

1. Screening and synthesizing porous materials that are promising for application in CO_2 separations.

2. Identifying and synthesizing polymer matrix that is well-matched with the filler prepared.

3. Fabricating composite membranes with ideal polymer-filler interfaces leading to a high CO_2 separation performance.

Chapter 2

Literature Review

2.1 Zeolite Molecular Sieve

2.1.1 Definition

Zeolites are crystalline microporous aluminosilicates composed of SiO_4 and AlO_4 tetrahedra as primary building units. The primary building units share the oxygen atoms to form a continual 3D structure with cavities and channels. Introducing AlO_4^- gives a negative charge to the overall silica framework, thus extra cations are required to make the entire framework neutral. The cations are typically from Group I (e.g., Li^+, Na^+, K^+) and Group II (e.g., Ca^{2+}, Mg^{2+}). Thus, the composition of zeolites can be expressed in the following form.

$$M_{y/a}^{a+} \times [Si_xAl_yO_{2(x+y)}] \times z\ H_2O$$

where M is the extraframework cation. In certain situations, there can be pure silica zeolites, which means y = 0 (e.g., Si-CHA zeolite and ITQ-12 zeolite) [30, 31].

Zeolites typically exhibit high thermal and chemical stability as well as well-defined 3-D pores allowing a sharp molecular discrimination. These advantages make zeolites ideal for CO_2 separation. Thus, numerous CO_2 separation studies have been performed with various commercial zeolite fillers, such as ZSM-5, Ca-A, Na-A, and Na-X [32-34]. Sorption and diffusion

properties of gases on/in zeolites materials are discussed in sections 2.1.2 and 2.1.3.

2.1.2 Equilibrium Separation

Equilibrium separation is based on the difference in the amounts of gases adsorbed at equilibrium. The majority of zeolites can demonstrate electric field strength due to the electrical field interaction of negative AlO_4^- and positive extraframework cations. The electric field strength, therefore, increases as the Si/Al ratio decreases. This behaviour makes low Si/Al zeolites interact strongly with CO_2, which has a high quadrupole moment (4.30×10^{-26} esu cm^2) [35]. In contrast, CH_4 and N_2, which have neither a dipole nor a quadrupole moment, are weakly bound to the zeolite surfaces and the changes in the Si/Al ratio will not have a significant effect on CH_4 adsorption. Corma et al. investigated the CO_2 and CH_4 uptakes on LTA zeolites with various Si/Al ratios (1 to $+\infty$). Increases in the Al content can give rise to the increase in isosteric heat of adsorption for CO_2. In contrast, the Al content has negligible effect on the isosteric heat of adsorption for CH_4. LTA zeolites with an Si/Al ratio of 1:1 demonstrated the highest CO_2/CH_4 selectivity, whereas an Si/Al ratio of 2:1 resulted in the highest CO_2 uptake [36]. A similar study to reveal the influence of the Si/Al ratio on CO_2 uptake has been performed with ZSM-5, KFI, MWW and CHA zeolites [37-40]. Zeolites with a low Si/Al ratio were observed to be

more sensitive to moisture. Water molecules compete for the active adsorption site in zeolites, resulting in a significant loss of CO_2 uptake.

The type and position of the extraframework cations can also modify the electric field of the zeolites and the available pore volumes [41]. Thus, ion-exchange can be a highly effective method for modifying CO_2/CH_4 selectivity [38, 39, 42]. Webley et al. investigated the effect of the cation type and Si/Al ratio of chabazite (CHA) zeolite on biogas separation and found that the CHA zeolite with large univalent cations (Rb^+, Cs^+) and a low Si/Al ratio (lower than 3) can exhibit a door-keeping effect, in which adsorbed CO_2 blocks the access of CH_4 and N_2, such that the CO_2/CH_4 selectivity can go up as high as 140 [39, 43, 44]. Bae et al. evaluated a series of ion-exchanged LTA and FAU zeolites, including Na-A, Ca-A, Mg-A, Na-X, Mg-X, and Ca-X. Among them, Ca-A and Na-X exhibited attractive CO_2 uptake at low CO2 partial pressure (0.15 bar) and can be considered as suitable candidates for post-combustion CO_2 capture [45]. Levan et al. have shown that, for X- and Y-type zeolites, the CO_2 capacity increased with a change in cation type in the following order: $Cs < Rb \approx K < Li \approx Na$ [46]. Derek Creaser has shown that Ba-ZSM-5 has a higher CO_2 uptake than Na-ZSM-5 and H-ZSM-5 [47].

The zeolite structure, which can affect the various zeolite properties, such as pore volume, pore size and surface area, can also have a considerable impact on the gas equilibrium uptake. Li et al. compared the CO_2 and CH_4 equilibrium

uptakes of 8-, 10-, and 12-membered-ring zeolites [48]. These zeolites, which are all high-silica zeolites, are DDR, silicalite-1 and zeolite beta, respectively. In that study, the changes in the BET surface area, pore volume and CO_2 uptake with changes of zeolite structure exhibited the following trend: 8-membered ring < 10-membered ring < 12-membered ring. The CO_2/CH_4 selectivity followed the order of 10-membered ring < 8-membered ring ≈ 12-membered ring.

2.1.3 Kinetic Separation

Kinetic separation is based on the difference in diffusion rates of permeating species. In this area, a computation tool has been actively used to understand how gas molecules can transport through the pores of zeolites. For example, Lobo and his co-workers have studied the potential energy of CO_2 and CH_4 passing through an 8-membered zeolite ring using density function theory [49]. The main parameters for the kinetic separation of CO_2/CH_4 are size, shape and dimensionality of the pores. The ideal pore size of the adsorbent should between the kinetic diameter of CO_2 (0.33 nm) and CH_4 (0.38 nm).

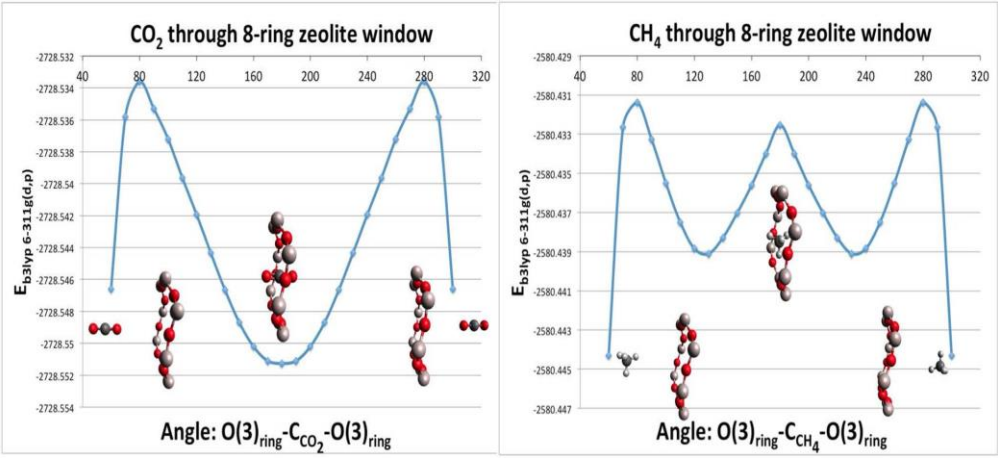

Figure 2-1 Potential energy as a function of angle out of plane of the 8-membered ring windows for the ideal geometry of CO_2 and CH_4 showing 8-ring zeolite is more likely to attract and store the CO_2 [50].

Sholl et al. used a molecular dynamics (MD) simulation to reveal that 3D pores have greater steric hindrance to light gas than 1D pores. It was also found that the diffusion rate increased significantly with pore size [51]. Thus, the ideal zeolites for kinetic separation of biogas are 8-membered-ring zeolites. However, the computational study often predicts higher gas selectivity than experimental measurement. For example, DDR zeolite showed CO_2/CH_4 selectivity of 58 in an experimental measurement while MD simulations yielded an even higher kinetic selectivity of up to 70 [52]. Experimental measured diffusion properties in zeolites and main characteristics of most common zeolites had been summarized in the tables 2-1 and 2-2, respectively.

Table 2-2 Experimentally measured diffusion rates of CO_2 and CH_4 in zeolites

Sorbents	**Temperature (K)**	**CH_4 Do (m^2/s)**	**E_{CH4} (kJ/mol)**	**CO_2 Do (m^2/s)**	**E_{CO2} (kJ/mol)**	**Method**
HZSM-5	334	$\sim 10^{-8}$	4	NA	/	PFG NMR
HZSM-5	250	3×10^{-9}	4	NA	/	QENS
DD3R	298	1.7×10^{-12}	NA	1.0×10^{-10}	/	FR
Na-A	300/500*	5×10^{-15}	24	3×10^{-12}	23	Gravimetric uptake

[a] All diffusion results are from the textbook: . *Diffusion in nanoporous materials*; John Wiley & Sons, 2012.

[b] The diffusion rate of CH_4 and CO_2 is a summary of the literature and do not have detailed temperature.

[c] QENS = quasi-elastic neutron scattering, PFG NMR = pulsed field gradient nuclear magnetic resonance.

[d] In the case of Na-A, Do of CH_4 and CO_2 was measure at 300 and 500 K respectively.

Table 2-3 Main characteristics of common zeolite fillers

	Zeolite Structure	Cation	Pore size (nm)	CO_2 Uptake (mmol/g)	Total Pore Volume (cm^2/g)	BET surface area(m^2/g)	Ref
4A	LTA	Na^+	0.38	3.07	0.21	422	[45]
5A	LTA	Ca^{2+}	0.48	5.02	0.29	689	[45]
13X	FAU	Na^+	0.74	5.67	0.33	724	[45]
LiX	FAU	Li^+	0.74	5.62	-	-	[46]
SAPO-34	CHA	NH_4^+	0.38	4.55	0.28	587	[53]
H-SSZ-13	CHA	H^+	0.38	3.98*	0.27	764	[50]
Cu-SSZ-13	CHA	Cu^{2+}	0.38	3.75*	0.25	710	[50]
DD3R	DDR	\	0.36×0.44	1.32	0.15	304	[54]
ZSM-5	MFI	Na^+	0.51×0.55	1.56	0.22	311	[55]
NaY	FAU	Na^+	0.74	5.18	0.34	-	[46]
LiY	FAU	Li^+	0.74	5.21	0.34	-	[46]
Li-ZK-5	KFI	Li^+	0.39	~4.9*	0.22	-	[56]
Na-ZK-5	KFI	Na^+	0.39	~4.0*	0.22	-	[56]
Li-RHO	RHO	Li^+	0.41	4.96**	0.36	-	[57]
K-RHO	RHO	K^+	0.41	4.50**	0.36	-	[57]
K-BEA	BEA	K^+	0.6	~3.0	0.41	446	[58]
Na-BEA	BEA	Na^+	0.6	~2.8	0.52	508	[58]
K-MCM-22	MWW	Na^+	0.40×0.59	~2.7	--	479	[40]

[a]Assume CO2 uptake is at the condition of 298 K and 1 bar, here * stands for 303K and 1 bar and ** stands for 303K and 0.8 bar.

[b] The data for pore size is from the database of international zeolite association if the reference does not give a specific result.

2.1.4 Chemical Treatment of Hierarchical Zeolites

The hierarchically zeolites are defined as zeolite possessing at least two levels of porosity, namely the microporosity of zeolite domain and additional pore domains. The additional pore domains are formed by the chemical treatment and range from 0.5 nm to 50 nm which random distributed in the framework.

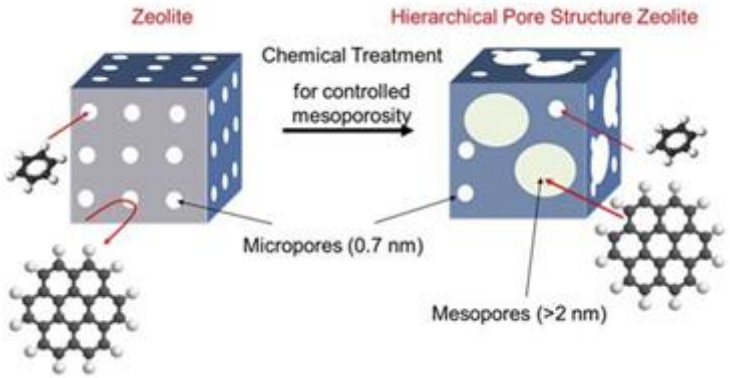

Figure 2- 2 Schematic Illustration of the hierarchical zeolites (Resource retrieved 16th, November, 2017 from http://news.engr.uconn.edu/dr-ioulia-valla-awarded-nsf-grant.php)

This structure can give additional possibilities for post-synthetic modification and increasing the rates of intercrystalline diffusion [59, 60]. The treatment of hierarchically zeolites can be divided into pre-synthetic route and post-synthetic route. The post-synthetic route is known as demetallation, in which acid or alkaline is used to partially decompose zeolite structure [61]. The amount of acid/alkaline and reaction condition should be precisely controlled in order to achieve a desired level of mesoporosity as well as to retain the certain level of crystallinity. Sulikowski had applied ethylenediaminetetraacetic acid to Na-Y zeolites for partial demetallation under a heating reflux (~800 ℃) condition [62]. This process could successfully remove some of aluminum atoms leading to mesoporous domains formed within the zeolite. Another successful example is the disilication of ZSM-5 zeolite with NaOH. The

process could increase the mesopore volume by factor 4 with a slight sacrifice of the micropore volume [63].

The pre-synthetic method for hierarchically zeolite is typically done by adding templates (hard templates or soft templates) into the precursor gel. This method is widely used in synthesis of nanomaterials with specific morphology [64, 65]. The hard templates are generally carbon nanomaterials including carbon nanoparticles, carbon nanofibers and carbon nanotube [66-68]. In this method, mesopore size is generally dependent on the shape of templates, such that the size distribution of mesopores formed in zeolite is generally narrow [61]. Unlike hard template method for which the resultant hierarchical zeolite is strongly depended on the nature of the template, the soft template method typically provides more flexibility. The mesoporosity can be tailored by adjusting several parameters including the amount and the packing density of the surfactant, the reaction temperature and pressure.

2.1.5 Zeolite as Membrane Filler

The first zeolite-based composite membrane which is also the first composite membrane for gas separation was introduced in 1973. In this work, Ca-A zeolite was incorporated into poly(dimethylsiloxane) (PDMS). A considerably longer diffusion time lag than that for the net polymers was observed together with a minor effect on CO_2/CH_4 permselectivity. However,

this result did not attract too much interest until 1990s when several scientists attempted to utilize zeolites as fillers to improve the performance of polymer membranes. The strong electrostatic interactions between the zeolites and CO_2 molecules and the size-exclusion mechanism could enhance the performance of the unfilled polymers, such that the performance of resulting composite membrane can surpass the Robeson upper bound limit established in 1991. Judicious matching of appropriate polymers and zeolites with optimal filler loading is considered the key requirement for a successful composite membrane fabrication. Glassy polymers with a rigid structure, low permeability and high selectivity are generally considered as the most appropriate candidates for composite membrane fabrication owing to good mechanical stability and processability [69]. Some important work about CO_2-selective composite membranes are introduced below.

The Ozturk group incorporated different loadings of K-A, Na-A and Ca-A zeolites into poly(ether imide) (PEI) and polyimide (PI) polymers for potential application in biogas separation. They found that PEI benefits more from the loading of the zeolites, particularly for the 10% wt. Ca-A zeolite, whereas Na-A zeolite is more suitable for polyimide composite membranes [70]. Chung and co-workers demonstrated after ion-exchange LTA zeolite with Ag^+ ions, the zeolite can display a stronger size-sieving mechanism toward CO_2/CH_4 separation. It was also speculated that Ag cations residing zeolite can facilitate the transport of CO_2. As a result, the Ag-A/PES composite membranes could

show a higher CO_2 permeability and a CO_2/CH_4 selectivity than those of Na-A/PES composite membranes [71]. Kazemin et al. synthesized several void-free polyimide-based composite membranes with Na-X and Na-A zeolites at loadings of 10, 20, 30, and 40 wt%. They found that 30% Na-X zeolite/polyimide composite membranes yielded the best separation performance with the 96% increase in CO_2 permeability together with the 280% increase in CO_2/CH_4 selectivity from those of pure polymers [72]. Balkus Jr et al. used surfactant CTABr to synthesize mesoporous ZSM-5 zeolite. The as-synthesized mesoporous zeolite exhibited a pore size of 2.7 nm [73]. After incorporation into Matrimid® polymers, mesoporous ZSM-5/Matrimid® mixed matrix membranes exhibited a dramatic increase in both CO_2 permeability and CO_2/CH_4 selectivity. In particular, when the loading reached 20%, the CO_2/CH_4 selectivity increased by 100% as compared to that of unfilled polymer. The authors attributed this result to the penetration of the polymer chain into the mesopores of ZSM-5 zeolites, resulting in perfect filler/polymer adhesion which finally lead to a desirable CO_2/CH_4 separation performance.

In addition to dense composite films introduced thus far, the zeolite-based composite membrane in an asymmetric structure which is closer to real industrial application has attracted vast amount of attentions. Leo et al. investigated the effect of loading SAPO-34 and SAPO-44 zeolites into asymmetric polysulfone membranes [74, 75]. The addition of both SAPO-34 and SAPO-44 can increase the CO_2 permeance considerably. In particular,

when the loading was 10% wt, the CO_2 permeance of the composite is more than 10 times higher than that of the unfilled polymer membrane. However, when the loading exceeded a certain number, extensive interfacial voids could be observed, causing the CO_2/CH_4 selectivity to decrease significantly. The authors found that the optimal loadings for SAPO-34 and SAPO-44 were 10% wt and 5% wt, respectively. The authors could successfully make a series of high performance membranes in a flat sheet type [74-76]. However, for real industrial application, a hollow fibre structure is more favourable because of the higher packing density. Chung et al. have incorporated zeolite beta into polysulfone to form a composite skin layer on the top of Matrimid® layer[77]. These structure could be made by one step called dual-layer spinning. The overall performance of the hollow fibre membrane increased with increasing loading. The optimal biogas separation performance was recorded as approximately 4 GPU with a CO_2/CH_4 selectivity of 39 when the loading was 30 wt%.

A few notable work in zeolite-based mixed matrix membrane are summaized in table 2-3. Theoretical model such as Maxwell model often predicted much higher the performance of zeolite-based mixed matrix membrane than the value realizable in real measurement. This discrepancy may attributed to the poor interfacial morphology between the fillers and polymers. Additional details about filler-polymer interfacial morphology and the methods for improving the adhesion are provided in the following section.

Table 2-4 CO_2 separation performance of zeolite-based mixed matrix membranes

Pure Polymer	Zeolite	Loading (wt%)	CO_2 permeability (barrer)	CO_2/CH_4 Selectivity	CO_2/N_2 Selectivity	Ref
Pebax 1657	ZSM-5	10	192.7 (57%)	32.7(55%)	N.A.	[78]
PES	Ag-A	50	1.2 (-52%)	59.6 (90%)	N.A.	[71]
PES	Na-A	20	2.3 (-31%)	31.2 (3%)	25.6(-3%)	[79]
PC	Na-A	10	4.9(-44%)	44.1(87%)	N.A.	[80]
PSF	Silicalite-1	16	~9.4 (16%)	~23.1 (-7%)	~22.2 (-1%)	[81]
6FDA-ODA	FAU-EMT	25	17.6 (7%)	80.0 (50%)	N.A.	[82]
Matrimid®	ZSM-5	10	8.3 (13%)	67.2 (94%)	59.1(78%)	[73]
Poly(RTIL)	SAPO-34	10	72.0 (682%)	30.0 (-23%)	44.0 (38%)	[83]
PDMS	ZSM-5	66	11648.0 (233%)	4.4 (34%)	11.1 (0%)	[84]
Matrimid®	MFI	35	31.0 (308%)	39.0 (11%)	N.A.	[85]
PVAc	Na-A	50	4.3 (101%)	33.5 (48%)	N.A.	[86]
PVDF	Na-A	32	3.3 (194%)	N.A.	27.2 (-8%)	[87]
6FDA-DAM	Silicalite-1	8	712.0 (5%)	31.1 (45%)	N.A.	[88]
Matrimid®	Silicalite-1	8	18.7 (146%)	N.A.	39.8 (50%)	[89]
P84	13X	30	11.2 (96%)	25.1(280%)	49.8(217%)	[72]

[a] The ( ) in the CO_2 permeability, CO_2/CH_4 and CO_2/N_2 means the enhancement compared with pure polymers

2.1.6 Engineering the Interfacial Morphology of Zeolite-Based Composite Membrane

Improving the interfacial adhesion between the polymers and fillers is critical for fabricating high-performance composite membranes. Various

methods for improving the compatibility between the two phases have been developed to date.

Silane chemistry is one of the most widely used methods for improving the interfacial adhesion. In this technique, silane coupling agents act as a compatibilizer between the polymer and filler. One component of silane coupling agents is reactive groups, such as alkoxides, which can interact with the zeolite surface by a condensation reaction. The other component of the silane coupling agents can attach to the polymer surface by forming covalent bonds. Thus, the compatibilization process between the polymers and fillers is accomplished by such chemical linking via silane agents. This functionalization not only controls the filler-polymer adhesion but also adds amine groups to further increase the CO_2 solubility of membrane. On the other hand, silane treatment can cause unfavourable interfacial problems such as pore blockage of the fillers or rigidification of polymer chains. A major focus in this area has been to determine the optimal functionalization conditions, namely, the amount of silane agent, the reaction temperature and the type of solutions.

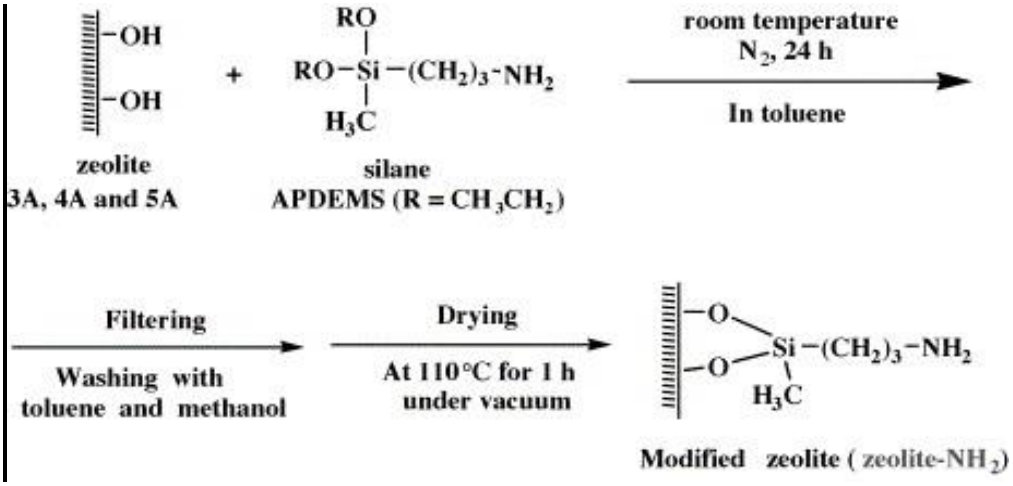

Figure 2- 3 The modification of zeoite surfaces with silane agents [90].

Kailaguine et al. used 3-aminopropylmethyldiethoxysilane (APMDES) to modify FAU/EMT zeolites which was subsequently loaded in the polyimide membranes [91]. They adjusted the grafting conditions, such as the grafting time and reaction temperature to have zeolite with a desired functionality. An ideal result was obtained at a temperature of 85 ℃ after 24 h (CO_2 permeability = 41.2 barrer, CO_2/CH_4 selectivity = 40.7). They also compared the influence of coupling agents (APTES, APMDES, and APDMES) and solutions (isopropanol and toluene) on CO_2/CH_4 separation performance of FAU/EMT zeolite/polyimide composite membranes [82].

Meanwhile, low-molecular-weight additives which can heal the voids between the polymers and fillers had been applied to composite membrane fabrication. For example, p-nitroaniline (pNA), 2-hydroxy5-methylaniline (HMA) and 2,4,6-triaminopyrimidine (TAP) were used as additives to improve

the interface void between glassy polymers and zeolites [80, 92, 93]. The addition of these additives effectively decreased the Tg of polymer matrix, such that the polymer behaved like more rubbery matrix during the membrane fabrication. This technique is considered easier to be implemented than silane chemistry. However, the resulting membrane often showed a dramatic reduction in CO_2 permeability. For example, the TAP/13X/PI composite membrane has only 8% of the permeability of the unfilled polymers. The effect of pNA and HMA is somewhat a trade-off between permeability and selectivity. An appropriate amount of these additives (4% HMA/20% SAPO/PES and 1% pNA/10% Na-A/polycarbonate) can tailor performance of unfilled polymers.

Another viable approach is to coat zeolites with high roughness inorganic structures (e.g., metal hydroxides and metal oxides). The metal hydroxide nanostructures formed on zeolite surfaces can increase the external surface area of zeolite considerably, enabling it to have more interfacial interactions with polymers. This method was first introduced by Shu et al. [94, 95], who applied the Grignard method to modify Na-A zeolites with $Mg(OH)_2$ nanowhiskers. The treated and untreated Na-A zeolites were then incorporated into poly(ether imide) and poly(vinyl acetate). The experimental results showed that both the permeability and selectivity were considerably improved as compared to pure polymeric membranes. These improvements were attributed to the better interaction with the polymers and the absence of voids. The unmodified zeolite-composite membrane permeation result suggested a sieve-in-cage

morphology of resulting membranes. Later, Bae et al. developed a more facile and environmentally friendly solvothermal method to deposit metal hydroxides, such as $Mg(OH)_2$ and $Ca(OH)_2$, on MFI zeolites [96]. The 35 wt% treated MFI zeolite/Matrimid® demonstrated a promising result: the CO_2 permeability increased from 7.6 to 31.0 barrer with a slight increase in CO_2/CH_4 selectivity. The relationship between deposition methods and the resulting composited membrane performance has been investigated by Lydon et al [97], who found that the ion-exchange functionalization methods yielded the best results for CO_2/CH_4 separation, with a CO_2 permeability of approximately 10 barrer and a CO_2/CH_4 selectivity of approximately 40. Although few studies have been performed on this topic, this method has great potential for overcoming the poor adhesion problems of composite membranes because it does not sacrifice the permeability of polymers in contrast to silane chemistry or additives.

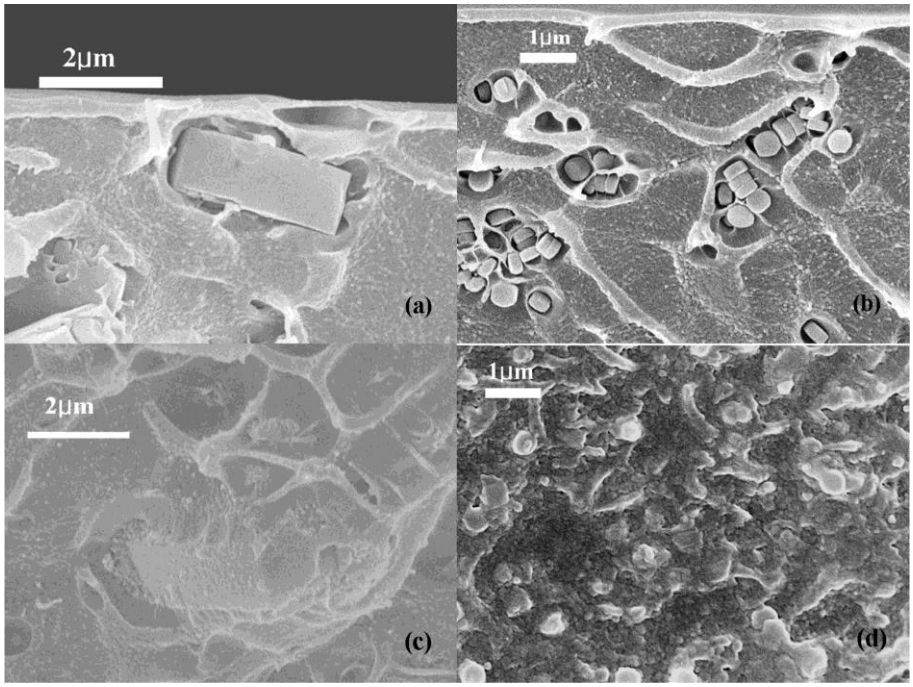

Figure 2-4 SEM images of cross sections of composite membranes composed of pure-silica-MFI and Ultem. (a) 5 μm untreated MFI, (b) 300 nm untreated MFI showing extensive voids between bare zeolites and polymers which can not be observed in (c) 5 μm solvothermally treated MFI, and (d) 300 nm solvothermally treated MFI [85].

The concept of polymerizable room-temperature ionic liquid/room-temperature ionic liquid (RTIL)/zeolite 3-component composite membranes was first introduced by Hudiono et al. [83]. The CO_2 permeability increased from 13.9 to 72 barrer with the addition of RTIL with a marginal decrease in CO_2/CH_4 selectivity. Another study compared the influence of RTIL-[emim][Tf_2N] loading and poly(RTIL) types [98]. The 24% vinyl-poly(RTIL)/36% RTIL/40% SAPO zeolites demonstrated the best results, with a CO_2 permeability of 527 barrer and a CO_2/CH_4 selectivity of 24.9.

Annealing can be considered a post-treatment for healing the voids between zeolites and polymers. This method can be useful when the heating temperature is above or close to the polymer glass transition temperature. Thus, selecting the appropriate polymer and heating temperature is critical for this treatment. Additional plasticizer can also be added to decrease the glass transition temperature if the polymer matrix has been fixed.

2.2 Metal-Organic Frameworks

2.2.1 Definition

Metal-organic frameworks (MOFs) are an emerging class of nanoporous material composed of metal ions coordinated with predesigned organic ligands. MOFs have several advantages over conventional porous materials, such as larger surface areas (~up to 7,000 m^2/g), lower densities (down to 0.19 g/cm^3), and higher porosity (greater than 50%). But the most fascinating character of MOF is the countless combinations of metal centers and organic linkers (e.g., imidazoles, pyridines, and carboxylates) that can result in an excellent tenability of chemical and physical properties. In addition, the unsaturated metal ions can be further functionalized with a post-synthetic route to improve targeted properties. Due to these advantages, active researches about MOF are currently in progress for potential applications in gas storage, gas separation and sensor technology [99-101].

2.2.2 Synthesis Methods

The developing new MOF structures had attracted widespread attention during the last 2 decades. Till now, more than 20000 types of MOFs had been synthesized from various methods [102]. Conventional synthesis methods, which are still mainstay for MOF synthesis, include slow-diffusion reaction, hydrothermal and solvothermal reactions. These methods usually requie a long synthesize time (~several days) and give large and nonuniform crystals with undesirable morphology [103]. In order to tackle these problems, alternative methods such as ultrasonic-assisted method, microwave-assisted method, mechanochemical method and electrochemical method had been developed.

The microwave-assisted method is based on the interaction between electromagnetic waves and electric field of the molecules. The intensive energy can be transferred from microwave (wavelength from 1 mm to 1m) to the target molecules via dipole rotation and ionic conductions. Thus the reaction is preferred to be carried out in a high dipole solution such as ionic liquid and water. External heat can accelerated this synthesis route and thereby the overall reaction is generally finished within several hours. A series of benchmark MOFs such as MOF-5, CuBTC, IRMOF-1, and MIL-53 had been successfully synthesized through this method [104-107]. Considerate reduction of synthesize time and crystal size had also been observed. In addition, this method is

believed to have better control of the crystal morphology which can finally lead to a better control of physical properties (mechanical and optical properties) of resultant MOF.

The ultrasonic-assisted method is considered as a facile and green synthesis route. This method can be operated with a sonication horn or sonication bath. In this technique, the powerful ultrasonic waves (20 KHz -10 MHz) can interact with liquid and formed bubbles. The bubbles will grow rapidly to their maximum sizes and then collapsed. This whole process can generate extremely high temperature (~5000K), pressure (~1000 bar) and heating and cooling rates (10^{10} K/s). Thus energy transferred from sound to the medium solution can initiate the reaction which is hardly triggered in hydrothermal or solvothermal methods. Ultrasonic-assisted method is believed to be more powerful than microwave-assisted method and have given even smaller crystal size and shorter reaction time (refer to the following table).

Table 2-5 MOF particle size from various synthesize methods.

MOF type	Conventional	Microwave-assisted	Ultrasonic-assisted	Ref
CuBTC	~20 μm	~10 μm	200-400 nm	[108]
MOF-5	500 μm	20-25 μm	N.A.	[109]
SIFSIX-3-Zn	~10 μm	N.A.	1 μm	[110]
ZIF-8	~250 μm	N.A.	700 nm	[111]
MIL-53-Al	~3-5μm	~1-3 μm	N.A.	[112]
MOF-177	0.5-1 mm	15-50 μm	5-20 μm	[113]
MIL-53-Fe	5-25 μm	1-2 μm	400-800 nm	[114]
MIL-88-A	250 nm	20 nm	100 nm	[115]
CPO-27-Co	~15 μm	5-7 μm	0.5-1 μm	[116]

[a] Most results are from the reference: Synthesis of metal-organic frameworks (MOFs) with microwave or ultrasound: Rapid reaction, phase-selectivity, and size reduction. Coordination Chemistry Reviews, 2015 – Elsevier [103].

[b] Conventional method including slow diffusion reaction, hydrothermal reaction and solvothermal reaction.

[c] ~ stands for roughly observed from SEM images.

Mechanochemical method refers to the chemical reaction which is triggered by mechanic energy such as grinding. The first MOF synthesized by mechanochemical method was reported in 2006 and then the method could be generalized to other popular MOFs such as HKUST-1, MOF-14, $Zn(EIm)_2$, and $Zn_2(BDC)_2(BPY)$ [117-120]. This method is favoured due to its convenience since it can be carried out in non-solvent media at room temperature. The short synthesize time is an additional advantage to this method. Unfortunately, till

now this method is only applicable to a limited number of MOFs and still need further development.

The electrochemical synthesis of MOF was first introduced by BASF in 2005 and then become an effective way to produce MOF thin film [121]. This method can also be used to synthesize powdered CuBDC particles by immersing Cu electrodes into organic solution which is full of the organic linkers. The specific electricity voltage leads to the continuous dissolution of Cu^{2+} ions and the reaction occurred in or near the electrodes. The final crystal morphology can also be controlled by tuning the electrolytes and voltage. Stirring is necessary in order to remove the as-synthesized MOF from the electrode and thus keep the reaction continues.

2.2.3 Ligand Design and Post-synthetic Treatment

Sava et.al, suggested that ideal MOF should: 1) contain large accessible pores, 2) be readily functionalized, 3) have sufficient chemical and thermal stability even in humid conditions [122]. The two key components of the MOFs are metal ions and organic linkers. A judicious selection of both components and applying property synthesis conditions that can give a high crystallinity with a minimum amount of defects are critical to meet these requirements.

For application in CO_2 separations which are the manor concerns in this thesis, the ligand should be chosen or synthesized to have additional characters

so that the resultant MOFs have a pore size ranged in between 0.33 nm and 0.38 nm as well as a good affinity for CO_2 molecules. For example, the ligand with imidazole groups is reported to be highly selective for CO_2 separation [123]. MOFs constructed with pyrazines such as SIFSIX-3-Zn and SIFSIX-3-Cu also showed impressive CO_2 sorption properties recently [124, 125]. Pachfule and his co-workers had developed a MOF with a mixed ligand of tetrazole and pyrimidine which had shown an extraordinary CO_2 sorption capacity [126].

The post-synthetic route is widely used to tailor the MOF's properties even further. Cohen and Wang had classified the post-synthetic modification into 6 categories which are: modification by non-covalent interaction, modification by coordinative interactions, modification by covalent bonds, Tandem reaction, protonation and Doping with metals [127]. Coordination of open metal sites and functionalizing organic ligands with specific functional groups to improve the CO_2 sorption property have been considered as an ideal way to modify the MOFs for applications in adsorptive and membrane separations.

2.2.4 Working Stability

As discussed in Chapter 2.2.1 and 2.2.3, MOFs have a strong potential to outperform conventional porous materials. However one of the main concerns for this material has been the stability in humid and harsh conditions.

Coordination bondings between metal centers and organic linkers can often be broken upon exposure to water or acid gas, resulting in decomposition

of whole MOF structure. If the thermal stability is too weak, the MOF can be collapsed prior to removing all guest molecules. Such unstable nature of MOF had restricted their applications in several industrial fields as adsorbents and membrane materials. One of highly stable MOFs is ZIF-8 which is reported in 2006 [128]. Since then, ZIF-8 which has a similar topology with sodalite zeolite had raised intensive attentions. The ZIF family usually have a higher stability than many other MOFs due to the strong chemical bonding between metal ions and imidazolate ligands which can remain their crystal structure even after soaking in the boiling water for several days. Zirconium based MOF such UIO-66 is also known to a robust framework that can withstand certain harsh conditions.

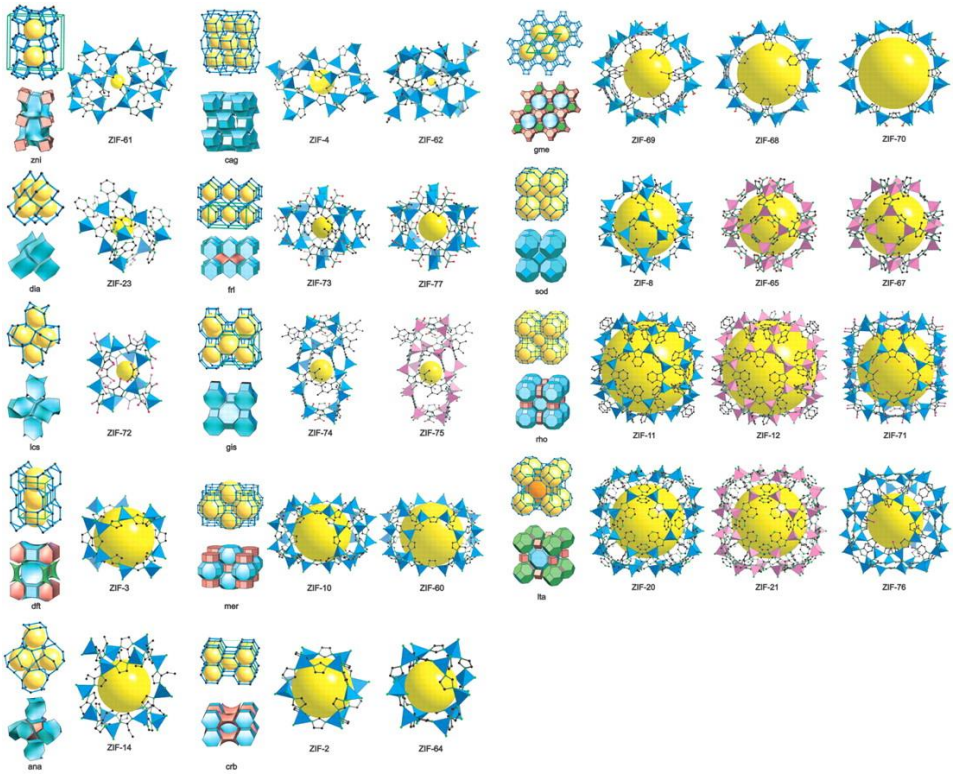

Figure 2-5 Representations of ZIF crystal structures [123].

In addition to example mentioned above, the urgent need for highly stable and high-performance MOFs had called out a series of attempts in the past few years. Long and his co-workers demonstrated that some alkylamine-functionalized MOF mmen-Mg_2(dobpdc) and Ni_2(dobpdc) can maintain or even increase CO_2 uptake in a moisture environment which is the most case for CO_2 capture applications [129]. This promising result can be explained by the presence of H_2O molecules improving the formation of ammonium carbamate, resulting in more efficient capture of CO_2 molecules by alkyl amines appended. Other promising fillers, such as SIFSIX-3-Zn, SIFSIX-3-Cu, ZnAtzOx, NBOFFIVE-1-Ni, ZJU-198 and Ni-4PyC, can retained the crystal structure in some humid conditions. However, the performance in realistic conditions such as in the presence of NO_2 and SO_x should be validated. [124, 125, 130-134].

2.2.5 MOFs as Membrane Filler

In contrast to hydrophilic inorganic crystals such as alumina silicate zeolites, the presence of organic ligands in MOFs can improve the compatibility with polymer matrix, such that the formation of defects can be restricted without any additional processing. MOF-based MMMs are an emerging research field compared with zeolite-based MMMs which was used be popular. Due to the advantages of MOFs which were mentioned in the previous sections,

vast amount of efforts have been devoted to designing high-performance MMMs made up with judiciously selected MOF-polymer pairs. Several important examples will be discussed below.

NH_2-MIL-53(Al) could be synthesized through several different routes, including a solvothermal method and microwave-assisted heating [107, 135]. This MOF is reported to have a weak dispersion force that can hold small pore windoes at low CO_2 partial pressures. However, the pores can be expanded at a relatively high pressure and reduce to its origin size at low pressure. This reversible movement which is so-called breathing effect is owing to the flexibility of the organic ligands[136]. Gascon and his co-workers incorporate this MOF into Matrimid® and studied the effect of several parameters, including MOF loading, operation temperature and trans-membrane pressure on the CO_2/CH_4 separation performance [137]. Rodrigue et al. studied the thermal stability of NH_2-MIL-53(Al)/6FDA-ODA MMMs. Their TGA curves indicated that MMM has good thermal stability; no significant weight loss was observed even above 400 ℃. A gas permeation test revealed that the membrane performance exceeded the Robeson upper bound established in 1991 with a high loading of MOF (30% and 32%). Mg_2(dobdc) is also considered a promising material for CO_2-selective MMM fabrication. The CO_2/N_2 selectivity (see Figure 1-2) and gravimetric CO_2 uptake of this compound are greater than those of many other porous materials, including Na-X zeolites [45].

Table 2-6 CO_2 separation performance of zeolite-based mixed matrix membranes

Pure Polymer	MOF	Loading	CO_2	CO_2/CH_4	CO_2/N_2	Ref
PSF	NH_2-MIL-53	25	~15 (60%)	~35.0	N.A.	[137]
6FDA-DAM	ZIF-90	15	720.0 (85%)	39.0	N.A.	[138]
6FDA-ODA	NH_2-MOF-199	25	26.6 (85%)	59.6	N.A.	[139]
Pebax 1657	ZIF-7	22	111.0 (54%)	30.0	97.0	[140]
SPEEK	IRMOF-1	30	20.2 (124%)	44.9	N.A.	[141]
6FDA-TMPDA	Mg_2(dobdc)	10	850.0 (31%)	N.A.	23 (64%)	[142]
Matrimid®	Cu-BPY-HFS	30	10.4 (42%)	27.5	33.4 (1%)	[143]
Matrimid®	ZIF-8	50	4.7 (-50%)	94.4	26.2	[73]
Matrimid®	Fe(BTC)	20	13.5 (59%)	33.8	N.A.	[144]
PSF	NH_2-MIL-125	30	40.0 (321%)	29.2	N.A.	[145]
Matrimid®	UiO-66	30	15.7 (166%)	35.8	N.A.	[146]
Matrimid®	MOF-5	30	20.2 (124%)	44.7 (7%)	38.8 (8%)	[147]
Matrimid®	$Cu_3(BTC)_2$	20	24.8 (226%)	37.8 (1%)	N.A.	[148]
PEI	MOF-5	25	5.4 (221%)	23.4	28.4	[149]
Poly(RTIL)	ZIF-8	18.9	198.8 (97%)	12.0 (-9%)	19.5 (-4%)	[150]

[a] The ( ) in the CO_2 permeability, CO_2/CH_4 and CO_2/N_2 means the enhancement compared with pure polymers

2.2.6 Crystal Size and Shape

Particles with processable particle size and well-defined morphology are desireable for composite membrane fabrication. In general, a small crystal size can beneficial as it could minimize the sedimentation problem in the dope

solution. Moreover, with the same filler loading, a small crystal can increase the interaction area with the polymer surface, and thus, it has better chance to be uniformly distributed in polymer matrix with good filler/polymer adhesion [110, 138, 142, 151]. At present, few studies have focused on the effect of filler shape on the composite performance. Recent studies have shown that a 2D nanosheet-type MOF can yield a more uniform distribution in the composite membrane and significantly promote the composite membrane performance even at low filler loadings [152-155].

Chapter 3

Solvothermal Deposition of Magnesium Oxides on LTA Zeolites for Composite Membrane Fabrication

3.1 Introduction

Recent study showed that 5A (or Ca-A) has a better CO_2 separation property than Na-A in terms of the uptake capacity, the binding energy, the adsorption kinetics and the selectivity over N_2 since Ca-A has larger pores and stronger binding sites for CO_2 than Na-A[45]. The results highlighted the potential of Ca-A for improving CO_2 separation property of especially polymeric membranes producible in a large industrial scale. However as mentioned in Chapter 2, the Ca-A zeolite also suffered poor compatibility with the polymer matrix. In order to overcome this problem various methods have been demonstrated to improve the polymer-zeolites interaction; one of which was chemical coupling of zeolites and polymer chain using a linker such as silane coupling agent which was described in Chapter 2[69, 82, 91, 156, 157]. However, this method is limited by its typical polymer-sieve pairs selectivity and often results in another non-ideal interfacial morphology such as the rigidified polymer chain which would adversely impact the permeability of gaseous molecules[29]. Furthermore, significant decrease in the pore volumes of the chemically treated zeolites which would impair its molecular sieving property have been reported. Meanwhile, enhancing surface roughness of zeolites crystals via the formation of nanostructures such as $Mg(OH)_2$ nanowhiskers could be a potential alternative to improve the polymer-zeolites interface through the adsorption and entanglement of polymer chains within the

nanostructures[94, 158]. Nonetheless, the conventional Grignard treatment method which have been commonly employed to synthesize the nanostructures entailed complex procedures and sensitive reactants[86, 97, 138]. To replace such complicated surface treatment, a simple solvothermal treatment to deposit $Mg(OH)_2$ nanostructures on surfaces of Silicalite-1 and Na-A (or 4A) zeolites has been developed [96, 159]. Composite membranes containing the surface treated zeolites demonstrated an improved gas separation performance as a result of an enhanced polymer-zeolites interfacial property. However, the solvothermal treatment is not environmentally benign since a large amount of ethylenediamine which is corrosive and difficult to be regenerated should be used in the reaction. As an alternative, a method to grow inorganic nanostructure on the surface of Na-A in an aqueous condition has been developed[97]. This reaction was induced by ion-exchange of extra-framework cation of aluminosilicate zeolites, such that $Mg(OH)_2$ nanostructure were formed only on the surface of zeolites. Defect-free membranes can be synthesized with the surface modified zeolites resulting enhanced CO_2/CH_4 selectivity of Matrimid® membrane.

In this Chapter, defect-free Matrimid®/Ca-A mixed-matrix membranes had been fabricated for enhanced CO_2/CH_4 separation. To improve polymer-zeolites adhesion, $Mg(OH)_2$ nanostructures were deposited on the surfaces of Ca-A. To this end, the previous ion-exchange based surface treatment has been systematically modified to give the best candidate for our composite membrane fabrication. A series of composite membranes was fabricated by varying the

loading of fillers and their CO_2/CH_4 binary mixture permeation properties were investigated.

3.2 Experimental Section

3.2.1 Materials

Sodium hydroxide (NaOH, ≥98%), sodium metasilicatepentahydrate (≥95%), sodium aluminate (technical grade), calcium nitrate ($Ca(NO_3)_2$, ≥99%), magnesium chloride ($MgCl_2$, ≥98%)and sodium nitrate ($NaNO_3$, ≥99%) were purchased from Sigma-Aldrich and used as received without further purification. Methanol (CH_3OH) and dichloromethane (DCM, ≥99.9%) were purchased from VWR. Commercial Matrimid® was used without further treatment.

3.2.2 Synthesis of Zeolites

Na-A or 4A zeolites were first synthesized based on the process as published by W.A. Khandayet et al [160]. 0.72g of NaOH was dissolved in 80 ml water. After the NaOH was completely dissolved, the solution was divided into two equal volumes. One half of the solution was further added with 8.258g sodium aluminate while the second half of the solution was mixed with 15.48g sodium metasilicate. Both solutions were mixed gently until they become clear. Subsequently, the sodium aluminate solution was transferred into

a round bottom flask. A gel will form as the silicate solution was being poured into the aluminate solution. The gel was stirred with egg shape stirrer for 4 h at 80 ℃. After the reaction, Na-A crystals were collected by filtration and washed with deionized water. Finally, the zeolite particles were dried in a convection oven.

3.2.3 Solvothermal Treatment

In this treatment, the magnesium source for the formation of $Mg(OH)_2$ nanostructure was supplied from inside the zeolite particles. To introduce Mg^{2+} ions to the substrates, 2 g of Na-A zeolite particles were dispersed into 100 mL of aqueous $MgCl_2$ solutions and the mixture was stirred for 1 h at room temperature. The amounts of Mg^{2+} ions in zeolites were varied by using three different $MgCl_2$ solutions of 0.1, 0.2, and 0.4 M, for the ion-exchange. Subsequently, 0.1 g of the hydrated Mg-containing zeolites which were not yet been activated, were added into 10 ml of 0.1 M $NaNO_3$ solutions of which pH were adjusted to 9.5 or 11 with a dilute aqueous NaOH solution [161-163]. Then, the mixture were transferred into a Teflon-lined autoclave and heated at 160 °C for 12 h. During this hydrothermal treatment, ion-exchange happened between Mg^{2+} ions introduced into the zeolites and Na^{+} ions in basic solution outside. As the free Mg^{2+} ions diffused out through micropores of the zeolites, $Mg(OH)_2$ nanostructures were formed at the zeolites surfaces by the reaction between the free Mg^{2+} ions and hydroxyl ions in bulk solution. After the reaction, the zeolites crystals were collected by filtration and washed with deionized water. Subsequently, an ion-exchange process was carried out at 60 °C for 20 h with 20 mL of 0.5M calcium nitrate to replace residual

extra-framework cations in zeolites with Ca^{2+}. This ion-exchange process was repeated twice for the same substrate collected via filtration. Bare Ca-A samples were also prepared by the ion-exchange of untreated Na-A with $Ca(NO_3)_2$. In summary, four different surface-treated (ST) Ca-A zeolites were prepared by a systematic modification of reaction conditions which are described in Table 3-1.

Table 3-1 Reaction conditions for surface treatment of zeolites

Samples	Mg loading		Hydrothermal treatment[(a)]	
	$Mg(Cl)_2$ concentration	Stirring Duration (h)	$NaNO_3$ concentration	pH
ST1-Ca-A	0.1 M	1	0.1 M	9.5
ST2-Ca-A	0.2 M	1	0.1 M	9.5
ST3-Ca-A	0.4 M	1	0.1 M	9.5
ST4-Ca-A	0.1 M	1	0.1 M	11

(a) conducted at 160 ^{o}C for 12h

3.2.4 Membrane Fabrication

A solution casting technique was employed to prepare dense films of mixed-matrix membranes. 0.2 g zeolite particles (bare or surface treated Ca-A, hydrated) were dispersed in 2.5 g DCM in a 20 ml glass vial followed by ultrasonication for 5 minutes. Subsequently, 0.8 g of polymer (Matrimid®) was added to the suspension following which the mixture was stirred overnight with an egg-shaped stirrer to obtain a homogenous solution. Subsequently, the solution was poured on a glass plate for casting of a nascent film using a "doctor's blade", in a glove bag saturated with DCM vapor. The membrane film on the glass plate was left to complete evaporation in the glove bag for 1 h before annealed at 230 °C for 1 day in a vacuum oven.

3.2.5 Characterization

The powder X-ray diffraction (XRD) of zeolite was characterized using a Bruker D2 phase diffractometer with Cu Kα radiation. N_2 adsorption-desorption analysis at 77K were carried out using AutoSorb-1 Quantachrome Instrument to determine the textural properties of zeolites such as specific surface area, pore size and pore volume. Differential scanning calorimetry (DSC) was employed to observe physical transformation of zeolite materials as a function of temperature using the Pyris Diamond Thermogravimetric Analysis. Temperature range was 50-500 °C, with an increase rate of 10 °C/min and air as the purging gas. Elemental composition of the zeolite materials were analyzed using an energy dispersive X-ray spectrometer (EDX) attached to the SEM (FESEM, JSM-7600F). The gas uptake properties of zeolites and membranes were measured by a high-pressure gas adsorption analyzer (Quantachrome, i-Sorp HP-1). The activation of the zeolites and membranes were carried out at 200℃ for 24 h under high vacuum whereby the samples were placed into a stainless steel chamber and heated by a heating bag. Following this, pure component CO_2 and CH_4 isotherms were obtained in a pressure range of 0 to 1 bar at 40 ℃. The morphology of the zeolites and cross-section of the membranes were observed with a field emission scanning electron microscopy (FESEM, JSM-7600F). The membranes were first cryogenically fractured in liquid nitrogen and coated with platinum prior to FESEM imaging. In the case of zeolites, the image was taken without any platinum coating to preserve the

inorganic morphological structure. Mechanical properties of membranes were also compared with and without fillers using Instron Tester 5543 Model System.

3.2.6 Gas Adsorption Analysis

To quantify the gas uptake properties, all gas adsorption isotherm data were fit with the following Langmuir model.

$$q = \frac{q_{sat} bp}{1 + bp} \quad (1)$$

Here q is the quantity adsorbed, q_{sat} represents the saturation loading of the adsorbent, b is the Langmuir parameter, and p is the partial pressure of gas. As the measurement of the saturation capacity of CH_4 at 40 ℃ is difficult, it was assumed that all adsorption sites for CO_2 in zeolites are accessible to CH_4. Thus, the saturation capacities for CO_2 and CH_4 were assumed to be equal in this work.

Then, using the fitting parameters in equation 1, Henry's coefficients (k_H) were estimated as follow,

$$\lim_{P \to 0} q = k_H p = q_{sat} bp$$
$$k_H = q_{sat} b \quad (2)$$

In this work, the sorption selectivity of CO_2 over CH_4 was defined as the ratio of Henry's coefficients for CO_2 over CH_4.

$$\text{selectivity} = k_{H,CO2} / k_{H,CH4} \quad (3)$$

3.2.7 Permeation Tests

Gas permeation tests were carried out using the method descried in our previous work[110]. The testing gas was CO_2/CH_4 (50/50) binary mixture supplied from Air Liquide. The membrane sample was first mounted onto the sample cell and then vacuum pumped to remove all the residual gases. Then, the upper chamber of the cell was pressurized with the test gas at 1 bar. The permeate gas in the downstream was swept by He and the composition was subsequently analyzed with a gas chromatograph (GC). The permeability of individual component was determined using the flow rate of sweeping gas (He), the composition of permeated gas measured by GC, and the properties of membrane such as effective exposed area and thickness. The operating temperature throughout the whole measurement process was fixed at 40°C. Gas permeation test was repeated for another 2 times using 2 other samples to determine reproducibility of the experiment.

3.3 Results and Discussion

3.3.1 Zeolite Synthesis and Surface Treatment

Figure 3-1 shows an SEM image of bare 5A crystals synthesized by a hydrothermal method. At given reaction conditions, cubic-shaped crystals with smooth surface were successfully synthesized.

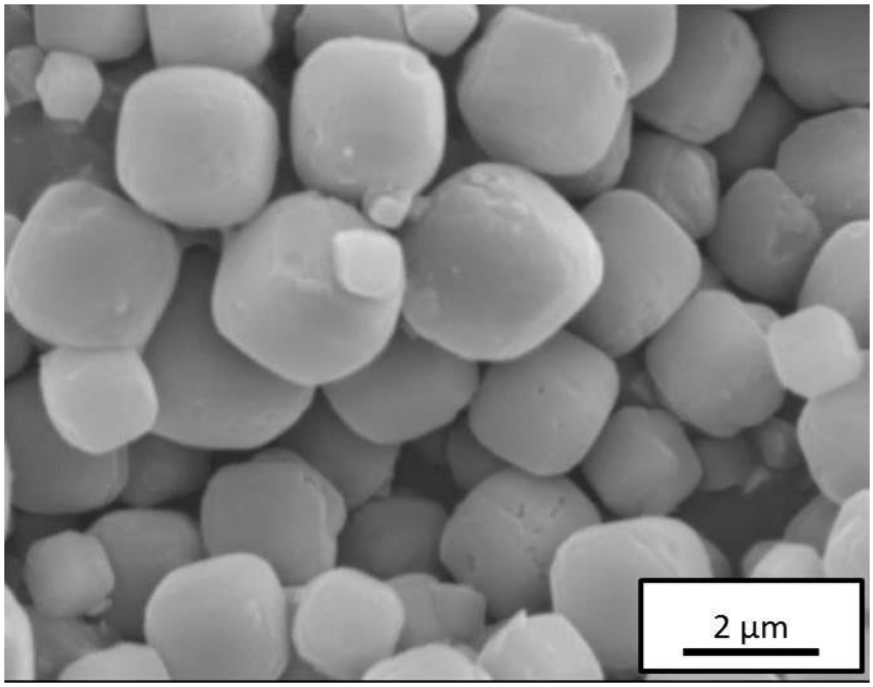

Figure 3-1 FESEM image of bare LTA zeolite particles prior to surface treatment (before ion exchange with $MgCl_2$).

Following the surface treatment, the surfaces of LTA zeolite was transformed into highly roughened surface owing to the formation of $Mg(OH)_2$ nanostructures; as clearly depicted in the FESEM images in Figure 3-2. A vivid morphological evolution of particles at different reaction conditions, in particular Mg loading in the substrate(LTA) and reaction pH, was observed. When the amount Mg loaded in the substrate is lowest, the surfaces of zeolites were coated with fine structure of $Mg(OH)_2$ as shown in Figure 3-2a. In this condition, the growth of $Mg(OH)_2$ was limited by the supply of Mg from the inside of substrate. However, as the amount of Mg loading in the substrate was increased by increasing concentration of aqueous $MgCl_2$ solution from 0.1 M to 0.2 M and 0.4 M, the size of $Mg(OH)_2$ structures formed on the surface of

zeolites increased which could enhance its overall surface roughness and surface area (Figure 3-2b and c). Meanwhile, when pH increased from 9.5 to 11.0 at the same Mg loading, overall morphology was evolved into a sphere enwrapped with $Mg(OH)_2$ nanostructures (Figure 3-2d). It may imply that a core-shell-like system where the ST4-5A (which was the core) was entirely enwrapped with a thick $Mg(OH)_2$ shell could have resulted in the spherical shape formation of ST4-5A. In general, this observation revealed that the final products could be tuned via adjustment of pH and Mg loading to attain different desirable properties for different application need and efficiency.

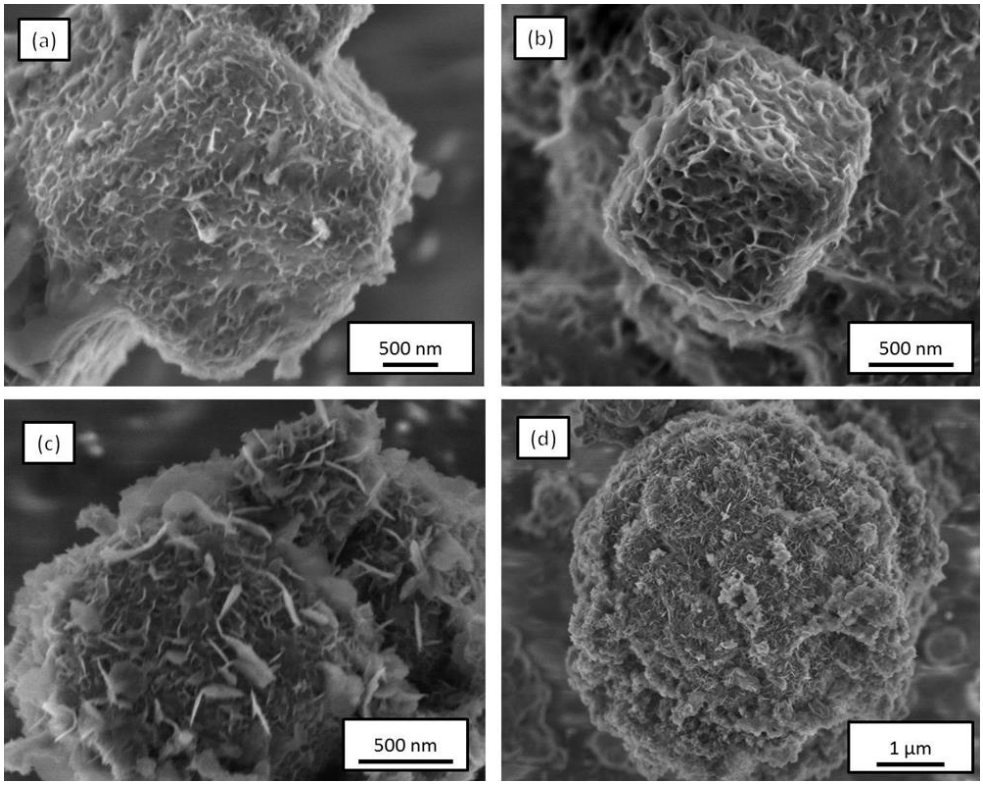

Figure 3-2 FESEM images of surface treated 5A zeolites (ST-5A) with different concentration of Mg ions in substrates and reaction pH: (a) 0.1 mol/L Mg, pH = 9.5, (b) 0.2 mol/L Mg, pH = 9.5, (c) 0.4 mol/L Mg, pH = 9.5, (d) 0.1 mol/L Mg, pH = 11.0 showing higher pH and Mg concentration will lead to a rougher external surface.

Figure 3-3 exhibits the XRD figures of bare 5A and surface modified 5A zeolites which were synthesized under various Mg loadings in the substrate and pHs of reaction medium. Both the untreated and treated 5A exhibited major peaks of LTA zeolites crystals [164] thus indicating that the crystallinity of zeolites was retained even after the surface treatments at 160 °C under basic conditions and not affected by different Mg loading and pH.

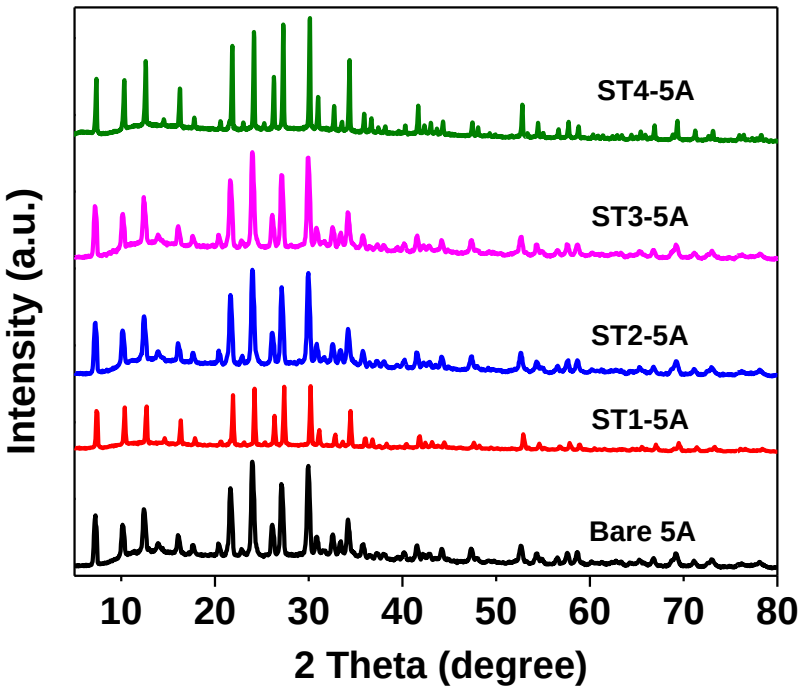

Figure 3-3 Powder X-ray diffraction patterns of bare 5A and ST-5A which were synthesized under different reaction conditions.

Interestingly, $Mg(OH)_2$ peaks were not prominent for all ST-5A samples which were synthesized at all the four different reaction conditions. The low

loading of $Mg(OH)_2$ and/or the possibly amorphous or lower degree of $Mg(OH)_2$ crystallinity relative to the 5A zeolites component could have limited the detection of $Mg(OH)_2$ via XRD. Nevertheless, the presence of Mg was evidenced through EDX spectrum of the surface modified 5A (Figure 3-4).

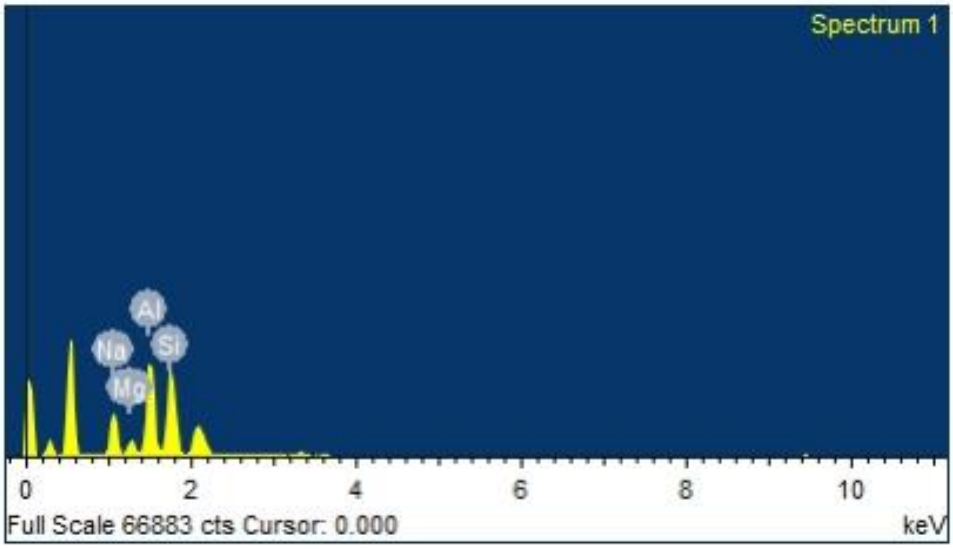

Figure 3-4 EDX spectrum of the surface modified LTA.

In addition, analysis using DSC further verified the successful formation on $Mg(OH)_2$ on LTA surfaces where a characteristic peak for transition of $Mg(OH)_2$ to MgO was observed at ~ 380 ^oC (as shown in Figure 3-5). With the observation of the peak in 380 degree, we can surely guarantee that $Mg(OH)_2$ had been formed successfully.

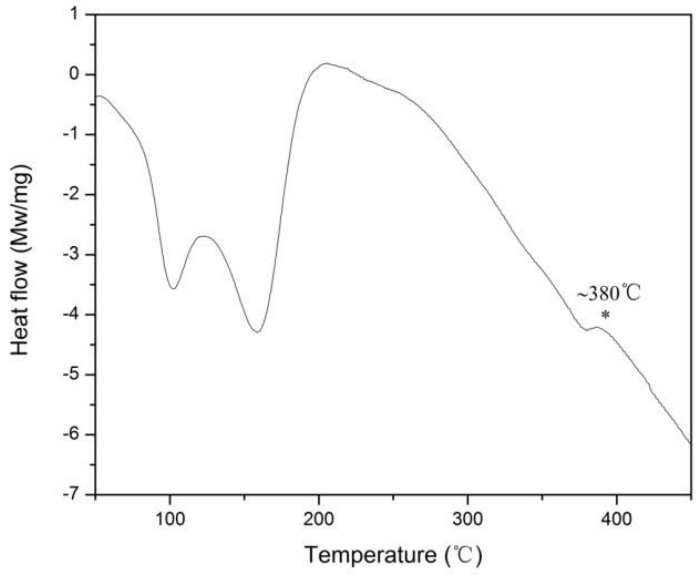

Figure 3-5 DSC Curve of the surface modified LTA zeolite.

Meanwhile, elemental analysis via EDX as summarized in Table 4-2 of the Supporting Information showed that the Mg/Na ratio increased with increasing concentration of Mg used. This implied that Na has been successfully exchanged by Mg. In essence, observation from XRD, DSC and EDX consistently evidenced the successful surface modification of LTA with $Mg(OH)_2$ without changing the crystal structure of LTA.

Sample name	Mg content (atomic %)	Na content (atomic %)	Mg/Na ratio	Degree of ion exchange
0.1M Mg-$NaNO_3$-Zeolite	5.08	13.05	0.39	44%
0.2M Mg-$NaNO_3$-Zeolite	6.28	12.78	0.49	50%
0.4M Mg-$NaNO_3$-Zeolite	8.79	13.80	0.64	56%

Table 3-2 EDX elemental analysis of Mg-containing zeolite (after ion-exchange with $MgCl_2$)

Figure 3-6 depicted the N_2 physisorption isotherms for bare 5A and ST-5A which evidenced the microporosity nature of 5A before and after its surface treatment. As concluded in Table 3-3, the reduction of micropore volume and BET specific surface area were marginal for ST1-5A which was treated at pH 9.5 using the substrate with the lowest Mg loading. Such small losses may be due to the increase in mass of sample by the formation of $Mg(OH)_2$ whiskers which are not porous. The pore channel and window of LTA seemed to be intact in this reaction condition. Nevertheless, increased loading of Mg in the substrate had considerably reduced the porosity of resulting surface-treated zeolites due to the growing coverage of the zeolites surface by $Mg(OH)_2$ and this was consistent with the FESEM images from Figure 3-2b-c. The microporosity of surface-treated zeolites was significantly changed by the pH of reaction medium. Even though both ST1-5A and ST4-5A were conducted with the same substrate containing the lowest Mg content, the micropore volume of ST4-5A treated at pH 11 were significantly lower than that of ST1-5A. The microporosity could be reduced at the expense of higher pH when the external layers of zeolites were partially dissolved under highly alkaline condition, leading to a morphological change as shown in Figure 3-2d. External surface area seemed to have increased at higher Mg loading and pH given the surface

roughness from the $Mg(OH)_2$ nanostructuresas corroborated by the FESEM images in Figure 3-2. In essence, sufficient micropore volume is necessary to ensure molecular diffusivity of gaseous products during gas separation, thus must not be overly compromised for filler enhancement. Thus, ST1-5A was chosen for the gas adsorption study and mixed-matrix membrane fabrications.

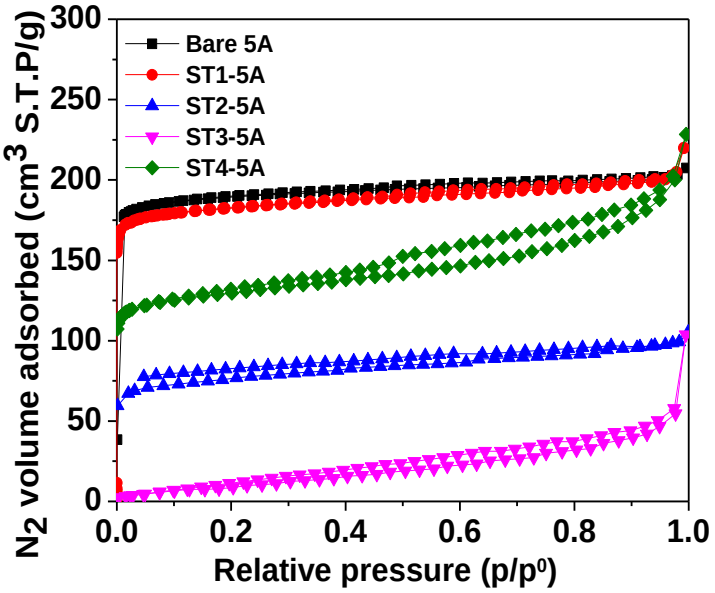

Figure 3-6 N_2 physisorption isotherms of bare 5A and surface treated 5A zeolites which were synthesized under different reaction conditions.

Table 3-3 Properties of bare and surface treated 5A zeolites calculated from N_2 physisoprtion at 77 K.

Zeolites	BET surface area (m^2/g)	External surface area[(a)] (m^2/g)	Micropore volume[(a)] (cm^3/g)
Bare 5A	830	20	0.29
ST1-5A	742	33	0.27
ST2-5A	273	35	0.11
ST3-5A	55	55	0
ST4-5A	510	80	0.17

(a) calculated by the t-plot method.

3.3.2 Gas Adsorption Properties of Zeolites

Figure 3-7 shows CO_2 and CH_4 uptake properties of bare 5A and ST1-5A zeolites measured at 40 ℃. Both zeolites selectively adsorb large quantity of CO_2 over CH_4 at the pressure range tested. For further analysis, all isotherms were fit with Langmuir model which successfully described all adsorption isotherms with the R^2 values greater than 0.99. All parameters used for curve fittings, Henry's coefficients, and sorption selectivity are concluded in Table 3-4. The surface modifications of 5A zeolites caused marginal decrease in both CO_2 adsorption capacity and CO_2/CH_4 selectivity compared to those of bare 5A zeolites, as $Mg(OH)_2$ nanostructures that couldn't contribute to CO_2 uptake were added to the zeolites. Nevertheless, the ST1-5A still retains a good potential to improve CO_2 separation property of certain polymeric membranes.

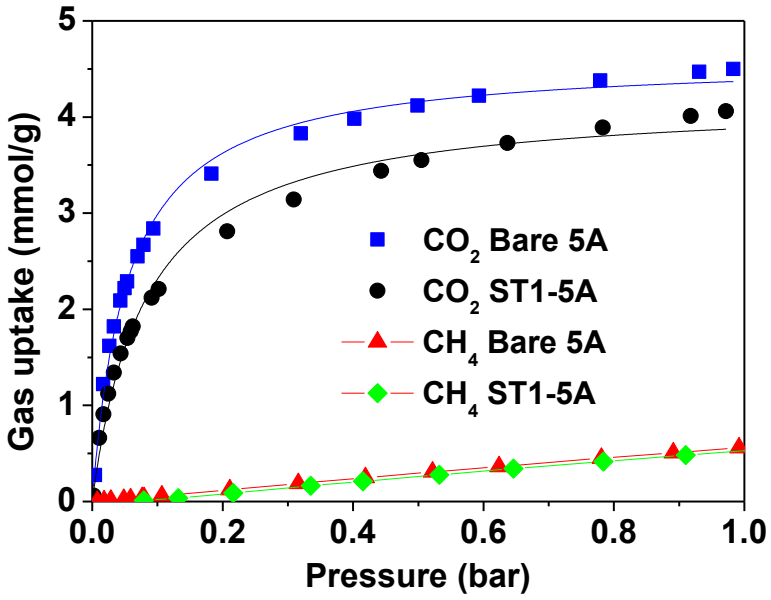

Figure 3-7 Pure components CO_2 and CH_4 adsorption isotherms of bare 5A and ST1-5A measured at 40 ℃, along with corresponding Langmuir fits (solid lines).

Table 3-4 Fitting parameters for Langmuir model, Henry's coefficients, and sorption selectivities.

Zeolites	**CO_2**		**CH_4**		**CO_2/CH_4 selectivity**	**R square**
	q_{sat} (mmol/g)	B (bar $^{-1}$)	q_{sat} (mmol/g)	B (bar $^{-1}$)		
Bare 5A	4.61	18.4	4.61	0.138	130	0.993
ST1-5A	4.20	12.3	4.20	0.138	89	0.981

3.3.3 Fabrications and Characterization of Composite Membranes

Figure 3-8 shows the cross-section morphology of mixed-matrix membranes made up from Matrimid®and zeolites (bare 5A and surface treated 5A). The appearance of undesirable common non-ideal polymer-zeolites interfacial morphology in particular the 'sieve-in-a-cage' as depictedin Figure 3-8a and b was seen alleviated in the mixed-matrix membrane made up of Matrimid® with ST1-5A, (Figure 3-8c and d). This was highly likely endowed by the surface roughness and enhanced surface area of the ST1-5A which favoured physical interaction thus facilitating ST1-5A's adhesion with the polymer chain via the $Mg(OH)_2$ nanostructures. Furthermore, owing to such improved interaction between zeolites and polymer, the surface treated zeolites particles were distributed uniform in the polymer matrix, which is highly desirable for an improved gas separation performance. Our results are remarkable because unlike the conventional research where pore volume was usually sacrificed to improve polymer-filler interfacial morphology, the synthesis herein was successfully optimized to minimize pore volume reduction of zeolites which facilitate gaseous diffusion while achieving better polymer-filler adhesion.

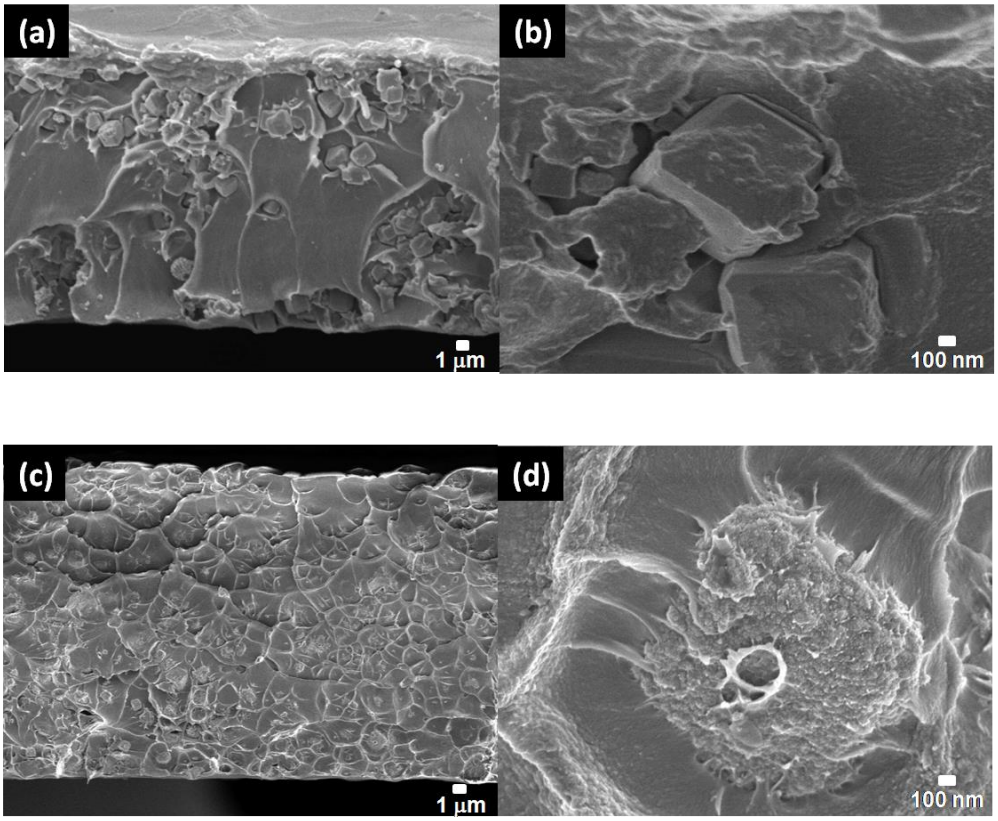

Figure 3-8 Cross section FESEM images of mixed-matrix membranes to show the enhanced polymer-zeolites interfacial morphology: (a) low magnification Matrimid®/bare 5A, (b) high magnification Matrimid®/bare 5A, (c) low magnification Matrimid®/ST1-5A, and (d) high magnification Matrimid®/ ST1-5A.

To further investigate polymer/filler adhesion property, the mechanical properties of mixed-matrix membranes were measured. Mixed-matrix membrane consisting of ST-5A exhibited greater mechanical strength than that made up from bare 5A, as shown in Table 3-5. Stress-strain curves for mixed-matrix membranes were included in Figure 3-9.

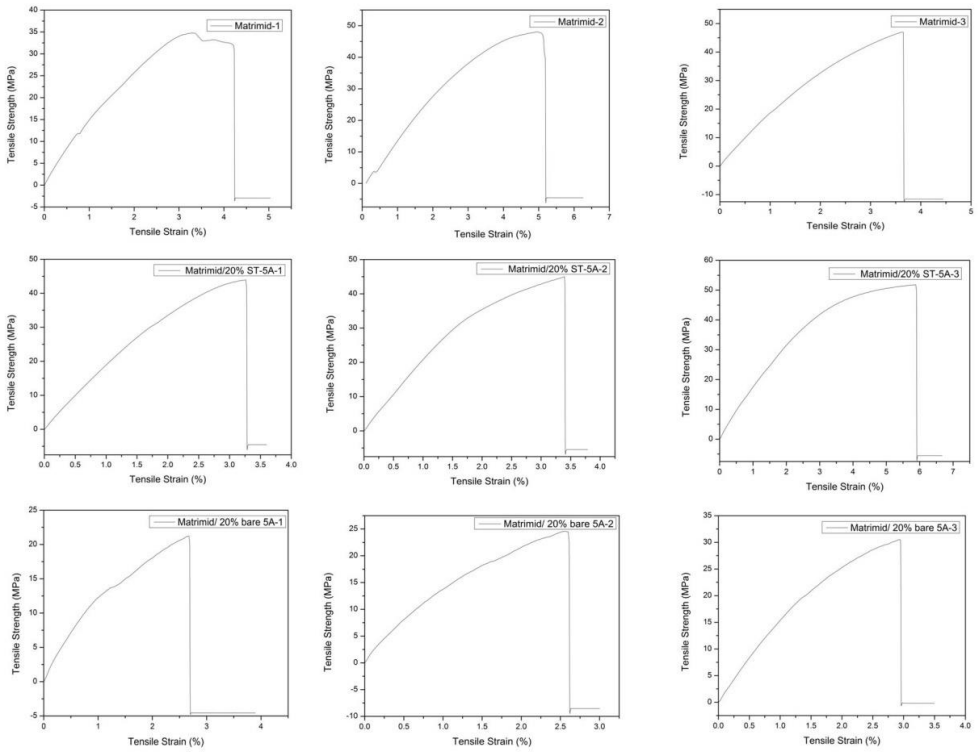

Figure 3-9 Stress-strain curves for Matrimid® membrane, Matrimid®-bare 5A mixed-matrix membranes, Matrimid®-surface treated 5A mixed-matrix membranes.

From Table 3-5 and Figure 3-9, it is noticed that the mechanical strength of Matrimid®-surface treated 5A composite membranes had outperformed pure polymers membranes and Matrimid® with bare zeolites a lot. This was possibly rendered by the $Mg(OH)_2$ flakes on zeolites 5A which have facilitated a stronger and more effective adhesion between Matrimid® and ST1-5A. On the other hand, with bare 5A, the voids at the polymer-zeolites interface could be the weak links which has led to the significantly lower tensile strength than even pure Matrimid® membrane. It is noteworthy that an enhanced mechanical strength observed for mixed-matrix membrane with ST1-5A is a highly

desirable property for production and application of membranes in industrial scales.

Table 3-5 Mechanical strength of mixed-matrix membranes.

Membranes	Tensile strength (MPa)	Modulus (MPa)
Matrimid®	42.7 ± 6.7	1711 ± 134
Matrimid®/20wt% Bare 5A	24.8 ± 4.8	1686 ± 416
Matrimid®/20wt% ST1-5A	45.2 ± 6.2	1995 ± 328

3.3.4 CO_2 Adsorption of Composite Membranes

Figure 3-10 shows the CO_2 adsorptions inpure polymer and mixed-matrix membrane containing ST1-5A. As expected, the amount of CO_2 uptake in mixed-matrix membrane was significantly higherthan that of pure polymer membrane owing to the addition of zeolites 5A that can capture a large quantity of CO_2 as illustrated in Figure 3-7. However, the CO_2 uptake in mixed-matrix membrane was observed to be slightly lower than its respective theoretical prediction calculated assuming the pores in all of the zeolites crystals in the membrane are available for CO_2 adsorption. The partial blockage of zeolites pores by the polymer chain following a strong polymer-zeolites binding might possibly limit the access of CO_2 to some of zeolites pores. Nevertheless, majority of zeolites pores are still available for CO_2 uptake and transport as the adsorption isotherm for the mixed-matrix membranes is closer to the theoretical calculation than the CO_2 isotherm of pure polymer membrane. Such enhanced CO_2 uptake property along with a good zeolites/polymer adhesion can render a high CO_2 separation efficiency to mixed-matrix membranes comprising ST1-5A.

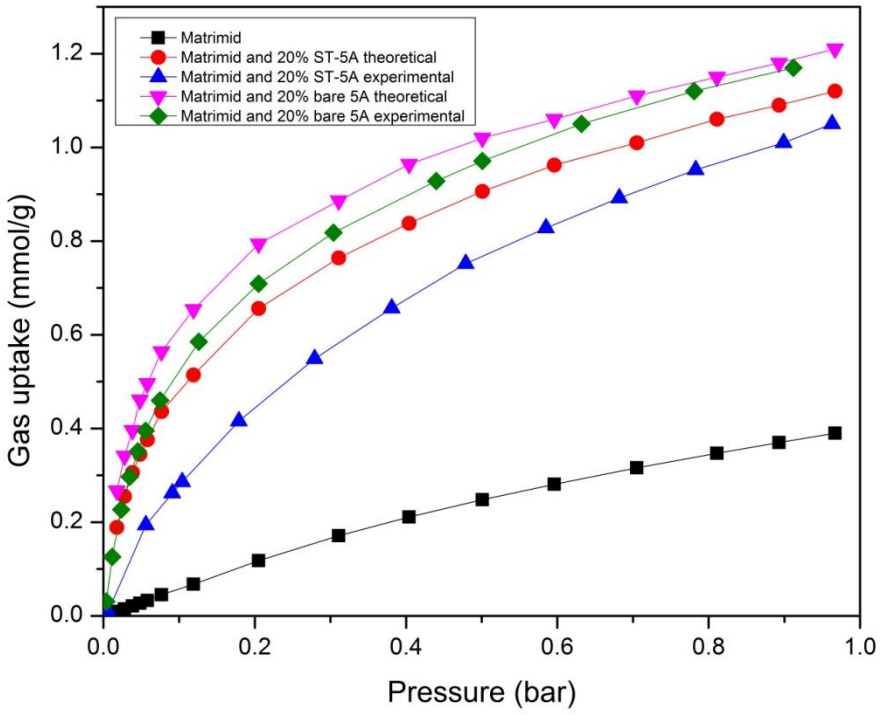

]

Figure 3-10 Pure component CO_2 adsorption by Matrimid®/20 wt% bare 5A and Matrimid®/20 wt% ST1-5A mixed-matrix membrane measured at 40 ℃.

3.3.5 Gas Permeation Properties of Composite Membranes

Table 3-6 shows CO_2/CH_4 binary mixture permeation properties of mixed-matrix membranes. The CO_2 permeabilities were significantly improved in mixed-matrix membranes containing ST1-5A capable of rapid transport of CO_2 molecules. For example, the CO_2 permeability of Matrimid®/20 wt% ST1-5A membrane was observed to be 22.4, which is 120 % greater than that of pure Matrimid® membrane. Such dramatic improvement of CO_2 permeability is highly attractive for industrial applications of Matrimid® membrane which is suffering from a low permeability in spite of its many advantages as a

membrane material such as inexpensive cost, good mechanical property, and excellent gas selectivity.

The selectivity of mixed-matrix membrane also gradually increased with increasing loading of ST1-5A in the polymer matrix owing to the selective uptake or transport of CO_2 through the pores of 5A. The CO_2/CH_4 selectivity of Matrimid®/20 wt% ST1-5A membrane reached 36.4, which is approximately 10 % higher than the selectivity of pure polymer. On the other hand, selectivity of mixed-matrix membrane seems to decrease with increasing bare 5A likely due to the increased presence of voids at the polymer-zeolites interface which promoted more non-selective bypass of CO_2 molecules. Such decreased selectivity observed for bare 5A-containing membranes indicates that our surface treatment is highly effective in improving polymer/zeolites adhesion thus minimizing the 'sieve-in-a-cage' morphology formation.

Table 3-6 Mixed-gas permeation properties of membranes at 40 °C and 1 bar total feed pressure with a 1:1 CO_2/CH_4 mixture.

Membranes	**CO_2 permeability (barrers)**	**CO_2/CH_4 selectivity**
Matrimid®	10.2 ±0.5	33.6 ±2.0
Matrimid®/10wt% bare 5A	26.7 ±3.0	31.3 ±2.0
Matrimid®/20wt% bare 5A	31.0 ±5.0	30.8 ±3.0
Matrimid®/10wt% ST1- 5A	19.6 ±2.0	35.4 ±2.0
Matrimid®/20wt% ST1- 5A	22.4 ±3.0	36.4 ±2.0

Since permeability depends on both solubility and diffusivity, the benefits of surface-modified zeolites were further analyzed by observing its effect on

solubility and diffusivity of the resulting mixed-matrix membranes. The solubility of CO_2 at 0.5 bar, which was the upstream CO_2 partial pressure for permeation testing, was obtained from CO_2 adsorption isotherms in Fig 3-10. Then, the diffusivity of CO_2 was estimated from the solubility and the permeability of membrane. The detailed procedure for calculations of solubility and diffusivity is described in our previous work [30]. As shown in Table 3-7, incorporating 20% surface modified zeolite could increase the CO_2 solubility of polymer by more than 150%. While marginal reduction in diffusivity of CO_2 was inevitable due to the strong binding of CO_2 onto zeolite pore surfaces, the overall improvement of CO_2 permeability for mixed-matrix membrane was significant owing to CO_2 solubility improvement.

Table 3-7 CO_2 solubility, diffusivity and permeability data for Matrimid® and Matrimid®/20wt% ST1-5A.

Membranes	**CO_2 permeability ($mol \times m/m^2 \times s \times bar$)**	**CO_2 solubility ($mol/m^3 \times bar$)**	**CO_2 diffusivity (m^2/s)**
Matrimid®	3.4×10^{-10}	340	10^{-12}
Matrimid®/20wt% ST1- 5A	7.5×10^{-10}	870	8.6×10^{-13}

1 barrer = $10^{-10}(mol \times m/m^2 \times s \times bar)$

3.4 Conclusions

5A zeolites with enhanced surface roughness were successfully prepared via a facile treatment in an aqueous phase through which nanostructures of $Mg(OH)_2$ were grown on the zeolites' surfaces. The systematic modification of

reaction conditions resulted in an optimized 5A zeolites (ST1-5A) for the fabrication of CO_2-selective composite membranes. The mixed-matrix membrane consisted of Matrimid® and ST1-5A possessed improved polymer-zeolites interfacial morphology given by the enhanced physical interaction between polymer and zeolites through the $Mg(OH)_2$ nanostructures. What is more, mixed-matrix membranes exhibited a greater mechanical strength thus stability, due to the improved polymer-zeolite interaction that has also led to a significant enhancement in CO_2 permeability (ca. 120%) along with a modest increase in CO_2/CH_4 selectivity compared to those of pure polymer membrane. This study is remarkable as it brought about an advancement througha simplified synthesis of surface-enhanced new filler candidate for use in fabricating mixed-matrix membranes witha more efficient CO_2 separation.

3.5 Declaration

The work presented in this chapter has been published in Microporous and Mesoporous Materials.

Heqing Gong[1], Siew Siang Lee[1], Tae-Hyun Bae*, Mixed-matrix membranes containing inorganically surface-modified 5A zeolite for enhanced CO_2/CH_4 separation, *Microporous and Mesoporous Materials*, **2017,** *237,* 82-89

[1]These authors contributed equally to this work.

Chapter 4

Amine Grafting LTA Zeolites for Composite Membrane Fabrication

4.1 Introduction

Zeolites possessing a sharp molecular sieving property owing to their rigid pore structures are currently produced in large scales with reasonable costs and used in many industrial processes. In particular, LTA(Linde Type A) zeolites is a promising filler for mixed-matrix membrane used in CO_2 capture due to their high CO_2 uptake as well as chemical and thermal stability[45]. Nevertheless, the preparation of high-quality mixed-matrix membranes containing zeolites has been greatly challenged by the formation of non-ideal polymer-zeolites interfaces. One of the main concerns is the sieve-in-a-cage (voids) morphology[29, 94, 95, 156] which resulted from the poor adhesion between organic polymer and inorganic zeolites crystals thus yielding poor gas separation performance due to non-selective bypass of gas molecules through voids[156]. Hence, the control of polymer-zeolites interface is essential to attaining a successful fabrication of composite membranes with good gas separation performance.

As mentioned in Chapter 2, the application of the amine grafting technique can be an effective way to improve the interfacial adhesion between the polymers and zeolites. Studies for this field should be applied to judicious select the right pair of silane coupling agents and zeolites. Furthermore, optimal

the details of amine grafting process such as amine loading, reaction temperature and purification condition.

In this work, hierarchical Ca-A zeolites were synthesized with mesoporous domain decorated with alkylamines for capturing a large amount of CO_2 even at low CO_2 partial pressure. Owing to the contributions of both alkylamine groups grafted on the mesopore surfaces and active sites in zeolites Ca-A, the amount of CO_2 uptake on such materials was observed to be much higher than that for conventional amine-appended silica materials. Furthermore, the adsorbent showed good stability and recyclability under a humid gas flow condition which is highly important for industrial application. Moving forward, a series of mixed-matrix membranes was fabricated using the new amine-grafted hierarchical mesoporous Ca-A for the first time, to investigate the unravelled potential of this filler material to develop mixed-matrix membranes with good CO_2 selectivity.

4.2 Experimental Section

4.2.1 Materials

Sodium metasilicatepentahydrate (Na_2SiO_3 $5H_2O$, 95%), calcium nitrate tetrahydrate ($Ca(NO_3)_2$ $4H_2O$, 99%), sodium hydroxide (NaOH, 98%), sodium silicate, sodium aluminate ($NaAlO_2$, Al_2O_3 (50-56%), Na_2O (40-45%), 3-aminopropyl trimethoxysilane (APTMS, 97%),

[3-(trimethoxysilyl)propyl]octadecyldimethylammonium chloride (TPOAC, 42% in methanol), and anhydrous toluene were all purchased from Sigma-Aldrich and used without further purification. Dichloromethane (DCM) was purchased from VWR and used without further purification. Commercial Matrimid® was used after drying in a convection oven.

4.2.2 Synthesis of Mesoporous LTA Zeolite

Mesoporous LTA (Na-A) zeolite was first synthesized via a hydrothermal synthesis procedure by mixing a solution containing 60 ml H_2O, 6.98 g sodium silicate, 1.98 g NaOH and 3.5 ml TPOAC with another solution of 30 ml H_2O and 4.01 g $NaAlO_2$. The mixture was well-shaken for 5 min and heated at 100 ℃ for 4 h with vigorous stirring. The precipitated product was filtered, washed with plenty of water, dried at 100 ℃ in an oven overnight followed by calcination in a furnace at 550 ℃ for 3 h. Mesoporous LTA zeolite was converted to mesoporous Ca-A zeolite by treating the resultant LTA zeolite in a solution of 0.5 M $Ca(NO_3)_2$ at 60 ℃ for 15 h followed by filtering. This procedure was repeated three times to exchange cations completely. Finally, the mesoporous LTA Ca-A zeolite was dried in a vacuum oven at 80 ℃ for 24 h.

4.2.3 Post-Synthetic Amine Grafting and Membrane Fabrication

1 g of the synthesized mesoporous Ca-A zeolite was dissolved in 100 mL of anhydrous toluene followed by 5 ml of APTMS. The solution mixture was

kept with stirring at ambient temperature for 24 h. Subsequently, the product was filtered, washed with toluene and dried in a vacuum oven at 60 ℃ for 24 h to obtain amine grafted mesoporous Ca-A zeolite.

Both bare mesoporous Ca-A and amine-grafted mesoporous Ca-A were used to make mixed-matrix membranes with two polymers, Matrimid® and cross-linked polyethylene oxide (XLPEO). For Matrimid® membranes, a homogeneous solution of DCM and Matrimid® was prepared. Subsequently, zeolite particles were added to the solution to form the doped solution containing a zeolite/polymer of 20/80 ratio. The resultant solution was cast on glass plates using a doctor blade in a glove box saturated by DCM. The cast membrane was dried in air for 12 h and then treated at 200 ℃ for 24 h in a vacuum oven. The XLPEO membranes were synthesized by the procedure described in our previous work [16]. Monomeric solution was prepared by mixing two PEO monomers, 1.6 g of PEGMEA and 0.4 g of PEGDA. Then, a small amount of AIBN (about 0.005 g) and amine-grafted mesoporous Ca-A were added to the PEO monomeric solution. The mixture was vigorously agitated for at least 1 d to disperse the zeolite particles in the solution before membrane fabrication. Subsequently, the solution prepared was sandwiched between two glass plates whose gap thickness was controlled by spacers. Finally, the membrane was solidified by polymerization of PEO monomers at 65 ℃ for 1 h.

4.2.4 Characterizations

A field emission scanning electron microscope (FESEM, JSM6700) was used to observe the morphology of zeolites and mixed-matrix membranes. The samples were coated with a thin layer of platinum before observation. Pore structure of zeolites was analyzed via nitrogen physiosorption at 77 K by using a volumetric adsorption analyzer (AS1, Quantachrome). The TGA curve was taken by using a thermogravimetric/differential thermal analyzer (Diamond TG/DTA, Perkin Elmer). The content of amine grafted on zeolites was determined via the weight loss on the curve in a temperature range between 200 to 600 ℃ after assuming two methoxy linkages to the surface [17]. A D8 Advance (Bruker) equipped with Cu Ka (40 KV, 40 mA) was used to obtain the XRD patterns. Gas adsorption of adsorbents was determined using a gas sorption analyzer (iSorb HP1, Quantachrome). The measurement was carried out in a pressure range of 0 to 1 bar at 25 ℃ while the samples were activated under a dynamic vacuum at 130 ℃ for 12 h. To investigate the filler/polymer adhesion properties, the tensile strengths of pure and composite membranes were measured by a tensile force tester (Instron Model 5543). The measurements were repeated 8 times for each membrane after preparing eight different specimens.

4.2.5 Permeation Tests

Gas permeation tests were performed with the permeation system produced by Labthink (G2110) following similar procedure as reported previous[18]. Testing gas was CO_2/CH_4 (50/50) binary mixtures, purchased from Air Liquide. The permeation system and membrane were degassed using a vacuum pump after the membrane was mounted in the testing cell. Operating temperature of the system was 25 ℃. Gas permeation properties of all membrane were measured three times with three different batches to verify experimental reproducibility and determine error bars of the results.

4.3 Results and Discussion

4.3.1 Synthesis of Mesoporous LTA Zeolite and Amine Grafting

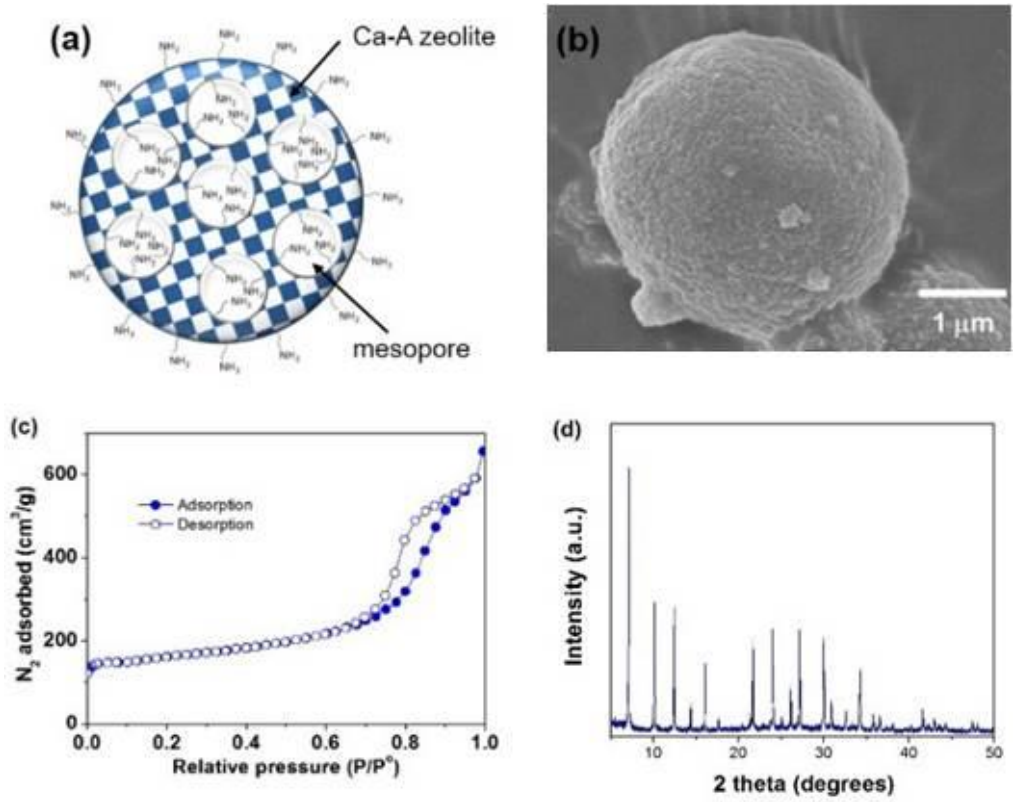

Figure 4-1 (a) A scheme of amine-appended hierarchical Ca-A and (b) SEM image, (c) N_2 physisorption at 77 K and (d) XRD pattern of hierarchical mesoporous Ca-A before amine-grafting.

Figure 4-1 b shows the SEM (scanning electron microscopy) image of a hierarchical mesoporous Ca-A zeolite, herein after referred to as mesoporous Ca-A. The small LTA crystals were assembled into a large particle and thus form the secondary pores, which were in the mesopore range. The characteristics of pores of hierarchical LTA zeolites were further investigated by measuring N_2 adsorption at 77 K. The co-existence of mesopores and

micropores within the sample was confirmed by the steep rise in N_2 uptake in the low-pressure region and the hysteresis loop in adsorption–desorption curves, respectively (Figure 4-1 c)[10]. The formation of LTA structure was also confirmed by the powder X-ray diffraction (XRD) pattern (Figure 4-1 d) which is matched with the reference in the zeolite structure database provided by International Zeolite Association [11]. Subsequently, in order to introduce the amine functional groups onto the mesopore surfaces of hierarchical Ca-A, a post-synthetic grafting with (3-aminopropyl)trimethoxysilane (APTMS) was carried out. The resulting fillers are termed as NH_2-mesoporous Ca-A herein after.

4.3.2 Characterization of Zeolites

Based on thermogravimetric analysis (TGA) of NH_2-mesoporous Ca-A (Figure 4-2), approximately 2.2 mmol NH_2 was grafted onto 1 g of mesoporous CaA.

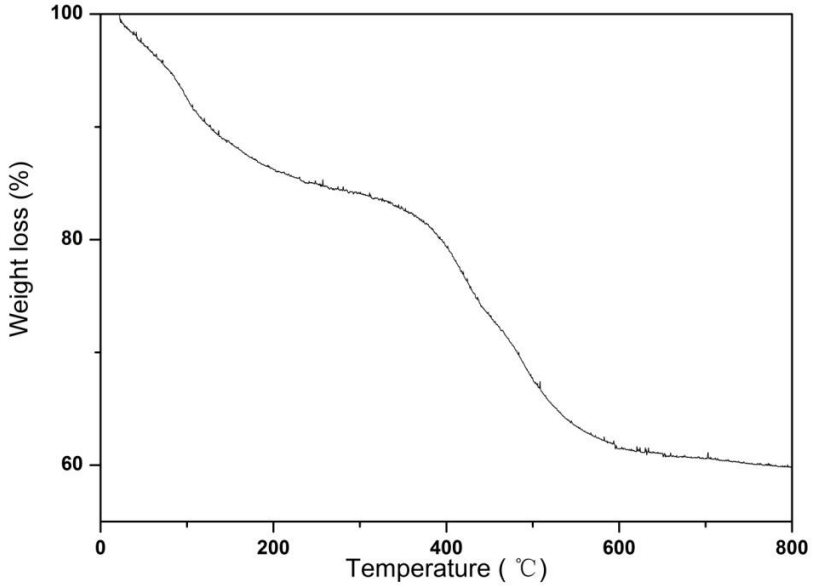

Figure 4-2 TGA curve of amine-functionalized hierarchical mesoporous Ca-A zeolite. (NH_2-mesoporous Ca-A).

Our previous work demonstrated that these amines are highly effective in capturing CO_2 [9]. The amine-grafting did not affect the crystal structure of mesoporous Ca-A as evidenced in the XRD pattern (Figure 4-1 d). As expected, a reduction in mesopore diameter due to occupancy of NH_2 groups within the mesopores was observed for NH_2-mesoporous Ca-A (Figure 4-3).

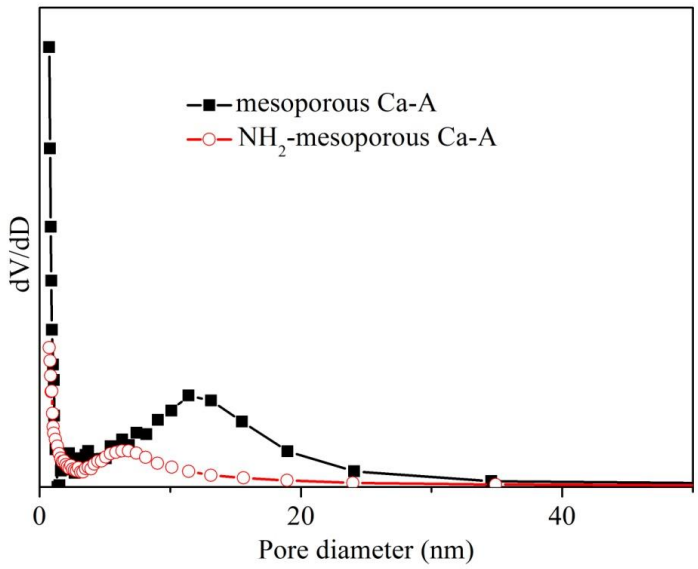

Figure 4-3 Pore size distribution of hierarchical mesoporous Ca-A zeolite before and after amine grafting.

The CO_2 and CH_4 uptake properties of the zeolites were investigated before and after the amine grafting. As depicted in Figure 4-5, the amount of CO_2 uptake significantly increased after grafting amine groups onto the mesopore surfaces.

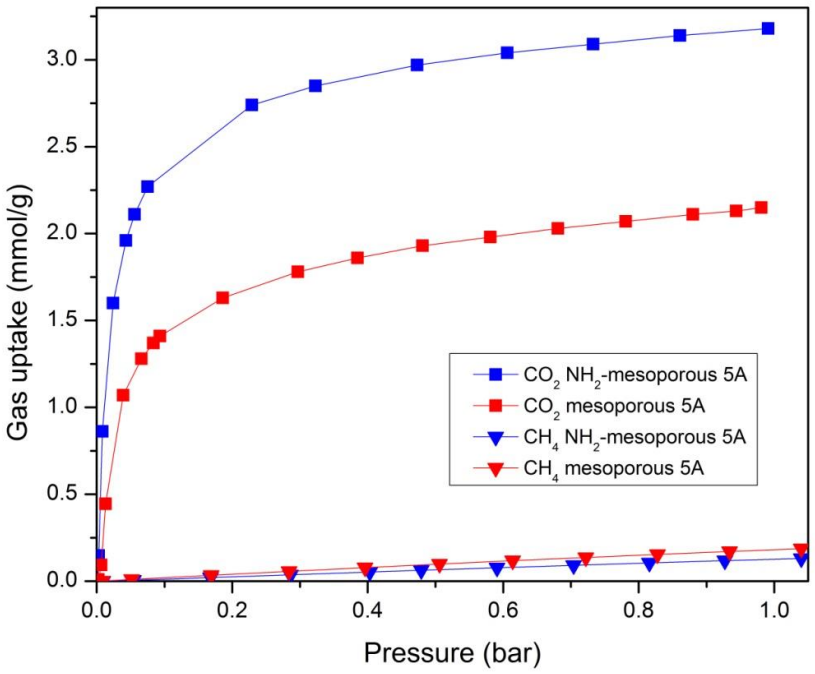

Figure 4-4 CO_2 and CH_4 adsorption isotherms of mesoporous Ca-A measured at 25°C.

Owing to the contributions of both the amine groups and Ca-A, NH_2-mesoporous Ca-A could take up a large amount of CO_2 even at low pressure, indicating a strong affinity for CO_2 molecules. Meanwhile, a decreased CH_4 uptake was observed for the amine-appended zeolite. As a result, the CO_2/CH_4 sorption selectivity, which is estimated by the ratio of Henry's constants for CO_2 and CH_4 in this work, dramatically increased from 189 to 874 after the amine grafting (Table 4-1).

Sample	BET surface area (m^2/g)	Total pore volume (cm^3/g)	Average mesopore diameter (nm)
Mesoporous Ca-A	520	1.01	11.4
NH_2-mesoporous Ca-A	158	0.32	5.8

Table 4-2 Physical properties of mesoporous Ca-A and NH_2-mesoporous Ca-A

4.3.3 Characterization of Composite Membranes

Figure 4-5 depicts the FESEM images of a series of mixed-matrix membranes fabricated between two different polymers (Matrimid® and cross-linked polyethylene oxide (XLPEO)) and mesoporous Ca-A zeolites. The sieve-in-a-cage morphology, which is typically found in mixed-matrix membranes made of bare zeolites and glassy polymers[9], was observed for the Matrimid®/bare mesoporous Ca-A membranes (Figure 4-5a and b). In contrast, defects formed at zeolite/polymer interface was vividly alleviated when NH_2-mesoporous Ca-A was used as the filler material (Figure 4-5c and d) owing to the chemical interaction between the NH_2 groups on external surface of zeolites and imide rings in Matrimid® backbone[4-5c, 10]. NH_2-mesoporous Ca-A zeolites were also successfully incorporated in XLPEO without forming defects as shown in Figure 4-5e and f, suggesting a wide usability potential of NH_2-mesoporous Ca-A for fabricating high quality mixed-matrix membranes.

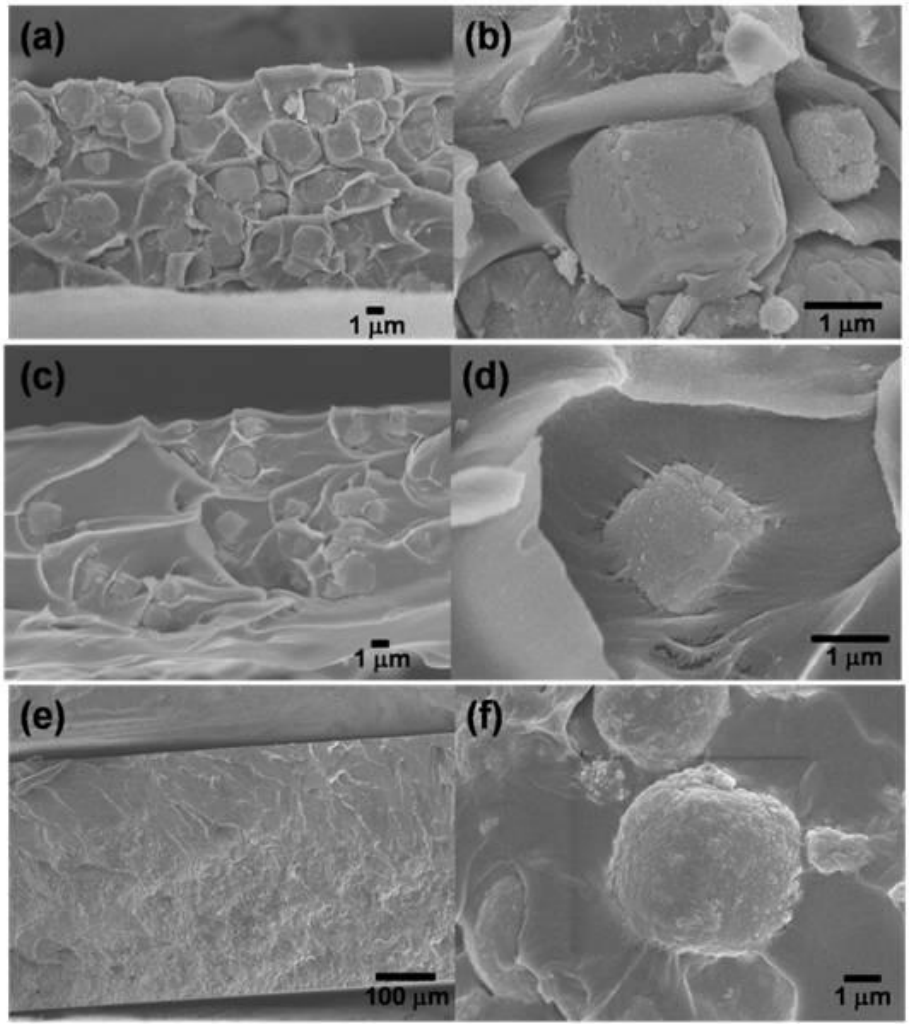

Figure 4-5 SEM images of a series of composite membranes. (a) and (b) low and high magnification of Matrimid®/20% wt bare mesoporous Ca-A; (c) and (d) low and high magnification of Matrimid®/20% wt NH_2-mesoporous Ca-A; (e) and (f) low and high magnification of XLPEO/NH_2-mesoporous Ca-A showing NH_2-decorated zeolite had a much better adhesion with the Matrimid® than the zeolite.

4.3.4 Permeation Result

CO_2/CH_4 binary mixture permeation properties of membranes are summarized in Table 4-2. The CO_2/CH_4 selectivity of Matrimid® membrane

increased from 34 to 39 by incorporating 20 wt% NH_2-mesorous Ca-A into the polymer membrane owing to the selective adsorption and transport of CO_2 through the filler. On the other hand, a decreased CO_2/CH_4 selectivity was observed for Matrimid®/bare zeolite membrane due to the non-selective bypass through the defects formed at zeolite/polymer interfaces.

Membranes	CO_2/CH_4 selectivity	CO_2 permeability (barrer)
Pure Matrimid®	34 ±2	10.2 ±0.5
Matrimid®/20 wt% bare mesoporous Ca-A zeolite	31 ±4	11.5 ±1.3
Matrimid®/20 wt% NH_2 mesoporous Ca-A zeolite	39 ±2	9.2 ±0.6
Pure XLPEO	18 ±2	380 ±20
XLPEO/20 wt% NH_2 mesoporous Ca-A zeolite	23 ±2	360 ±20

Table 4-3 Mixed-gas permeation properties of membranes at 40 °C and 1 bar total feed pressure with a 1:1 CO_2/CH_4 mixture.

Thus, amine groups grafted onto mesoporous Ca-A played two roles, in particular for (1) enhancing CO_2 uptake property of mesoporous Ca-A and (2) improving zeolite/polymer adhesion in mixed-matrix membranes. When NH_2-mesopores Ca-A zeolites were incorporated in XLPEO possessing a higher permeability but a lower selectivity than Matrimid®, CO_2/CH_4 selectivity was increased more significantly from 15 to 23. Although some reduction of CO_2 permeability was observed, likely attributed to strong affinity between NH_2 groups and CO_2 molecules which restricted the diffusivity of CO_2 through the membrane, the performance of XLPEO mixed-matrix membranes is located

closer to the upper bound limit of polymeric membranes than that of pure polymer membrane (Figure 4-6). It is noteworthy that XLPEO is an inexpensive polymer that can be used in a large-scale membrane production. The performance beyond the upper bound can potentially be realized by incorporating NH_2-mesoporous Ca-A into a polymer whose performance is close to the upper bound such as polyimides based upon 6FDA monomer.

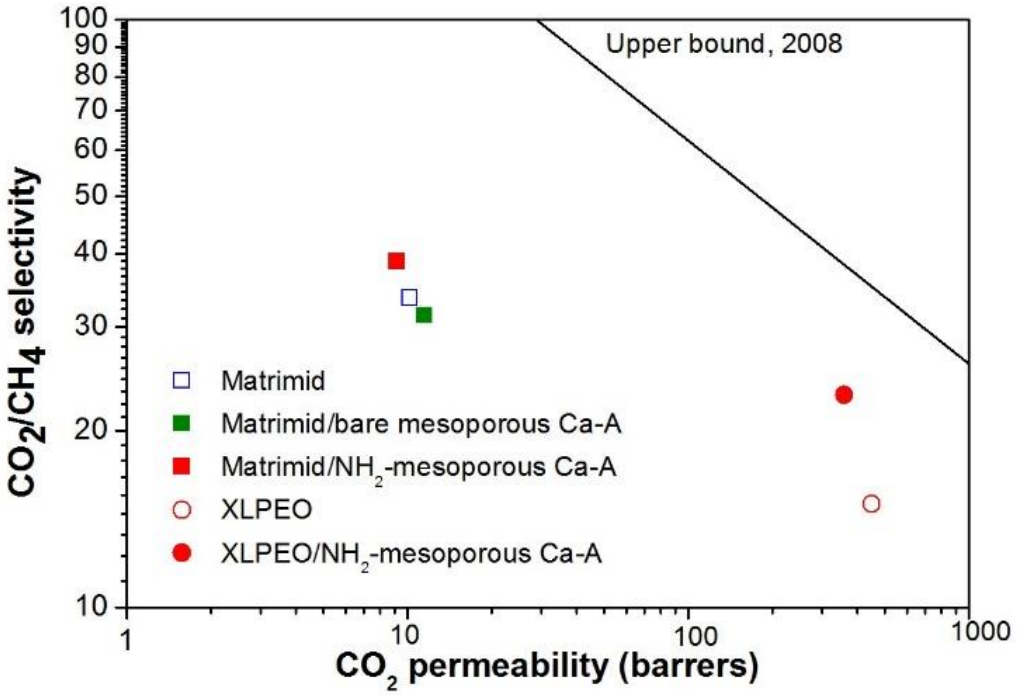

Figure 4-6 Mixed-gas permeation properties of membranes at 25°C and 1 bar total feed pressure with a 1:1 CO_2/CH_4 mixture. The filler loading was 20 wt% for all mixed-matrix membranes. The solid line is the upper bound limit for polymer membranes established in 2008.

4.4 Conclusions

In summary, new mixed-matrix membranes containing NH_2-grafted mesoporous Ca-A were successfully fabricated for the first time. The resulting

membranes showed an improved CO_2/CH_4 selectivity owing to the strong affinity of filler for CO_2 molecule. Amine groups introduced in mesoporous Ca-A also played an important role in controlling filler/polymer adhesion property which is a prerequisite for fabricating high-performance mixed-matrix membranes. The membranes developed in this work have potential utilities in biogas upgrading, natural gas treatment and CO_2 capture in power plants.

4.5 Declaration

The work presented in this chapter has been published in ChemPhysChem.

Tien Hoa Nguyen[1], **Heqing Gong[1]**, Siew Siang Lee, Tae-Hyun Bae*, Amine-appended hierarchical Ca-A zeolite for enhancing CO_2/CH_4 selectivity of mixed-matrix membranes, *ChemPhysChem*, **2016**, *17*, 3165-3169

[1]These authors contributed equally to this work.

Chapter 5

Submicron Crystals of Metal-Organic Framework and Their Applications in Carbon Capture

5.1 Introduction

While inorganic zeolites have been a mainstay for this application,[29] metal-organic frameworks which comprise metal center and organic linkers to form three-dimensional porous structure have attracted vast research interests in the recent years as potential fillers for mixed-matrix membrane fabrication owing to their larger pore volumes and more tunable functionalities than that of their zeolites counterpart (details can refer to Chapter 2.2) [165-168]. This is especially so in the development of high-performance CO_2-selective membranes owing to their wide range of potential applications including CO_2 capture, hydrogen purification, biogas upgrading, and natural gas treatment[165, 167, 169]. So far, a large number of studies have focused on improving the molecular sieving property of membrane by incorporating metal-organic frameworks with small pore size. Meanwhile, to improve the sorption selectivity, frameworks with functional groups that selectively interact with CO_2 molecule have also been incorporated into polymer matrices [139, 170-172]. Mg_2(dobdc) crystals, for example, featuring an outstanding CO_2 uptake property among the metal-organic frameworks tested so far, have been employed as the filler of mixed-matrix membranes for application in

post-combustion CO_2 capture.[171] All previous studies have strongly suggested that a metal-organic framework possessing both an optimum pore size for selective CO_2 permeation and a strong affinity for CO_2 molecule is an ideal filler to design a high-performance CO_2-selective membrane, as improvements in both size exclusion and sorption selectivity can be expected.

Recently, a new metal-organic framework $Zn(pyrz)_2(SiF_6)$ (or SIFSIX-3-Zn) possessing such properties has been reported[173, 174]. The compound $Zn(pyrz)_2(SiF_6)$ is composed of square grids of Zn and pyrazine pillared by hexafluorosilicate (SiF_6^{2-}) anions which form one-dimensional channels having a 3.8 Å diagonal dimension. Gas adsorption analysis on this framework demonstrated a steep rise in CO_2 uptake capacity at low partial pressure range, indicating a strong affinity of the framework to CO_2 molecule[174]. Furthermore, owing to the size exclusion property through pores in the framework, CO_2/CH_4 and CO_2/N_2 adsorption selectivities measured by the binary mixture adsorption technique at 25 ℃ were reported to be 350 and 1700, respectively[174]. These results suggest that not only $Zn(pyrz)_2(SiF_6)$ is a good solid adsorbent but also an outstanding candidate for synthesizing a high-performance CO_2-selective membrane.

In this Chapter, mixed-matrix membranes comprising $Zn(pyrz)_2(SiF_6)$ submicron crystals were synthesized via a facile sonochemical mean. Crosslinked polyethylene oxide (XLPEO) was employed as a polymer matrix in

this work, since it has a decent CO_2 separation property as well as a high chain mobility that strongly inhibits the formation of polymer/filler interfacial gaps which could result in an undesirable gas separation property[158, 175]. Subsequently, CO_2/CH_4 and CO_2/N_2 mixture gas permeation properties of membranes were measured at the conditions relevant to biogas upgrading and post-combustion CO_2 capture, respectively.

5.2 Experimental Section

5.2.1 Materials

Zinc hexafluorosilicate ($ZnSiF_6$) and pyrazine were purchased from Sigma-Aldrich and used as received without further purifications. 4,4'-(hexafluoroisopropylidene)diphthalic anhydride (6FDA), N,N,N',N'-Tetramethyl-1,3-propanediamine(TMPDA), Acetic Anhydride (AA), Triethylamine (TEA), N-Methyl-2-Pyrrolidone (NMP). Other Organic solvents such as Dichloromethane (DCM), methanol were purchased from VWR and also used as received without further purifications.

5.2.2 Synthesis of Submicron $Zn(pyrz)_2(SiF_6)$ Crystals

The bulk crystals of $Zn(pyrz)_2(SiF_6)$ were synthesized by the procedure described elsewhere[20, 21]. A solution of pyrazine prepared by dissolving 1.3 mmol (0.10g) of pyrazine in 2 ml of methanol was added to a solution of $ZnSiF_6$ comprising 0.6 mmol (0.13g) $ZnSiF_6$ and 2 ml of methanol and let the

reagents react at room temperature without agitation for 3 d. After the reaction, harvested crystals were washed with a copious amount of methanol and dried at 60 ℃ in a convection oven. Then, the crystals were gently ground before use in membrane fabrications.

The submicron crystals of $Zn(pyrz)_2(SiF_6)$ were synthesized by a sonochemical mean. The reagent solution comprising pyrazine, $ZnSiF_6$ and methanol was prepared using the same method used in the bulk crystal synthesis. Then, the solution in a vial was sonicated in an ultrasonic bath (Symphony) at room temperature for 2 h. During this period, the formation of white solid particles could be visually identified. Next, a filtration was conducted to collect the crystals formed and a copious amount of methanol were added to the filter cake to wash out residual unreacted reagents. Prior to using them in membrane fabrication, $Zn(pyrz)_2(SiF_6)$ crystals were dried at 60 ℃ in a convection oven.

5.2.3 Fabrication of Crosslinked Polyethylene Oxide (XLPEO) Membranes

The XLPEO membranes were synthesized by the procedure described in our previous work[17]. Monomeric solution was prepared by mixing two PEO monomers, 1.6 g of PEGMEA and 0.4 g of PEGDA. Then, a small amount of AIBN (about 0.005 g) and fully activated $Zn(pyrz)_2(SiF_6)$ crystals were added to the PEO monomeric solution. The mixture was vigorously agitated for at least 1 d to disperse $Zn(pyrz)_2(SiF_6)$ crystals in the solution before membrane

fabrication. Subsequently, the solution prepared was sandwiched between two glass plates whose gap thickness was controlled by placing “spacers”. Finally, the membrane was solidified by polymerization of PEO monomers at 65 ℃ for 1 h.

5.2.4 Characterizations of $Zn(pyrz)_2(SiF_6)$ Crystals and Membranes

Gas adsorption properties of $Zn(pyrz)_2(SiF_6)$ crystals were measured by a high-pressure gas adsorption analyzer (Quantachrome, i-Sorp HP-1). After activation of the crystals at 120 ℃ for 15 h under high vacuum, pure component CO_2, N_2, and CH_4 isotherms were obtained in a pressure range of 0 to 1 bar at 25 ℃ that is precisely controlled by a recirculating fluid. The size of $Zn(pyrz)_2(SiF_6)$ crystals were analyzed using a dynamic light scattering method (BIC PALS Zeta Sizer). Themo gravimetric analysis (TGA) was carried out with Perkin Elmer TGA/DTA in a temperature range of 30 to 500 ℃ with a ramping rate of 10 ℃/m. The powder X-ray diffraction (XRD) analysis was performed with Bruker D2 phaser diffractometer with a Cu Kα radiation. The morphology of $Zn(pyrz)_2(SiF_6)$ crystals and cross-sections of composite membranes were observed using a field emission scanning electron microscopy (FESEM, JSM-7600F). Both MOF crystals and composite membranes were coated with gold prior to imaging using FESEM. In the case of membranes,

the samples were first cryogenically fractured in liquid nitrogen prior to sputtering with gold.

5.2.5 Mixture Gas Permeation Tests

Gas permeation tests were carried out with the permeation system produced by Labthink (G2-110). Testing gases, namely, CO_2/N_2 (20/80) and CO_2/CH_4 (50/50) binary mixtures, were purchased from Air Liquide. After mounting a membrane in the testing cell, all residual gases in the permeation system and the membrane were removed using a vacuum pump. Next, the upstream chamber of the cell was pressurized to 1 bar with the feed gas. The downstream gas permeated through the membrane was swept by He and fed to Gas Chromatograph to analyze the composition. The permeability of individual component was calculated using the flow rate of sweeping gas (He), the composition of permeated gas measured by Gas Chromatograph, and the properties of membrane such as effective exposed area and thickness. Throughout the whole operation, the temperature of entire system was maintained at 25 ℃. Prior to the testing membranes prepared in this work, the reliability of the permeation system was validated with several pure polymeric membranes including pure XLPEO by comparing our experimental data with the figures reported in the literature. In addition, to check the reproducibility of experiments and obtain the error bars of results, three samples of each mixed-matrix membrane were tested.

5.2.6 Prediction of Membrane Performance with the Maxwell Model

The permeability of a hypothetical mixed-matrix membrane was predicted by the Maxwell model shown below [29, 176].

$$P_{MMM} = P_p[\frac{P_s + 2P_p - 2\varphi_s(P_p - P_s)}{P_s + 2P_p + \varphi_s(P_p - P_s)}]$$

where, P_p and P_s are the permeabilities of polymer and sieve (metal-organic framework) phases, respectively, and φ_s is the volume fraction of the sieve.

5.3 Results and Discussion

5. 3.1 Synthesis of $Zn(pyrz)_2(SiF_6)$ Metal-Organic Framework Crystals

Fig 5-1a shows the $Zn(pyrz)_2(SiF_6)$ crystals synthesized by the reaction at room temperature for 3 d as described in the previous work. [173, 174] Large crystals of up to 10 μm were formed under these reaction conditions with an average particle size of 5.7 μm, as estimated by a dynamic light scattering (DLS). However, crystals with sizes smaller than 1 μm are more desirable for the fabrication of high-quality composite membranes with ideal morphology such as good filler/polymer adhesion and uniform distribution of filler crystals in polymer matrix[138, 151, 171, 177]. Hence, in this work, a sonochemical

synthesis route was employed to obtain submicron-sized $Zn(pyrz)_2(SiF_6)$ crystals. As shown in the Fig 5-1b, crystals apparently far smaller than 1 μm were successfully synthesized. The formation of submicron crystals was further verified by the DLS analysis which showed an average particle diameter of 860 nm. Furthermore, unlike the conventional method which takes 3 d due to a slow reaction kinetics, the crystals are rapidly formed under the ultrasonic radiation, such that the reaction was completed within 2 h.

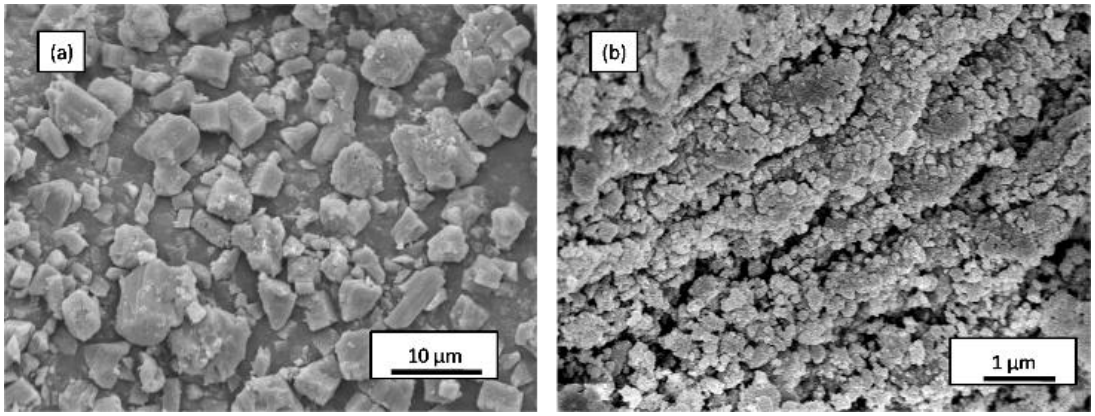

Figure 5-1 FESEM images of $Zn(pyrz)_2(SiF_6)$ crystals synthesized by (a) the conventional and (b) the sonochemical approaches.

The structure of the sonochemically synthesized submicron crystals was confirmed by collecting a powder x-ray diffraction, as depicted in Fig 5-2. A peak broadening, as compared to the peak widths of bulk crystals, was observed for the submicron crystals presumably due to their smaller crystallites. Thermal stabilities of the metal-organic framework crystals in the air were analyzed with TGA and results are demonstrated in Fig 5-3. The sonochemically synthesized

submircon crystals exhibited the similar thermal stability with bulk crystals. Both crystals started to decompose at around 150 ℃ in the air, similar to the result previously reported for bulk crystals[173]. Initial weight loasses below 150 ℃ are attributed to the evaporation of solvents in the pores of $Zn(pyrz)_2(SiF_6)$ crystals.

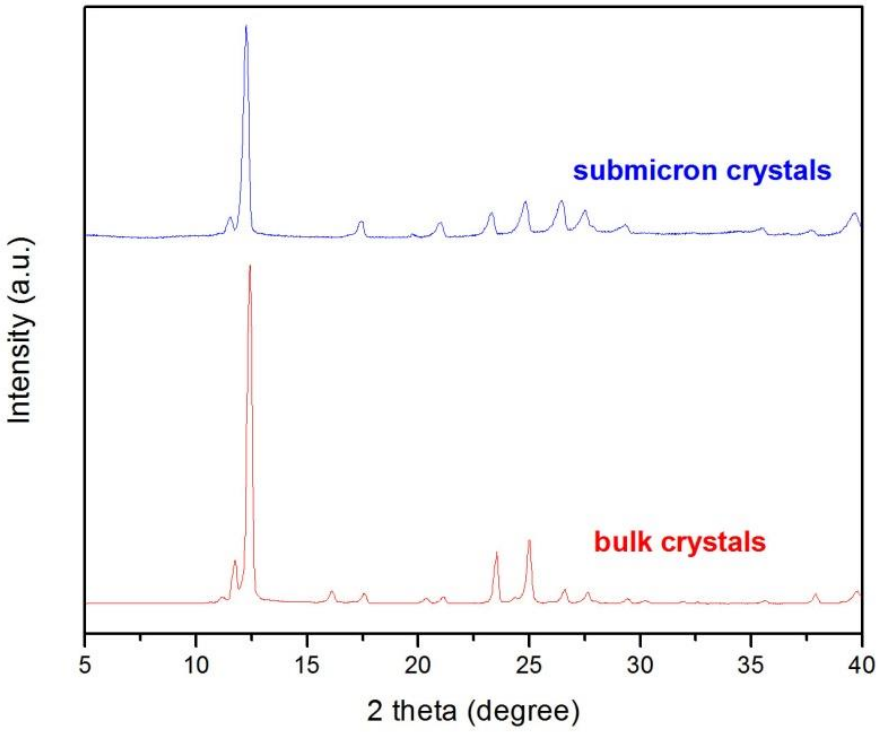

Figure 5-2 Powder X-ray diffraction patterns of $Zn(pyrz)_2(SiF_6)$ crystals.

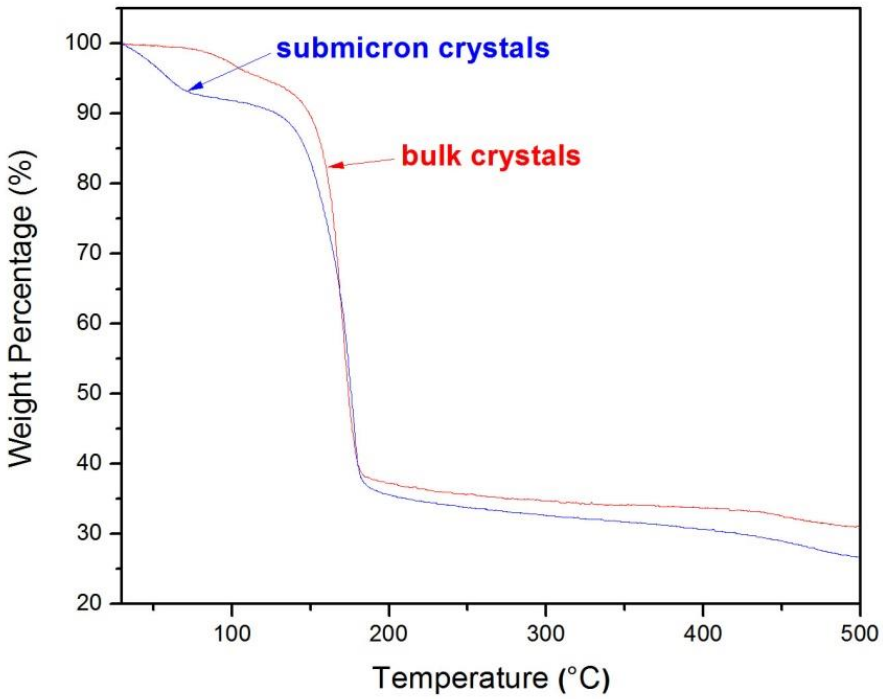

Figure 5-3 TGA curves of $Zn(pyrz)_2(SiF_6)$ crystals.

5.3.2 Gas Adsorption Properties of $Zn(pyrz)_2(SiF_6)$ Crystals

Pure component gas adsorption isotherms were measured at 25 ℃ to investigate the adsorptive gas separation property of $Zn(pyrz)_2(SiF_6)$ submicron crystals (Fig 5-4). In consistent with that reported for the bulk material,[21] the $Zn(pyrz)_2(SiF_6)$ crystals exhibited an excellent CO_2 adsorption capacity at low CO_2 partial pressure. Note that the amount of CO_2 uptake for the submicron crystals is slightly lower than that for bulk crystals, presumably due to the smaller crystallites formed. In contrast, the amounts of CH_4 and N_2 uptakes were observed to be zero (0 ± 0.01 mmol/g) throughout the whole pressure range tested (0 to 1 bar), indicating inaccessibility of $Zn(pyrz)_2(SiF_6)$'s pores by

CH_4 and N_2 at 25 ℃ below 1 bar. The result of gas adsorption analysis strongly suggested that $Zn(pyrz)_2(SiF_6)$ submicron crystals synthesized in this work is a good candidate for fabricating membranes for CO_2/CH_4 and CO_2/N_2 separations under a low pressure range.

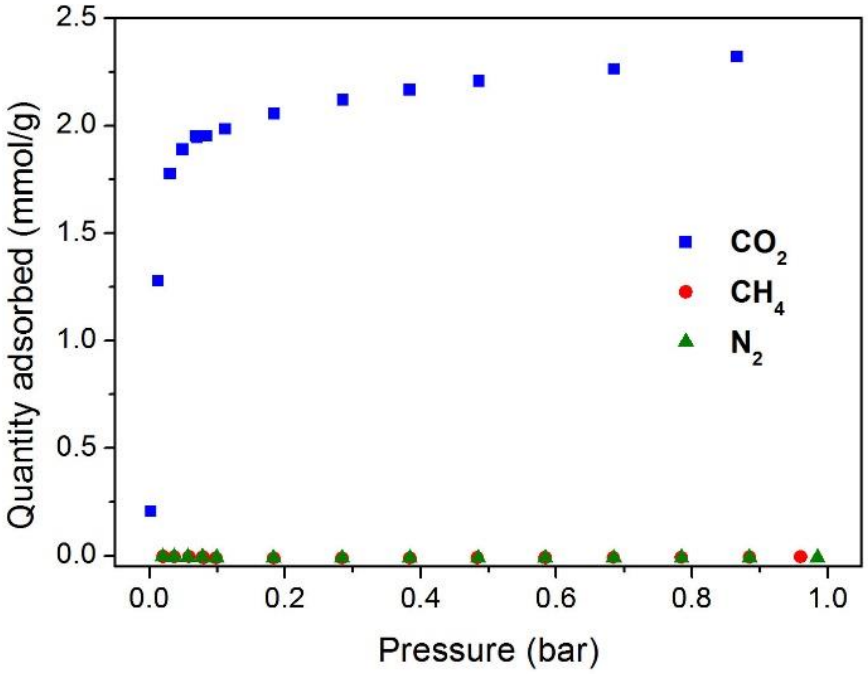

Figure 5-4 Pure component CO_2, CH_4, and N_2 adsorptions on $Zn(pyrz)_2(SiF_6)$ submicron crystals measured at 25 ℃.

5.3.3 Fabrications of Composite Membranes

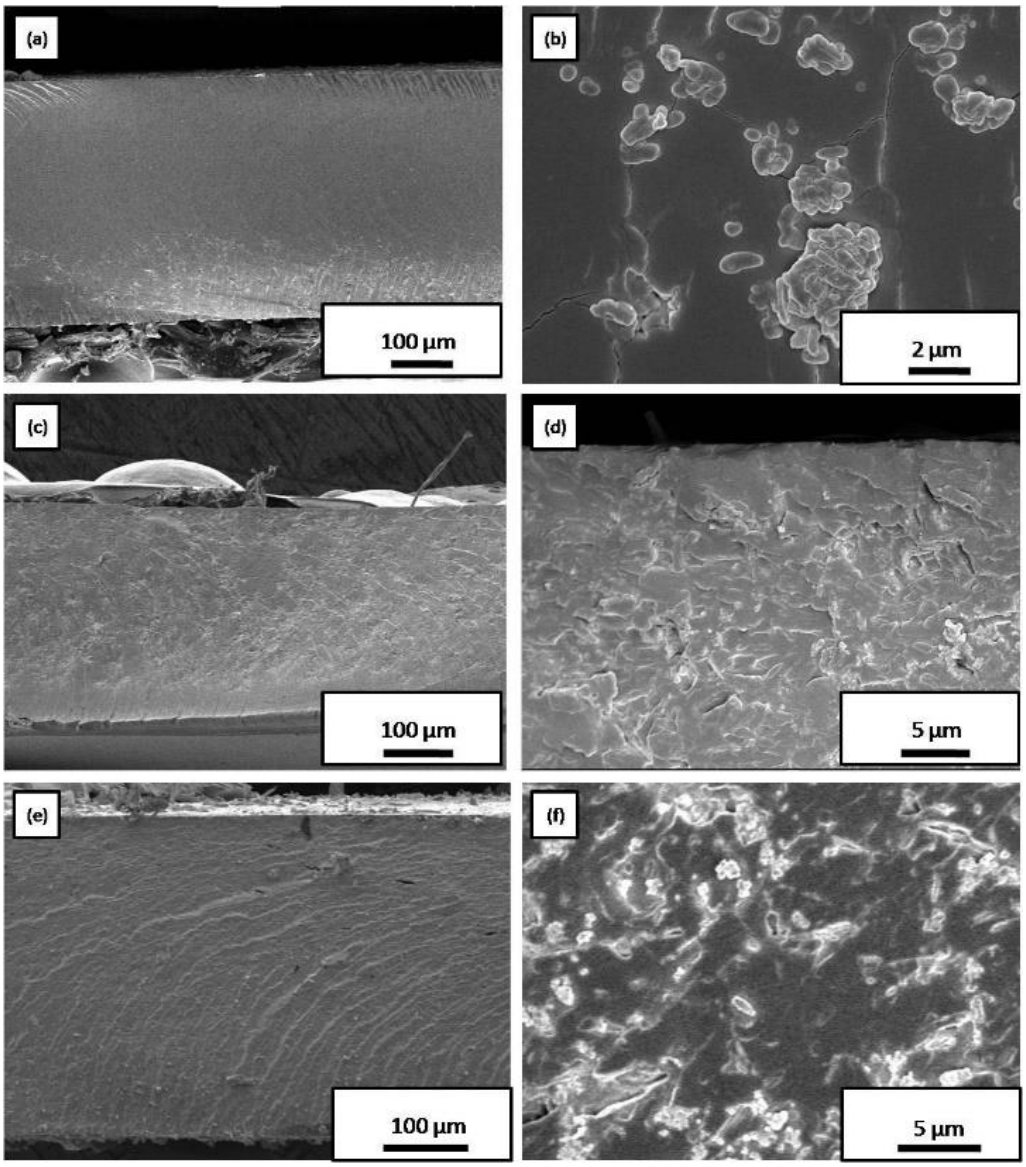

Figure 5-5 FESEM images of cross-sections of composite membranes containing $Zn(pyrz)_2(SiF_6)$ crystals. (a) and (b) 10 wt % bulk $Zn(pyrz)_2(SiF_6)$ crystals in XLPEO; (c) and (d) 10 wt % submicron crystals in XLPEO; (e) and (f) 20 wt % submicron crystals in XLPEO demonstrating both the submicron and bulk crystals can have a desirable interfacial morphology with the XLPEO, while the submicron crystal's distribution in membrane is better than the bulk crystals.

Mixed-matrix membranes comprising $Zn(pyrz)_2(SiF_6)$ crystals were fabricated using XLPEO as a polymer matrix. While a "sieve in a cage" morphology has been frequently observed for zeolite/polymer composite membranes due to the poor compatibility between the two phases,[85, 97, 159, 176] all membrane prepared in this work has showed good adhesion property (Fig 5-5). This was attributed to a good affinity of the organic ligand in the framework to the PEO chain which possesses a high mobility at room temperature. In the case of membrane containing the bulk crystals, majority of crystals were located at the bottom of membrane, since the crystals settled down during the membrane fabrication (Fig 5-5a and b). However, a different morphology was observed for the membranes comprising the submicron crystals. Figure 5-5d and f showed that the submicron crystals could form clusters in the polymer matrix, probably due to the high viscosity of the dope solution which resulted from the direct dispersion of the crystals in the PEO monomers without an aid of solvent, thus impeding an effective suspension of crystals during the solution agitation. Despite that, the submicron crystals were overall effectively stabilized by the surrounding PEO chains in the monomeric solutions, resulting in a relatively uniform distribution of crystals in the polymer matrix.

5.3.4 Gas Permeation Properties of Composite Membranes

Table 5-1 shows the CO_2/CH_4 mixture gas permeation properties measured at 25 ℃ and 1 bar of total upstream pressure. The CO_2 permeability and the CO_2/CH_4 selectivity of pure polymeric membrane were 450 barrers and 15, respectively, comparable with that reported before[175]. Incorporation of 10 wt% $Zn(pyrz)_2(SiF_6)$ bulk crystals into the membrane showed an improved separation property, with CO_2 permeability and CO_2/CH_4 selectivity increased to 540 barrers and 23, respectively. When 10 wt% $Zn(pyrz)_2(SiF_6)$ submicron crystals were used instead of the bulk material, the CO_2 permeability and CO_2/CH_4 selectivity were further enhanced to 620 barrers and 27, respectively. In comparison with the performance of pure polymeric membrane, this enhancement translates to 38% and 80% of CO_2 permeability and CO_2/CH_4 selectivity, respectively. At 20 wt% $Zn(pyrz)_2(SiF_6)$ submicron crystals loading, CO_2/CH_4 selectivity further increased to 30 with the modest change in CO_2 permeability. However, the effect of increasing the filler content was observed to be less significant than expected in this study. Non-ideal effects such as a change in polymer chain mobility derived from the increased polymer/filler contact area, as well as an increased amounts of agglomerated crystals in polymer matrix, might decrease the effect of the filler[29, 159, 178].

Table 5-1 CO_2/CH_4 (50/50) mixture gas permeation properties of membranes measured at 25 ℃ and 1 bar of upstream pressure.

$Zn(pyrz)_2(SiF_6)$/XLPEO mixed-matrix membranes	**CO_2 permeability (barrer)**	**CH_4 permeability (barrer)**	**CO_2/CH_4 selectivity**
Pure XLPEO	450	30	15
10 wt% bulk crystals	540 ±50	23 ±2	23 ±1
10 wt% submicron crystals	620 ±110	23 ±4	27 ±2
20 wt% submicron crystals	590 ±130	20 ±4	30 ±2

As shown in Table 5-2, enhanced gas separation properties by incorporating the metal-organic framework crystals into XLPEO polymer membrane were also observed in CO_2/N_2 mixture gas permeation tests. In consistent with the result observed in the CO_2/CH_4 permeation test , the incorporation of the bulk crystals was less effective than that with submicron crystals. CO_2 permeability and CO_2/N_2 selectivity of mixed-matrix membranes comprising 10 wt% $Zn(pyrz)_2(SiF_6)$ submicron crystals increased by 43% to 670 barrers and by 53% to 29, respectively, from those of pure polymeric membranes.

Table 5-2 CO_2/N_2 (20/80) mixture gas permeation properties of membranes measured at 25 ℃ and 1 bar of upstream pressure.

$Zn(pyrz)_2(SiF_6)$/XLPEO mixed-matrix membranes	**CO_2 permeability**	**N_2 permeability (barrers)**	**CO_2/N_2 selectivity**
Pure XLPEO	470	25	19
10 wt% bulk crystals	540 ± 100	22 ± 4	24 ± 2
10 wt% submicron crystals	670 ± 120	23 ± 4	29 ± 2
20 wt% submicron crystals	630 ± 120	22 ± 4	29 ± 2

The improvements in gas separation properties of mixed-matrix membranes were attributed to the selective adsorption/transport of CO_2 through the pores of $Zn(pyrz)_2(SiF_6)$ crystals. As evidenced in Table 5-1 and 2, the incorporation of $Zn(pyrz)_2(SiF_6)$ in XLPEO effectively increased CO_2 permeability. On the other hand, decreased N_2 and CH_4 permeabilities were observed for mixed-matrix membranes, since transport of these two gas molecules in membranes were hindered by the embedded $Zn(pyrz)_2(SiF_6)$ crystals which impede the access of N_2 and CH_4 to their pores. Such size exclusion property of $Zn(pyrz)_2(SiF_6)$ crystals was consistent with the gas adsorption data in Fig 5-4.

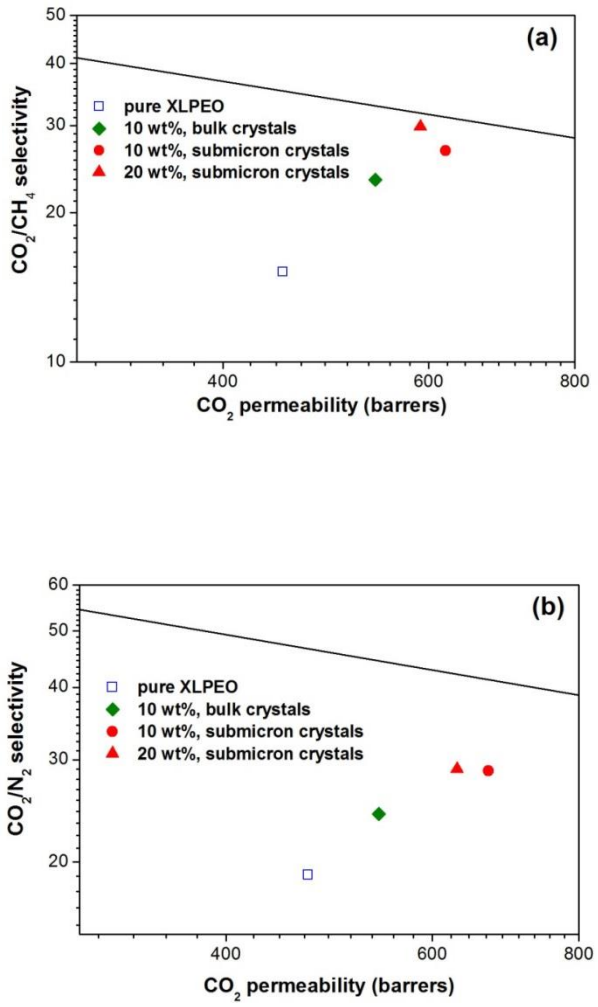

Figure 5-6 Robeson plots of (a) CO_2/CH_4 (50/50) and (b) CO_2/N_2 (20/80) mixture gas permeation data presented in Table 5-1 and 2. The solid lines represent the upper bound limit for polymeric membranes established in 2008[17].

5.3.5 Prediction of Performance of Hypothetical Membranes Comprising $Zn(pyrz)_2(SiF_6)$ Crystals

Figure 5-6 depicts that the CO_2/CH_4 separation property of the best performing membrane in this work was very close to the upper bound limit established in 2008[17]. Although the significant improvement in CO_2/CH_4 permeation property was achieved by incorporating $Zn(pyrz)_2(SiF_6)$ submicron

crystals into XLPEO, the overall performance was still lower than the upper bound limit owing to the relatively low separation performance of pure polymeric membrane. To realize the better performance of resulting mixed-matrix membrane, polymer membranes performing better than XLPEO, such as polyimides base upon 6FDA monomer, can be employed as matrices[179, 180]. To investigate the feasibility of such idea, the gas permeation properties of hypothetical membranes synthesized by incorporating $Zn(pyrz)_2(SiF_6)$ submicron crystals into three different polyimides, namely, 6FDA-durene, 6FDA-TMPDA and 6FDA-TMPDA/DAT, were calculated using the Maxwell model. As shown in Figure 5-7, CO_2/CH_4 separation properties of the resulting composite membranes are predicted to be located beyond the upper bound limit in all three scenarios. However, owing to the crystalline nature of polyimides, the polymer/filler adhesion property should be carefully controlled to realize such performance.

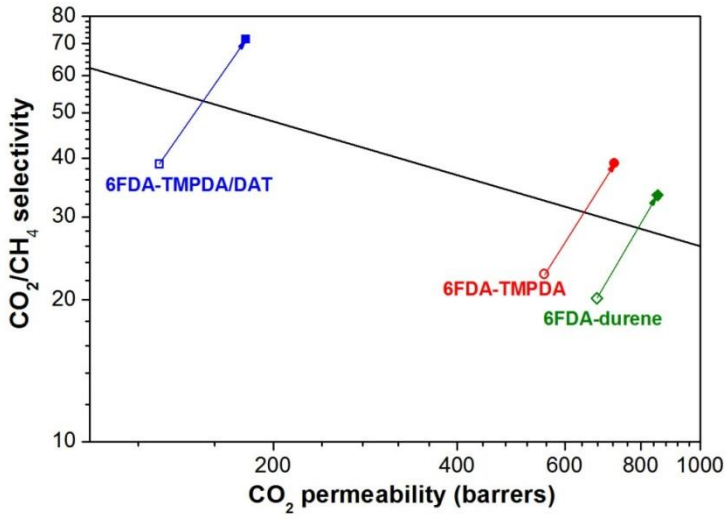

Figure 5-7 Predicted CO_2/CH_4 permeation properties of hypotheticals composite membranes synthesized by incorporating 20 wt% $Zn(pyrz)_2(SiF_6)$ submicron crystals into various 6FDA polyimides. Solid and empty symbols represent predicted composite membranes and pure polymer membranes respectively. The calculations were carried out using the Maxwell model describe indicating the as-made composite membranes will show extraordinary CO_2 separation performance if combine the $Zn(pyrz)_2(SiF_6)$ submicron crystals together with high performance 6FDA-based polymers[179, 180].

5.4 Conclusions

Mixed-matrix membranes comprising $Zn(pyrz)_2(SiF_6)$ submicron crystals were fabricated for potential applications in biogas upgrading and post-combustion CO_2 capture. In essence, the foregoing results demonstrated that the CO_2 separation performance of polymer membrane at relatively low CO_2 partial pressure can be significantly enhanced by incorporating $Zn(pyrz)_2(SiF_6)$ submicron crystals within a polymer. Future efforts will be devoted to fabricating high-performance membranes based on 6FDA

polyimides and $Zn(pyrz)_2(SiF_6)$ submicron crystals. Eventually, we aim to produce membranes in an asymmetric hollow fiber configuration in which a thin skin layer containing a large fraction of metal-organic framework crystals is supported by the porous polymer layer, for application in biogas upgrading and post-combustion CO_2 capture.

5.5 Declaration

The work presented in this chapter has been published in Journal of Membrane Science.

Heqing Gong, Tien Hoa Nguyen, Rong Wang, Tae-Hyun Bae*, Separations of Binary Mixtures of CO_2/CH_4 and CO_2/N_2 with Mixed-Matrix Membranes Containing $Zn(pyrz)_2(SiF_6)$ Metal-Organic Framework, *J. Membrane Science.* **2015**, *495,* 169-175

Chapter 6

High Performance Composite Membranes Comprising $Zn(pyrz)_2(SiF_6)$ Nanocrystals for CO_2/CH_4 Separation

6.1 Introduction

In Chapter 5, we have demonstrated the potential utility of $Zn(pyrz)_2(SiF_6)$ (or SIFSIX-3-Zn) MOF as a membrane material that can improve both solubility and diffusivity of CO_2[110]. Owing to the ideal pore size of 3.8 Å and hexafluorosilicate (SiF_6^{2-}) anions that have strong affinity for CO_2 in the network,[124, 173] $Zn(pyrz)_2(SiF_6)$ could increase the CO_2/N_2 and CO_2/CH_4 selectivities of cross-linked polyethylene oxide (XLPEO) membrane. However, the overall performance of resulting membrane was still not satisfactory owing to the large size of filler, inefficient distribution of filler owing to the high viscosity of monomeric solution as well as the poor gas transport property of polymer matrix. Furthermore, XLPEO which is a rubbery polymer having limited processability is mechanically unstable as compared to glassy polymers[171, 175, 181].

In this chapter, $Zn(pyrz)_2(SiF_6)$ nanocrystals were sonochemically synthesized in a facile manner via modification of the reaction conditions

previously reported. Subsequently, the nanoparticles were incorporated into a house-made polyimide possessing a high free volume to design high performance CO_2/CH_4 separation membranes. Owing to the selective CO_2 transport through the pores of $Zn(pyrz)_2(SiF_6)$, performance of resulting mixed-matrix membrane was observed to be far greater than that of pure polymer membrane and thereby surpassed the upper bound limit of polymer membranes established in 2008. Detailed analysis on the effect of the filler on gas solubility and diffusivity was also conducted to understand how such enhanced performance was realized.

6.2 Experimental Section

6.2.1 Materials

4,4'-(hexafluoroisopropylidene)diphthalic anhydride (6FDA), N,N,N',N'-Tetramethyl-1,3-propanediamine (TMPDA), zinc hexafluorosilicate, pyrazine, N-methyl-2-pyrrolidone (NMP), acetic anhydride, triethylamine, poly(ethylene glycol) diacrylate (PEGDA, M_n = 700), poly(ethylene glycol) methyl ether acrylate (PEGMEA, M_n = 480) and azobisisobutylonitrile (AIBN) were purchased from Sigma-Aldrich. 6FDA and TMPDA were first purified via vacuum sublimation process prior to the synthesis. The other chemicals were used as received without further purifications. Organic solvents such as dichloromethane (DCM) and methanol were purchased from VWR and used as received without further purifications.

6.2.2 Synthesis of Submicron $Zn(pyrz)_2(SiF_6)$ Crystals

It has been shown that the sonochemical synthesis is a useful method to produce metal-organic framework crystals in a facilitated manner[110, 124]. In this work, nanocrystals of $Zn(pyrz)_2SiF_6$ were synthesized by a sonochemical method under a strong ultrasonic irradiation. First, two separate solutions were prepared in vials by dissolving 0.3 g pyrazine in 6 ml of methanol and 0.38 g of zinc hexafluorosilicate in 6 ml of methanol, respectively. Next, while zinc hexafluorosilicate solution was sonicated with an ultrasonic horn (Qsonica, Q125), the solution of pyrazine was added dropwise. The whole sonication process was carried out for 30 minutes in an ice bath with the pulse setting of ten-second-on-five-second-off so as to prevent a sudden rise of the solution temperature. After the reaction, the white solid particles were collected by a vacuum filtration and washed with a copious amount of methanol. Prior to the membrane fabrication, the nanocrystals were dried in a convection oven at 60 ℃. On the other hand, the synthesis of sub-micron $Zn(pyrz)_2(SiF_6)$ nanocrystals were conducted by referring to our previous work [110].

6.2.3 Synthesis of 6FDA-TMPDA Polyimide

The 6FDA-TMPDA polyimide was synthesized using the method described elsewhere[182-184]. The whole reaction was conducted under argon atmosphere. Firstly, 0.444 g of 6FDA (1 mmol) was added gradually into a

round-bottom flask containing a solution of NMP (1.6 ml) and 0.150 g of TMPDA (1 mmol). The mixture was stirred at room temperature for about 30 minutes and subsequently diluted with NMP (9.6 ml). The mixture was agitated for 5 hours at room temperature until a viscous polyamic acid solution was formed. Next, chemical imidization was conducted by adding a mixture of 0.202 g of triethylamine (2 mmol) and 0.816 g of acetic anhydride (8 mmol) to the polyamic solution at 0 ℃ which was set by ice water. The reaction was conducted for 20 hours to ensure the completion of imidization. Subsequently, the polymer formed was precipitated in methanol and then washed with the same solvent. The polymer was further purified by dissolving the polymer into chloroform and reprecipitating in methanol. The white polymer powder was collected by a vacuum filtration and dried in a vacuum oven at 150 ℃ for 12 hours.

6.2.4 Fabrication of Membranes

A solution casting technique was employed to prepare dense films of mixed-matrix membranes. $Zn(pyrz)_2SiF_6$ nanocrystals were dispersed in DCM using ultrasonic bath. 6FDA-TMPDA polyimide was then added to the suspension following which the mixture was stirred overnight to obtain a homogenous solution. Subsequently, the solution was poured on a glass plate for casting of a nascent film using a "doctor's knife", in a glove bag saturated

with DCM vapor. The membrane film was left in the glove bag for 1 hour for the completion of solvent evaporation and subsequently annealed at 230 °C for 1 day in a vacuum oven.

In order to investigate the effect of smaller nanoparticles on the overall morphology of the mixed-matrix membrane, the fabrication of cross-linked polyethylene oxide (XLPEO) membranes containing submicron $Zn(pyrz)_2(SiF_6)$ were conducted as same as Chapter 5 described.

6.2.5 Characterization

The gas adsorption properties of $Zn(pyrz)_2(SiF_6)$ crystals and membranes were measured by a high-pressure gas adsorption analyzer (Quantachrome, iSorb HP1). After activation of the crystals at 150 ℃ for 15 hours under a dynamic vacuum, pure component CO_2 and CH_4 isotherms were obtained in a pressure range of 0 to 1 bar at 25 ℃ that is precisely controlled by a recirculating fluid. The size of $Zn(pyrz)_2(SiF_6)$ crystals was analyzed using a dynamic light scattering method (BIC PALS Zeta Sizer). Prior to the measurement the crystals were first sonicated and dispersed in methanol. Thermogravimetric analysis (TGA) was carried out using a thermogravimetric/differential thermal analyzer (PerkinElmer, Diamond TG/DTA) under pure nitrogen purging at a temperature range of 30 to 500 ℃ with a ramping rate of 10 ℃ per minute. The powder X-ray diffraction (PXRD)

analysis was performed at a step size of 0.02 °(Bruker D2). The morphology of $Zn(pyrz)_2(SiF_6)$ crystals and the cross-sections of mixed-matrix membranes were observed with a field emission scanning electron microscopy (FESEM, JSM-7600F). Both $Zn(pyrz)_2(SiF_6)$ nanocrystals and mixed-matrix membranes were sputtered with gold prior to the imaging with FESEM. For the case of membranes, the samples were cryogenically fractured in liquid nitrogen prior to goal coating. The density of membranes was determined using a pycnometer [144, 185] so as to investigate the possible dedensification of polymer in mixed-matrix membrane.

6.2.6 Mixture Gas Permeation Tests

Gas permeation tests were carried out using the method and the system descried in our previous work[59, 186]. Helium (He) and CO_2/CH_4 (50/50) mixture gas were purchased from Air Liquide. After mounting a membrane in the testing cell, the vacuum pump was used to remove all residual gases in the permeation system and the membrane. Subsequently, the upstream chamber of the cell was pressurized to 1 bar with the feed gas. The downstream gas permeated through the membrane was swept by He and the composition was analyzed by Gas Chromatograph (GC). The permeability of individual component was calculated based on the flow rate of sweeping gas (He), the properties of membrane (effective exposed area and thickness) and the

composition of permeated gas measured by GC. The temperature of the whole system was maintained at 25 ℃. Three samples of each mixed-matrix membranes were tested so as to check the experimental errors and reproducibility of the results.

6.2.7 Gas Adsorption Analysis

The solubility of gas in membrane in, *S*, was estimated using the following relationship:

$$S = \frac{q\rho}{p} \dots (1)$$

where q is CO_2 uptake per mass of the membrane at the pressure, p is the pressure and ρ is the density of the membrane. The density of mixed-matrix membrane was calculated from the densities of pure 6FDA-TMPDA and $Zn(pyrz)_2(SiF_6)$ reported in literature [187, 188]. From permeability, *P* and solubility, *S* that are expressed as $\mathrm{mol \cdot m/m^2 \cdot s \cdot bar}$ and $\mathrm{mol/m^3 \cdot bar}$ respectively, the diffusivity of gas in membrane, *D*, could be determined by dividing permeability with solubility.

6.2.8 Density of membranes

The density of the membranes (pure polymeric and mixed-matrix membrane) were estimated by using pycnometer, using methanol as the solvent.

The general procedure is as follows: The mass of the membrane, m_m was first weighed using the weighing balance. Next, the membrane was placed into the pycnometer, m_o and was weighed together as $m_o + m_m$. The pycnometer was filled with methanol and registered as m'_m (= $m_m + m_o + m_{methanol}$), which allows the computation of added methanol, $V'_{methanol}$.

$$V'_{methanol} = \frac{m'_m}{\rho_m} \dots (2)$$

where ρ_m is the density of methanol. With this, the volume of the membrane, V_m, can be computed by the difference between $V'_{methanol}$ and the volume of methanol that was used to fill the empty pycnometer, V, as shown in the expression:

$$V_m = V - V'_{methanol} = \frac{m''_m - m'_m}{\rho_m} \dots (3)$$

where m''_m is the mass of the methanol that was used to fill the empty pycnometer. With this, the density of membrane can be calculated using:

$$\rho_m = \frac{m_m}{V_m} \dots (4)$$

With the determination of the density of the mixed-matrix membrane, the density of the polymer in mixed-matrix membrane can be back-calculated using the expression:

$$\rho_m = \rho_p v_p + \rho_f \rho_f \dots (5)$$

where: ρ_m, ρ_p and ρ_f are the density of mixed-matrix membrane, polymer and filler, and v_p and v_f are the mole fractions of polymer and filler in

mixed-matrix membrane. This expression was used considering the assumption that ideal morphology was formed in mixed-matrix membrane.

6.3 Results and Discussion

6.3.1 Synthesis of $Zn(pyrz)_2(SiF_6)$ Nanocrystals

As reported in Chapter 5,[110] the sonochemical synthesis is a facile tool to downsize $Zn(pyrz)_2(SiF_6)$ crystals to a submicron size as well as shorten synthesis time as compared to conventional solvothermal synthesis. Nonetheless, the size of crystal synthesized in the previous work was not small enough to achieve a uniform distribution of fillers into polymer matrix which is desirable to realize a high separation performance. Therefore, in this study, the synthesis method was further optimized to obtain $Zn(pyrz)_2(SiF_6)$ nanocrystals. A major change we made is utilizing a sonication horn which is feasible in creating a strong acoustic cavitation with high-intensity ultrasound thereby creating nano-sized crystallites in a facilitated manner[189].

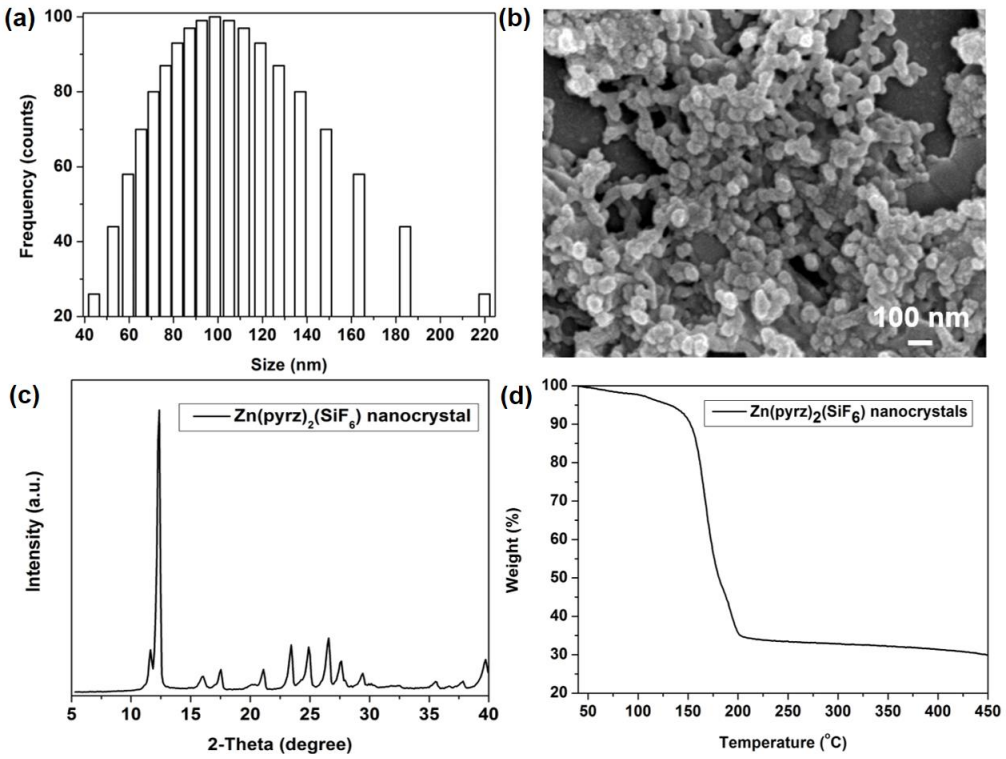

Figure 6-1 (a) Particle size distribution, (b) SEM image, (c) powder X-ray diffraction pattern, and (d) TGA curve of $Zn(pyrz)_2(SiF_6)$ nanocrystals.

Successful formation of nanocrystals by the sonochemical method could be verified with the dynamic light scattering analysis and FESEM imaging. As shown in Fig. 6-1a, the majority of particles was found to be in the range of 70 – 150 nm. FESEM observation on the morphology of nanocrystals also confirmed the formation of nanocrystals of which the average size is about 100 nm (Fig. 6-1b). An XRD analysis revealed that $Zn(pyrz)_2(SiF_6)$ was succesfully synthezed by the sonochemical method (Fig. 6-1c). Note that a significant peak broadening was observed in the XRD pattern, indicating the formation of small crytallites. A thermogravimetric analysis demonstrated a decent thermal

stability of $Zn(pyrz)_2(SiF_6)$ nanocrystals up till 150 ℃ (Fig. 6-1d), which is similar to the previously reported results for bulk and submicron crystals of $Zn(pyrz)_2(SiF_6)$[110]. Overall, the sonochemical method employed in this work was proved to be an effective way to synthesis $Zn(pyrz)_2(SiF_6)$ nanocrystals without sacrificing the integrity of framework.

6.3.2 Gas Adsorption Properties of $Zn(pyrz)_2(SiF_6)$ Nanocrystals

Fig. 6-2 shows CO_2 and CH_4 adsorption isotherms of $Zn(pyrz)_2(SiF_6)$ nanocrystals measured at 25 ℃. A steep rise in CO_2 uptake at low pressure was observed indicating a strong affinity between CO_2 and $Zn(pyrz)_2(SiF_6)$. A slight decrease in CO_2 adsorption (c.a. 0.4 mmol/g at 1 bar) as compared to that for bulk crystals may be attributed to the formation of smaller crystallites that could lead to a decrease in the total pore volume. Note that N_2 physisorption at 77 K couldn't be conducted as N_2 molecules cannot access the pore of $Zn(pyrz)_2SiF_6$ nanocrystals[110]. On the other hand, the CH_4 adsorption on $Zn(pyrz)_2(SiF_6)$ nanocrystal reported to be zero (0 ± 0.01 mmol/g), indicating the pores of $Zn(pyrz)_2(SiF_6)$ nanocrystals are not accessible for CH_4 as reported previously[110]. The results obtained from the gas adsorption analysis suggest that $Zn(pyrz)_2(SiF_6)$ nanocrystals synthesized in this work is a good membrnae material for CO_2/CH_4 separation.

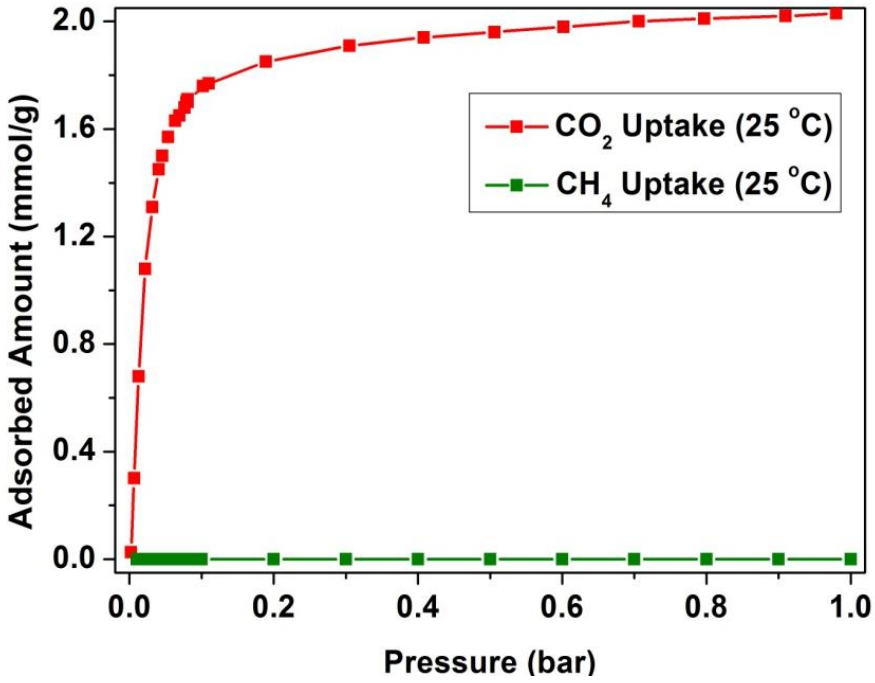

Figure 6-2 CO_2 and CH_4 adsorption of $Zn(pyrz)_2(SiF_6)$ nanocrystals at 25 ℃.

6.3.3 Fabrications of Composite Membranes

In this work, 6FDA-TMPDA polyimide was synthesized and used as the polymer matrix for the fabrication of composite membrane comprising $Zn(pyrz)_2(SiF_6)$ nanocrystals. The stability of the cast solution was investigated via a series of photographic images of the cast solution were conducted at several periods of time as depicted from Fig 6-3. The fillers were remained stable without settling down in the solution even after 1 day, indicating the $Zn(pyrz)_2(SiF_6)$ nanocrystals could be successfully stabilized by the polymer chains in the casting solution. Such excellent stability of the casting solution

may ensure a uniform distribution of the fillers in the resultant mixed-matrix membrane.

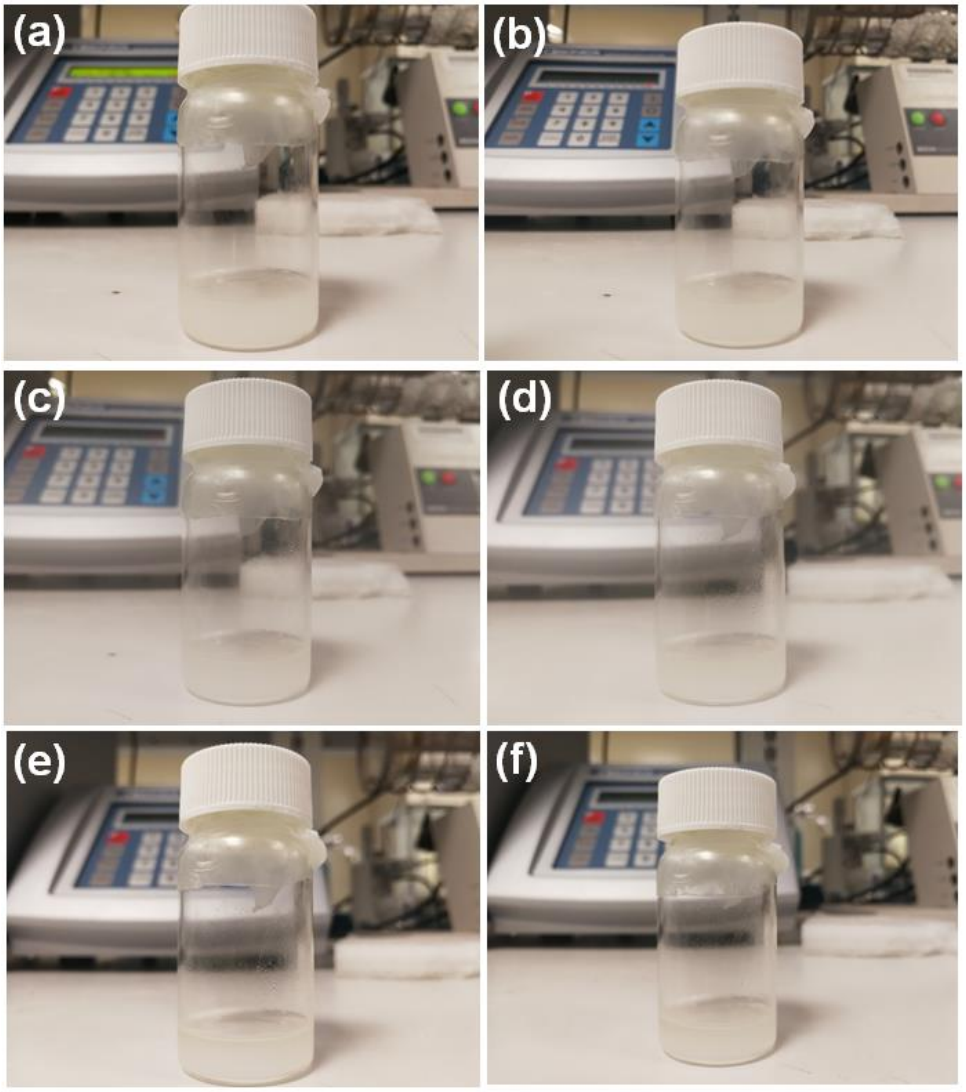

Figure 6-3 Photographic images of the as-made cast solutions after **(a)** 1 hour **(b)** 2 hours **(c)** 4 hours **(d)** 8 hours **(e)** 16 hours and **(f)** 24 hours. The as-made cast solution was based on 20 wt% $Zn(pyrz)_2(SiF_6)$ nanocrystal in DCM containing 15 wt% 6FDA-TMPDA

The cross-section of the fabricated mixed-matrix membrane at 10 and 20 wt% loading of $Zn(pyrz)_2(SiF_6)$ nanocrystals were conducted as shown in Fig. 6-4. “Sieve-in-a-cage” morphology, which typically arises from the poor compatibility between inorganic fillers such as zeolite and polymer,[96, 97, 190] was not observed in this study. This is due to the strong affinity between the organic ligand presented in $Zn(pyrz)_2(SiF_6)$ and 6FDA-TMPDA polymer. It is noteworthy that, as demonstrated in previous studies, downsizing the MOF crystals could help the dispersion of filler within polymer matrix as well as the filler/polymer adhesion as it can effectively increase filler/polymer interface areas[171].

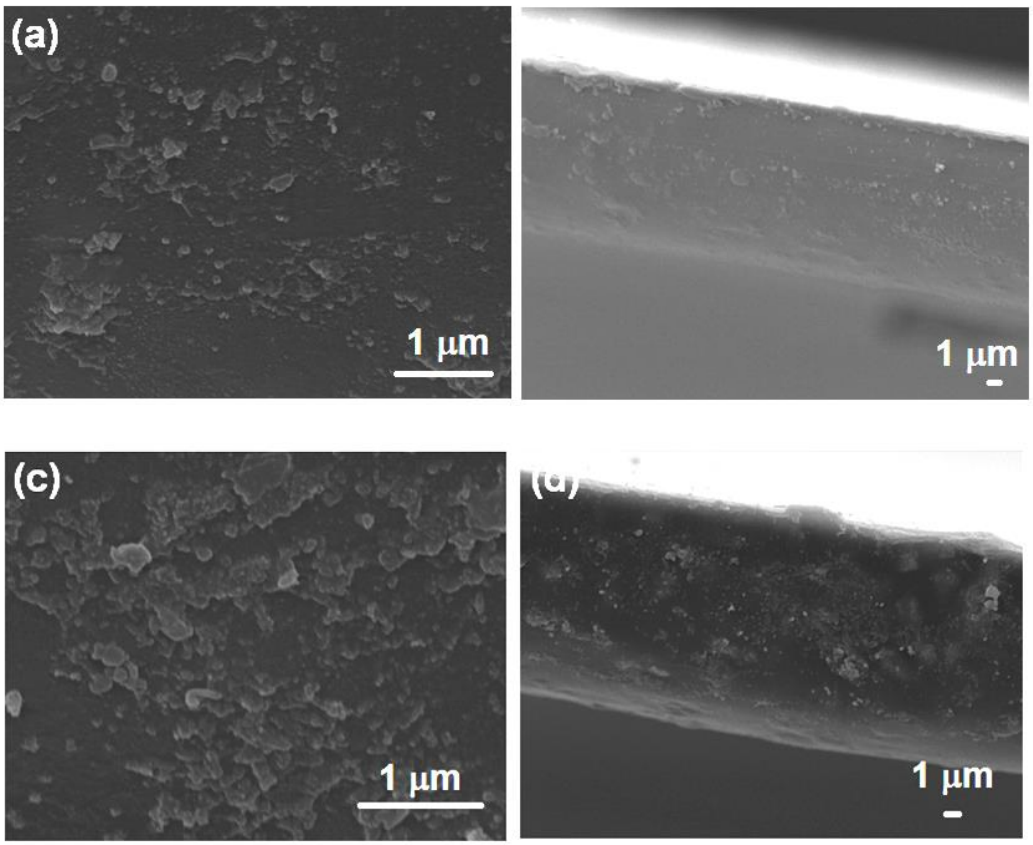

Figure 6-4 FESEM images of the cross-section of 6FDA-TMPDA mixed-matrix membrane containing **(a, b)** 10 wt% $Zn(pyrz)_2(SiF_6)$ nanocrystals and **(c, d)** 20 wt% $Zn(pyrz)_2(SiF_6)$ nanocrystals at **(a, c)** high magnification and **(b, d)** low magnification

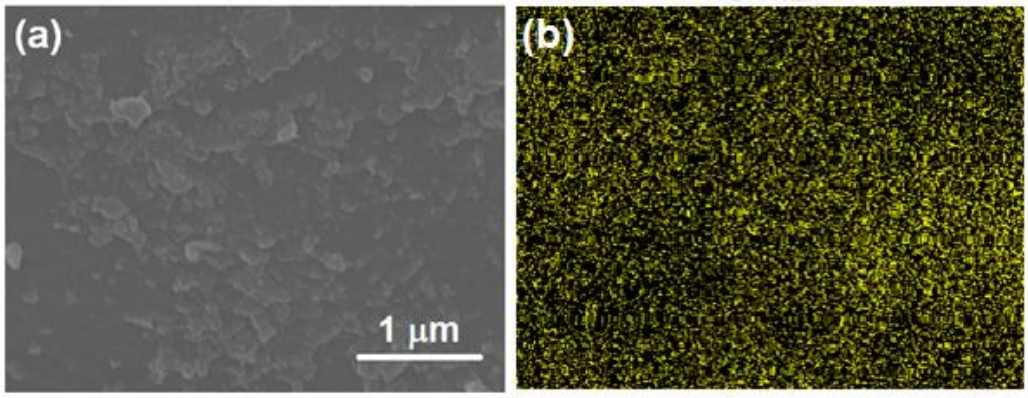

Figure 6-5 EDX mapping of **(a)** 20 wt% $Zn(pyrz)_2(SiF_6)$ nanocrystals in 6FDA-TMPDA membrane with the corresponding elemental distribution of Si **(b)**

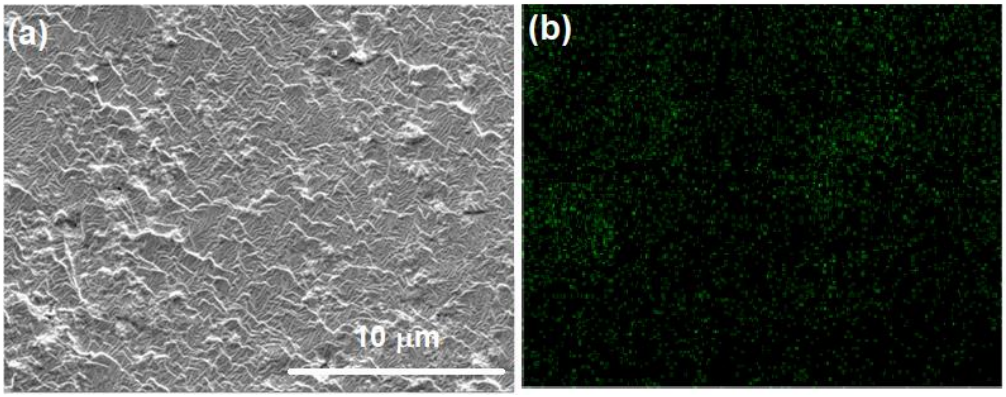

Figure 6-6 EDX mapping of **(a)** 20 wt% sub-micron $Zn(pyrz)_2(SiF_6)$ crystals in XLPEO membrane with the corresponding elemental distribution of Si **(b)**

Indeed, an improved dispersion of $Zn(pyrz)_2(SiF_6)$ nanocrystals within the polymer matrix confirmed by EDX mapping data. As shown in Fig 6-5, Si atoms that are from $Zn(pyrz)_2(SiF_6)$ nanocrystals were uniformmly distributed in 6FDA-TMPDA. In contrast, submicron-sized $Zn(pyrz)_2(SiF_6)$/XLPEO membrane which was reported in our previous work showed a relatively poor distribution of the filler as shown in Fig. 6-6. This result may suggest that downsizing the MOF filler to nanocrystals is an effective way to realize the desired mixed-matrix membrane morphology as the increased filler/polymer interface area can improve the dispersibility of filler within the polymer matrix. Choosing a good solvent in which the MOF crystals are well dispersed is also important to make a homogeneous dope solution leading to a mixed-matrix membrane with a uniform distribution of fillers. In this work, the $Zn(pyrz)_2(SiF_6)$ nanocrystals were readily dispersed in DCM when sonicated.

Fig. 6-7 shows CO_2 and CH_4 uptake properties of membranes measured at 25 ℃. Mixed-matrix membrane containing $Zn(pyrz)_2(SiF_6)$ nanocrystals demonstrated an enhanced CO_2 uptake property as compared to pure polymer membrane, indicating the filler in membrane is still intact and can effectively capture CO_2. Such enhancement was more prominent at high pressure region near 1 bar. Meanwhile, as demonstrate in Fig 6-2, $Zn(pyrz)_2(SiF_6)$ possesses the pore window that is not allowing the access of CH_4 molecules. Thus, the addition of $Zn(pyrz)_2(SiF_6)$ nanocrystals decreased the CH_4 uptake of membrane as shown in Fig. 6-7b. These results indicate that $Zn(pyrz)_2(SiF_6)$ is an ideal filler for designing CO_2/CH_4 separation membrane allowing selective sorption/transportation of CO_2. Detailed quantitative analysis on the sorption and the diffusion of gases within membranes is described in the next section.

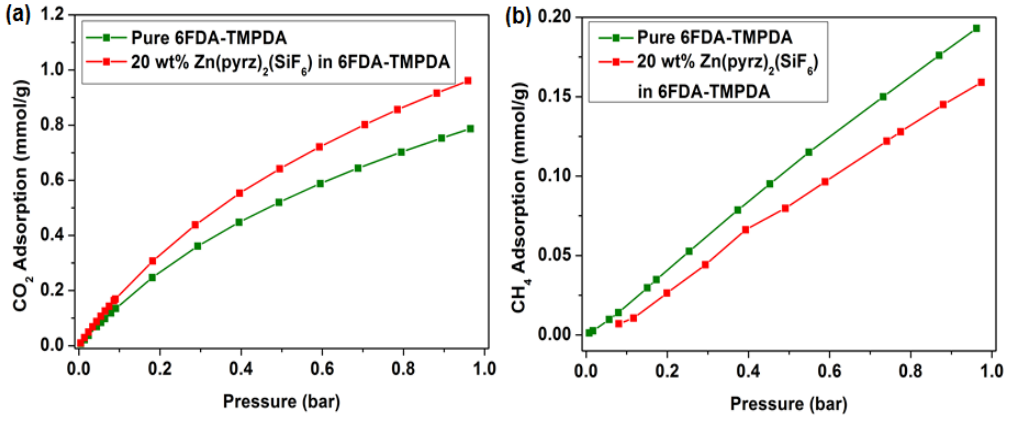

Figure 6-7 Pure component (a) CO_2 and (b) CH_4 adsorption properties of 20wt% $Zn(pyrz)_2(SiF_6)$/6FDA-TMPDA and pure 6FDA-TMPDA membranes at 25 ℃.

6.3.4 Gas Permeation Properties

Table 6-1 demonstrates the CO_2/CH_4 (50:50) mixture gas permeation properties of membranes that are measured at 25 ℃ and 1 bar of total upstream pressure. The CO_2 permeability and the CO_2/CH_4 selectivity of pure polymeric membrane were measured to be 590 barrers and 29, respectively, that were comparable to the reported values[187]. Mixed-matrix membrane containing 10 wt% $Zn(pyrz)_2(SiF_6)$ nanocrystals showed an enhanced performance, such that the CO_2 permeability and the CO_2/CH_4 selectivity increased to 840 barrer and 33, which can be translated into 42.4 % and 13.7 % improvements, respectively. When the loading was further increased to 20 wt%, even higher CO_2 permeability and CO_2/CH_4 selectivity were observed, which are 89.8 % and 31.0 % higher than those of pure polymer membrane, respectively. Note that the performance reported in this work is far better than the data we previously reported with the membrane made up of 20 wt% $Zn(pyrz)_2(SiF_6)$ and XLPEO and thereby surpasses the Robeson upper bound established in 2008. This can be attributed to the synergistic effect from the filler which allows selective sorption/transport of CO_2 over CH_4 and the high performance polymer matrix which has desirable membrane properties.

Table 6-1 Mixture gas (CO_2/CH_4, 50/50) permeation properties of membranes measured at 1 bar upstream pressure and 25 ℃.

Membranes	CO_2 Permeability (barrer)	CH_4 Permeability (barrer)	CO_2/CH_4 Selectivity
Pure 6FDA-TMPDA	590 ± 50	20 ± 2	29 ± 3
10 wt% $Zn(pyrz)_2(SiF_6)$	840 ± 70	25 ± 3	33 ± 3
20 wt% $Zn(pyrz)_2(SiF_6)$	1120 ± 150	29 ± 5	38 ± 5

Subsequently, to understand how such improvement was realized in composite membranes, the diffusivity and the solubility of CO_2 and CH_4 in membranes were quantified using the data presented in Fig. 6-7 and Table 6-1. As summarized in Table 6-3, $Zn(pyrz)_2(SiF_6)$ nanocrystals were effective in improving both the solubility and the diffusivity of CO_2, resulting in a significant increase in CO_2 permeability in mixed-matrix membrane. On the contrary, the addition of $Zn(pyrz)_2(SiF_6)$ nanoparticles decreased the amount of CH_4 sorption in mixed-matrix membrane, despite an increase in the diffusivity of CH_4 in mixed-matrix membrane was observed. This was attributed to the dedensification of the mixed matrix membrane in view of the packing of the polymer chain that had been hindered by the presence of filler. This has been proven by comparing the density of pure polymeric membrane and mixed-matrix membrane, as summarized in Table 6-2. As depicted in Figure 6-8a, an increase in overall permselectivity of the mixed-matrix membrane as compared to pure polymeric membrane is attributed to the noticeable increase

in sorption selectivity despite the filler causes a marginal decrease in CO_2/CH_4 diffusion selectivity.

Table 6-2 Comparison between the density of polymeric membrane and mixed-matrix membrane

Membrane	Density (g cm^{-3})[1]
6FDA-TMPDA	1.316
20 wt% $Zn(pyrz)_2(SiF_6)$ in 6FDA-TMPDA[2]	1.344

Note:

[a] Bulk density of the resultant membrane

[b] By back-calculation, the density of polymer (6FDA-TMPDA) in mixed-matrix membrane can be estimated, assuming perfect adhesion between the filler and polymer. Thus, the density of polymer in mixed-matrix membrane is 1.288 g/cm^3

However, unexpectedly, a significant increase in the diffusivity of CH_4 in mixed-matrix membrane was observed. Note that the pore window of $Zn(pyrz)_2(SiF_6)$ (3.8 Å) is too small to increase the diffusivity of CH_4 of which the kinetic diameter is 3.8 Å. To understand the reason for the increased CH_4 diffusivity in mixed-matrix membrane, we have measured the densities of polymers in both pure polymer and mixed-matrix membranes. As shown in Table 6-2, the polymer was dedensified in the mixed-matrix membrane because the packing of the polymer chains might be hindered by the presence of nano-sized fillers. Such dedensification of polymer might also cause the decrease in CO_2/CH_4 diffusion selectivity in mixed-matrix membrane (Fig. 6-8a).

Table 6-3 CO_2 and CH_4 solubility and diffusivity data for pure 6FDA-TMPDA and 20 wt% $Zn(pyrz)_2(SiF_6)$/6FDA-TMPDA membranes.

Membrane	CO_2 Permeability, x 10^{-8} $(mol \cdot m/m^2 \cdot s \cdot bar)$	CO_2 Solubility $(mol/m^3 \cdot bar)$	CO_2 Diffusivity, x 10^{-11} (m^2/s)	CH_4 Permeability, x 10^{-10} $(mol \cdot m/m^2 \cdot s \cdot bar)$	CH_4 Solubility $(mol/m^3 \cdot bar)$	CH_4 Diffusivity, x 10^{-12} (m^2/s)
6FDA-TMPDA	2.0	610	3.3	6.8	150	4.5
20 wt% $Zn(pyrz)_2(SiF_6)$	3.8	720	5.3	9.8	120	8.2

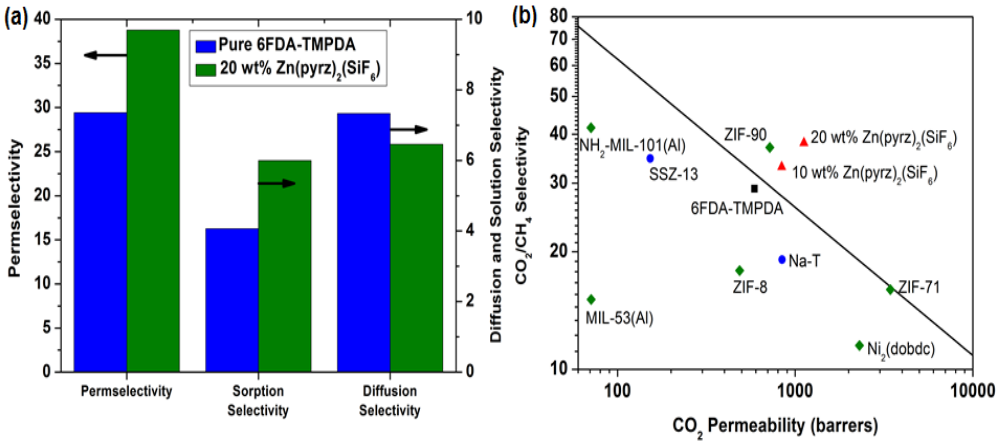

Figure 6-8 (a) Permselectivity, sorption selectivity and diffusion selectivity of membranes and (b) CO_2/CH_4 separation performance of membranes together with literature data for mixed-matrix membrane made up of 6FDA-based polymers; The exact data points are presented in **Table 6-4**. The black solid line represents the Robeson upper bound limit for polymeric membrane established in 2008. [191]

Performances of the membranes were benchmarked against literature data for mixed-matrix membranes made up of 6FDA polyimides of which

CO_2/CH_4 separation properties were reported to be near the upper bound limit established in 2008. As shown in Fig. 6-8b and Table 6-4, performances of our membranes which surpassed the upper bound limit are far better than those of the other composite membranes reported thus far. In fact, most of fillers employed in composite membrane fabrication, except for ZIF-90, were not effective enough to push the performance of resulting mixed-matrix membrane above the upper bound. In contrast, $Zn(pyrz)_2(SiF_6)$ nanocrystals used in this study was proved to be highly efficient in improving performance. This is attributed to the presence of pore window that can effectively sieved CO_2 from CH_4, together with the presence of SiF_6^{2-} anion that possess high affinity towards CO_2. These synergistic effects that is present in $Zn(pyrz)_2(SiF_6)$ nanocrystals possesses the capability of generating a remarkably high CO_2/CH_4 separation capability as compared to other microporous materials. Therefore, $Zn(pyrz)_2(SiF_6)$ nanocrystal can be served as an ideal candidate for mixed-matrix membrane in CO_2/CH_4 separation.

Table 6-4 Comparison of mixed-matrix membrane performance reported in **Figure 6-8 (b).**

Filler	Polymer	Filler loading (wt%)	Testing Condition		Permeability (barrer)	CO_2/CH_4 Selectivity	Ref
			Pressure (bar)	Temperature (^oC)			
Na-T	6FDA-durene	1	3.5	30	843.6	19.1	[192]
SSZ-13	6FDA-DAM: DABA (3:2)	25	4.5	35	153	34.7	[193]
MIL-53(Al)	6FDA-DAM:HAB (1:1)	15	10	35	71.1	15.1	[194]
NH_2-MIL-101 (Al)	6FDA: DSDA (1:1)-4MPD-4,4’	10	3	35	70.9	41.6	[195]
Ni_2(dobdc)	6FDA-durene	21	1	35	2300	11.5	[196]
ZIF-8	6FDA-durene	20	10	35	487	17.9	[197]
ZIF-71	6FDA-durene	20	7	35	3435	16.0	[198]
ZIF-90	6FDA-DAM	15	2	25	720	37.0	[199]
$Zn(pyrz)_2(SiF_6)$	6FDA-TMPDA	10	1	25	840	33.0	This Work
$Zn(pyrz)_2(SiF_6)$	6FDA-TMPDA	20	1	25	1120	38.0	This Work

Note:

DAM: 2,4,5-trimethyl-*m*-phenylenediamine; DABA: 3,5-diaminobenzoic acid; HAB: 3,3’-dihydroxy-4,4’-diamino-biphenyl; DSDA: 3,3’,4,4’-diphenylsulfonetetracarboxylic dianhydride; 4MPD: 2,3,5,6-tetramethyl-*p*-phenylenediamine

As the performance of pure polymeric membranes has been significantly improved by developing novel materials such as thermally rearranged (TR) polymer and polymer of intrinsic microporosity (PIM), best performing

polymer membranes are plotted together with the performance of the composite membranes reported in this paper for more effective benchmarking. As shown in Fig. 6, some state-of-the-art polymer membranes showed the performance surpassing the upper bound limit established in 2008. Nevertheless, the performance our composite membrane comprising 20 wt% $Zn(pyrz)_2(SiF_6)$ nanocrystals is competitive with most of TR polymers and PIMs reported thus far.

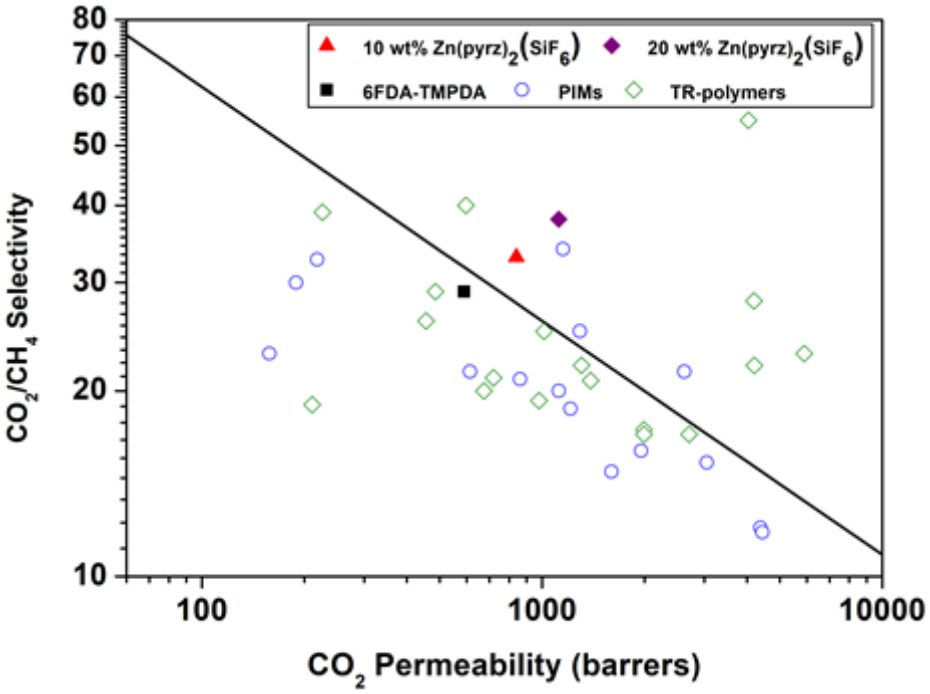

Figure 6-9 CO_2/CH_4 separation of our membranes together with the literature data for high permeable polymers. The exact number are summarized in table 6-5 and 6-6. The black solid line represents the upper bound limit for polymeric membrane constructed in 2008 [17].

Table 6-5 Performance of TR-polymer reported in **Figure 6-9**

TR-polymer	Polymer Structure	Testing Condition		Permeability (barrer)	CO_2/CH_4 Selectivity	Ref
		Pressure (bar)	Temperature (ºC)			
450-3	6FDA + 6FBAHPP	1	-	486	29	[200]
APAF-6FDA	6FDA + APAF	3	35	1993	17	[201]
CPBOc	6FDA + HAB(85) + bisAHPF(15)	3.5	35	1306	22	[202]
HAB:4MPD 1:3	6FDA + HAB(1) + 4MPD(3)	-	35	226	39	[203]
mTR450	6FDA + *m*HAB PBO	1	30	720	21	[204]
PBO400	TAC + bisAPAF	10	35	456	26	[205]
PI-*g*-CD-450	6FDA + DABA + *β*-CD	10	35	2707	17	[82]
PI-S1-425	6FDA + DA-6FDA-DABA +	2	35	1389	20.8	[206]
PPM-γ-CD-425	6FDA + durene(9) + DABA(1) + γ-CD	10	35	4211	22	[207]
Spiro TR-PBO-6F	PMDA + spiro diamino	1	35	675	20	[13]
*s*PBO	6FDA + bisAPAF	1	-	5903	23	[208]
TR-1	BPDA + bisAPAF	1	25	4045	55	[209]
TR-2	BPDA + bisAPAF	1	25	597	40	[209]
TR400	6FDA + HAB-*Pac*	-	35	211	19	[210]
TR450	6FDA + HAB	1	25	1993	17.3	[201]
*t*PBO	6FDA + bisAPAF	1	-	4201	28	[208]
TR-PBO	6FDA + bisAPAF	1	30	1014	25	[211]
XTR-PBO1-10	6FDA + bisAPAF + DABA (10)	1	25	980	19.3	[212]

Note: 6FDA: 4,4'-hexafluoroisopropylidene diphthalic anhydride, 6FBAHPP: 2,2,-bis(4-(4-amino-3-hydroxyphenoxy)-phyenyl)hexafluoropropane, APAF: 2,2-bis(3-amino-4-hydroxyphenyl)hexafluoropropane, HAB: 3,3'-dihydroxybenzidine, bisAHPF: 9,9-bis(3-amino-4-hydroxyphenyl)fluorene, 5MPF: 2,3,5,6-tetramethyl-1,4-phenylenediamine, *m*HAB: 3,3'-diamino-4,4'-dihydroxybiphenyl, TAC: Trimellitic anhydride chloride, DABA: 3,5-diaminobenzoic acid, *β*-CD: *β*-cyclodextrin, DA: durene diamine, γ-CD: γcyclodextrin

Table 6-6 Performance of PIM-polymer reported in **Figure 6-9**

High-Permeable Polymer	Testing Condition		Permeability (barrer)	CO_2/CH_4 Selectivity	Ref
	Pressure (bar)	Temperature (^oC)			
6FDA-DAT1	1	35	189	30	[213]
AO-PIM-1	2	35	1153	34	[214]
CoPI-TB-1	1	35	158	23	[215]
DC-PIM5	-	-	1291	25	[216]
DPPD-TMPD	3	30	1600	14.8	[217]
KAUST-PI-7	2	35	4391	12	[218]
PI-TB-3	1	35	218	32.7	[219]
PIM-CH_3-HPB	1	25	2620	21.5	[220]
PIM-1/Matrimid (90/10)	3.5	35	1953	16	[221]
SBFDA-DMN	2	35	3049	15.3	[222]
SPDA-SBF	2	35	614	21.5	[223]
TBDA1-SB1-PI	1	35	1213	18.7	[224]
TBPIM25	1	35	4441	11.8	[225]
Thioamide-PIM-1	-	-	1120	20	[226]
TPE-PIM	2	35	862	20.9	[227]

Note: DAT-1: 2,6-diaminotriptycene, AO: Amidoxine, TB: Troger's Base, DPPD: 3,8-diphenylpyrene-1,2,6,7-tetracarboxylic dianhydride, TMPD: trimetyl-*m*-phenylenediamine, SPDA: spirobisindane-based dianhydride, SBF: spirobifluorene , DMN: 3,3'-dimethylnaphthidine, TBDA1: 2,8-diamino-4,10-dimethyl-6H,12H-5,11-methanodibenzo[1,5]diazocine, TPE: 3,3,3',3'-tetramethyl-1,1-spirobisindane-5-5'-diamino-6,6'-diol

6.4 Conclusions

$Zn(pyrz)_2(SiF_6)$ nanocrystals that can selectively capture/transport CO_2 over CH_4 were successfully synthesized using a facile sonochemical method. The $Zn(pyrz)_2(SiF_6)$ nanocrystals were proved to be an efficient filler in improving CO_2/CH_4 separation property of polymer membrane, such that the

performance that surpassed the upper bound limit for polymer membranes were realized when it was incorporated into 6FDA-TMPDA polyimide. Detailed analysis revealed that the filler we used effectively enhanced the solubility and the diffusivity of CO_2 as well as CO_2/CH_4 sorption selectivity. Eventually, our future efforts will be devoted to fabricating a thin skin layer containing $Zn(pyrz)_2(SiF_6)$ nanocrystals on the top of a porous support, which is a necessary step to demonstrate the potential utility of our membrane in large industrial applications.

6.5 Declaration

The work presented in this chapter has been accepted in Journal of Industrial and Engineering Chemistry.

Chapter 7

Conclusions and Future Work

7.1 Conclusions

In this thesis, a series of high-performance gas separation composite membranes were developed and all these membranes demonstrated enhanced and promising separation performance toward CO_2/CH_4 or CO_2/N_2 separation, mainly due to the well-matched combination of filler and polymers and the desirable interfacial morphology, which can maximize the effect of the filler. The significant contributions of this thesis, which is the result of four years of study and both successful and unsuccessful attempts, can be summarized as follows:

1. Silane chemistry can be an effective way to decrease the interfacial defects between fillers and polymers, which arise due to the interaction between the amine groups on the external surface of zeolites and the polymer chains. However, the amine grafting conditions, such as post-synthetic amine grafting temperature, amine agents, and amine loadings, and a suitable zeolite candidate are critical to design a successful composite membrane, and their determination requires considerable time and effort.

2. Mesoporous fillers are desirable for amine grafting because when the right size opening pores is available the amine groups can easily enter the pores and can have a coordination effect with the pores toward a high CO_2 affinity, even at low partial pressure.

3. Amine grafting remains a mainstay for improving the adhesion between zeolite and polymers. However, the deposition of inorganic structures to increase the roughness of the zeolites has shown greater potential than traditional amine grafting because of its low cost and the lack of need to wash the organic modifier, which is typically difficult to remove. However, studies in this area are mainly limited to LTA and MFI zeolites.

4. If the modifying conditions (e.g. pH of the reaction medium and the amount of magnesium loaded in the substrates) are not ideal, the metal oxide nanowhisker will have an undesirable morphology which can cover the external surface of the zeolites, and lead to a dramatic decrease in total pore volume.

5. Compared to large crystals, submicron or nano-fillers are more desirable for composite membrane fabrication, as they can effectively reduce the filler sedimentation during the traditional membrane-casting procedure and petri dish procedure, which will lead to a more uniform filler distribution in resulting membranes.

6. MOFs, which are a new emerging class of materials, have shown great potential for composite CO_2 separation membrane. The ideal MOF should possess a critical pore size to enable size or shape discrimination for the targeted gas molecule.

7. High-permeable 6FDA-family polymers are always desirable for high-performance gas separation composite membrane fabrication because they will not block the pores of fillers.

8. For composite membrane fabrication, rubbery Polymers such as XLPEO barely face the problem of interfacial voids. However, the particles may sediment or agglomerate due to the gravity if the crystal size is not ideal.

9. Higher polymer concentration in organic solvents can lead to a higher viscosity which finally result a better filler distribution. On the other hand if the polymer concentration is too high, the as-made membranes's thickness may be nonuniform.

7.2 Recommendations for Future Work and Expectations

Based on the experience thus far, I would recommend that the following work should be pursued in the future:

1. Modify the zeolite and zeolite surface with a facile chemical method: The main method used to improve the surface roughness of zeolites with inorganic nanostructures is the use of the Grignard treatment, which entails complex procedures and sensitive reactants. Except for the treatment used in Chapter 4, other facile chemical treatments, such as hydrothermal treatments and even room-temperature reactions, will be highly attractive. To the best of my knowledge, although this method has been a technique-viable route for improving the interfacial adhesion between the polymers and fillers, limited zeolites (MFI and LTA) have been studied. Other zeolites structures, such as CHA, DDR, RHO and KFI zeolites, which possess ideal pore sizes (from 0.33 to 0.40 nm) for kinetic separation CO_2, are also suitable candidates for this application. Aside from zeolites, titanosilicate and coppersilicate microporous materials, whose structures are highly similar to those of zeolites, have shown great potential for CO_2 separation and composite membrane fabrications [188, 228-230]. However, similar to zeolites, they suffer from poor adhesion to the polymer matrix. Expanding this treatment to these materials is highly possible and attractive to the gas separation membrane community.

2. Explore a new class of MOFs with a 2D shape: As noted in Chapter 3, MOFs are an emerging new class of materials in composite membrane fabrication. The future trend will be to apply chemically and water stable MOFs, such as SIFSIX-3-Cu, ZnAtzOx and ZJU-198, into membranes. The

2D layer structure is extremely favourable as low filler loading can provide several advantages such as low production cost and desirable mechanical stability.

3. Explore the potential application of covalent organic framework in mixed matrix membrane fabrication: Based on the theory of the similarity and the intermiscibility, covalent organic framework which is completely composed of organic components can display even better filler-polymer affinity than metal organic framework [153, 231, 232]. Moreover, another advantage of covalent organic framework is that they can display excellent stability in harsh conditions such as humid and acid [233]. The major efforts for this area may include but not limit to: 1) control of size and shape of crystals since the nanocrystals which are less than 100 nm are highly desirable for membrane fabrications and 2) explore new classes of covalent organic frameworks possessing ideal pore size and desirable CO_2 affinity.

4. Asymmetric membrane fabrication: to date, majority composite membranes developed are fabricated in dense form and stayed in the labs. However, asymmetric membranes that give a high permeation flux is required for industrial applications. It would be more attractive to fabricate membranes in a hollow fibre configuration which can provide the highest packing density allowing a small footprint of entire membrane system.

Reference

[1] A. Sieminski, Annual Energy Outlook 2015, US Energy Information Administration, (2015).

[2] G.P. Peters, R.M. Andrew, T. Boden, J.G. Canadell, P. Ciais, C. Le Quéré, G. Marland, M.R. Raupach, C. Wilson, The challenge to keep global warming below 2 C, Nature Climate Change, 3 (2013) 4-6.

[3] J.T. Houghton, Y. Ding, D.J. Griggs, M. Noguer, P.J. van der Linden, X. Dai, K. Maskell, C. Johnson, Climate change 2001: the scientific basis, The Press Syndicate of the University of Cambridge, 2001.

[4] C.W. Jones, CO_2 capture from dilute gases as a component of modern global carbon management, Annual Review of Chemical and Biomolecular Engineering, 2 (2011) 31-52.

[5] P. Feron, C. Hendriks, CO2 capture process principles and costs, Oil & Gas Science And Technology, 60 (2005) 451-459.

[6] N. McCann, M. Maeder, M. Attalla, Simulation of enthalpy and capacity of CO_2 absorption by aqueous amine systems, Industrial & engineering chemistry research, 47 (2008) 2002-2009.

[7] T. Kosugi, A. Hayashi, T. Matsumoto, K. Akimoto, K. Tokimatsu, H. Yoshida, T. Tomoda, Y. Kaya, Time to realization: Evaluation of CO_2 capture technology R&Ds by GERT (Graphical Evaluation and Review Technique) analyses, Energy, 29 (2004) 1297-1308.

[8] S. Wong, Building Capacity for CO_2 Capture and Storage in the APEC Region, Asia-Pacific Economic Cooperation, (2009).

[9] M. Gupta, I. Coyle, K. Thambimuthu, CO_2 capture technologies and opportunities in Canada, in: 1st Canadian CC&S Technology Roadmap Workshop, 2003, pp. 19.

[10] L.S. White, K.D. Amo, T. Wu, T.C. Merkel, Extended field trials of Polaris sweep modules for carbon capture, Journal of Membrane Science, 542 (2017).

[11] L.S. White, X. Wei, S. Pande, T. Wu, T.C. Merkel, Extended flue gas trials with a membrane-based pilot plant at a one-ton-per-day carbon capture rate, Journal of Membrane Science, 496 (2015) 48-57.

[12] L.M. Robeson, Correlation of separation factor versus permeability for polymeric membranes, Journal of membrane science, 62 (1991) 165-185.

[13] S. Li, H.J. Jo, S.H. Han, C.H. Park, S. Kim, P.M. Budd, Y.M. Lee, Mechanically robust thermally rearranged (TR) polymer membranes with spirobisindane for gas separation, Journal of membrane science, 434 (2013) 137-147.

[14] X. Zhu, C. Tian, S.M. Mahurin, S.-H. Chai, C. Wang, S. Brown, G.M. Veith, H. Luo, H. Liu, S. Dai, A superacid-catalyzed synthesis of porous membranes based on triazine frameworks for CO_2 separation, Journal of the American Chemical Society, 134 (2012) 10478-10484.

[15] L.M. Robeson, M.E. Dose, B.D. Freeman, D.R. Paul, Analysis of the transport properties of thermally rearranged (TR) polymers and polymers of intrinsic microporosity (PIM) relative to upper bound performance, Journal of Membrane Science, 525 (2017) 18-24.

[16] S. Wang, X. Li, H. Wu, Z. Tian, Q. Xin, G. He, D. Peng, S. Chen, Y. Yin, Z. Jiang, Advances in high permeability polymer-based membrane materials for CO_2 separations, Energy & Environmental Science, 9 (2016) 1863-1890.

[17] L.M. Robeson, The upper bound revisited, Journal of Membrane Science, 320 (2008) 390-400.

[18] M.A. Carreon, S. Li, J.L. Falconer, R.D. Noble, Alumina-supported SAPO-34 membranes for CO_2/CH_4 separation, Journal of the American Chemical Society, 130 (2008) 5412-5413.

[19] M. Bernal, J. Coronas, M. Menendez, J. Santamaria, Separation of CO2/N2 mixtures using MFI‐type zeolite membranes, AIChE journal, 50 (2004) 127-135.

[20] Y. Hasegawa, T. Tanaka, K. Watanabe, B.-H. Jeong, K. Kusakabe, S. Morooka, Separation of CO_2-CH_4 and CO_2-N_2 systems using ion-exchanged

FAU-type zeolite membranes with different Si/Al ratios, Korean Journal of Chemical Engineering, 19 (2002) 309-313.

[21] S. Himeno, T. Tomita, K. Suzuki, K. Nakayama, K. Yajima, S. Yoshida, Synthesis and permeation properties of a DDR-type zeolite membrane for separation of CO_2/CH_4 gaseous mixtures, Industrial & Engineering Chemistry Research, 46 (2007) 6989-6997.

[22] T. Tomita, K. Nakayama, H. Sakai, Gas separation characteristics of DDR type zeolite membrane, Microporous and Mesoporous Materials, 68 (2004) 71-75.

[23] K. Sato, K. Aoki, K. Sugimoto, K. Izumi, S. Inoue, J. Saito, S. Ikeda, T. Nakane, Dehydrating performance of commercial LTA zeolite membranes and application to fuel grade bio-ethanol production by hybrid distillation/vapor permeation process, Microporous and Mesoporous Materials, 115 (2008) 184-188.

[24] B. Huang, Q. Liu, J. Caro, A. Huang, Iso-butanol dehydration by pervaporation using zeolite LTA membranes prepared on 3-aminopropyltriethoxysilane-modified alumina tubes, Journal of Membrane Science, 455 (2014) 200-206.

[25] D. Wu, G. Maurin, Q. Yang, C. Serre, H. Jobic, C. Zhong, Computational exploration of a Zr-carboxylate based metal-organic framework as a membrane material for CO_2 capture, Journal of Materials Chemistry A, 2 (2014) 1657-1661.

[26] D. Paul, D. Kemp, The diffusion time lag in polymer membranes containing adsorptive fillers, in: Journal of Polymer Science: Polymer Symposia, Wiley Online Library, 1973, pp. 79-93.

[27] X.Y. Chen, H. Vinhthang, A.A. Ramirez, D. Rodrigue, S. Kaliaguine, Membrane gas separation technologies for biogas upgrading, Rsc Advances, 5 (2015) 24399-24448.

[28] R. Mahajan, Formation, characterization and modeling of mixed matrix membrane materials, 2000.

[29] T.-S. Chung, L.Y. Jiang, Y. Li, S. Kulprathipanja, Mixed matrix membranes (MMMs) comprising organic polymers with dispersed inorganic fillers for gas separation, Progress in Polymer Science, 32 (2007) 483-507.

[30] D.H. Olson, M.A. Camblor, L.A. Villaescusa, G.H. Kuehl, Light hydrocarbon sorption properties of pure silica Si-CHA and ITQ-3 and high silica ZSM-58, Microporous and Mesoporous Materials, 67 (2004) 27-33.

[31] P.A. Barrett, T. Boix, M. Puche, D.H. Olson, E. Jordan, H. Koller, M.A. Camblor, ITQ-12: a new microporous silica polymorph potentially useful for light hydrocarbon separations, Chemical Communications, (2003) 2114-2115.

[32] N. Heymans, B. Alban, S. Moreau, G. De Weireld, Experimental and theoretical study of the adsorption of pure molecules and binary systems containing methane, carbon monoxide, carbon dioxide and nitrogen. Application to the syngas generation, Chemical engineering science, 66 (2011) 3850-3858.

[33] A. Alonso-Vicario, J.R. Ochoa-Gómez, S. Gil-Río, O. Gómez-Jiménez-Aberasturi, C. Ramírez-López, J. Torrecilla-Soria, A. Domínguez, Purification and upgrading of biogas by pressure swing adsorption on synthetic and natural zeolites, Microporous and Mesoporous Materials, 134 (2010) 100-107.

[34] T. Montanari, E. Finocchio, E. Salvatore, G. Garuti, A. Giordano, C. Pistarino, G. Busca, CO_2 separation and landfill biogas upgrading: a comparison of 4A and 13X zeolite adsorbents, Energy, 36 (2011) 314-319.

[35] V. Mulgundmath, F. Tezel, T. Saatcioglu, T. Golden, Adsorption and separation of CO_2/N_2 and CO_2/CH_4 by 13X zeolite, The Canadian Journal of Chemical Engineering, 90 (2012) 730-738.

[36] M. Palomino, A. Corma, F. Rey, S. Valencia, New Insights on CO_2−Methane Separation Using LTA Zeolites with Different Si/Al Ratios and a First Comparison with MOFs, Langmuir, 26 (2009) 1910-1917.

[37] G. Calleja, J. Pau, J. Calles, Pure and multicomponent adsorption equilibrium of carbon dioxide, ethylene, and propane on ZSM-5 zeolites with

different Si/Al ratios, Journal of Chemical & Engineering Data, 43 (1998) 994-1003.

[38] T. Remy, S.A. Peter, L. Van Tendeloo, S. Van der Perre, Y. Lorgouilloux, C.E. Kirschhock, G.V. Baron, J.F. Denayer, Adsorption and separation of CO_2 on KFI zeolites: effect of cation type and Si/Al ratio on equilibrium and kinetic properties, Langmuir, 29 (2013) 4998-5012.

[39] J. Shang, G. Li, R. Singh, P. Xiao, J.Z. Liu, P.A. Webley, Determination of composition range for "molecular trapdoor" effect in chabazite zeolite, The Journal of Physical Chemistry C, 117 (2013) 12841-12847.

[40] A. Zukal, J. Pawlesa, J. Čejka, Isosteric heats of adsorption of carbon dioxide on zeolite MCM-22 modified by alkali metal cations, Adsorption, 15 (2009) 264-270.

[41] Q. Wang, J. Luo, Z. Zhong, A. Borgna, CO_2 capture by solid adsorbents and their applications: current status and new trends, Energy & Environmental Science, 4 (2011) 42-55.

[42] M.M. Lozinska, J.P. Mowat, P.A. Wright, S.P. Thompson, J.L. Jorda, M. Palomino, S. Valencia, F. Rey, Cation Gating and Relocation during the Highly Selective "Trapdoor" Adsorption of CO_2 on Univalent Cation Forms of Zeolite Rho, Chemistry of Materials, 26 (2014) 2052-2061.

[43] J. Shang, G. Li, R. Singh, Q. Gu, K.M. Nairn, T.J. Bastow, N. Medhekar, C.M. Doherty, A.J. Hill, J.Z. Liu, Discriminative separation of gases by a "molecular trapdoor" mechanism in chabazite zeolites, Journal of the American Chemical Society, 134 (2012) 19246-19253.

[44] J. Shang, G. Li, Q. Gu, R. Singh, P. Xiao, J.Z. Liu, P.A. Webley, Temperature controlled invertible selectivity for adsorption of N_2 and CH_4 by molecular trapdoor chabazites, Chemical Communications, 50 (2014) 4544-4546.

[45] T.-H. Bae, M.R. Hudson, J.A. Mason, W.L. Queen, J.J. Dutton, K. Sumida, K.J. Micklash, S.S. Kaye, C.M. Brown, J.R. Long, Evaluation of

cation-exchanged zeolite adsorbents for post-combustion carbon dioxide capture, Energy & Environmental Science, 6 (2013) 128-138.

[46] K.S. Walton, M.B. Abney, M.D. LeVan, CO_2 adsorption in Y and X zeolites modified by alkali metal cation exchange, Microporous and Mesoporous Materials, 91 (2006) 78-84.

[47] S.K. Wirawan, D. Creaser, CO_2 adsorption on silicalite-1 and cation exchanged ZSM-5 zeolites using a step change response method, Microporous and mesoporous materials, 91 (2006) 196-205.

[48] J. Yang, J. Li, W. Wang, L. Li, J. Li, Adsorption of CO_2, CH_4, and N_2 on 8-, 10-, and 12-membered ring hydrophobic microporous high-silica zeolites: DDR, silicalite-1, and beta, Industrial & Engineering Chemistry Research, 52 (2013) 17856-17864.

[49] C.A. Grande, Biogas upgrading by pressure swing adsorption, INTECH Open Access Publisher, 2011.

[50] M.R. Hudson, W.L. Queen, J.A. Mason, D.W. Fickel, R.F. Lobo, C.M. Brown, Unconventional, highly selective CO_2 adsorption in zeolite SSZ-13, Journal of the American Chemical Society, 134 (2012) 1970-1973.

[51] A.I. Skoulidas, D.S. Sholl, Molecular dynamics simulations of self-diffusivities, corrected diffusivities, and transport diffusivities of light gases in four silica zeolites to assess influences of pore shape and connectivity, The Journal of Physical Chemistry A, 107 (2003) 10132-10141.

[52] J. Kärger, D.M. Ruthven, D.N. Theodorou, Diffusion in nanoporous materials, John Wiley & Sons, 2012.

[53] D. Wang, P. Tian, M. Yang, S. Xu, D. Fan, X. Su, Y. Yang, C. Wang, Z. Liu, Synthesis of SAPO-34 with alkanolamines as novel templates and their application for CO 2 separation, Microporous and Mesoporous Materials, 194 (2014) 8-14.

[54] S. Himeno, T. Tomita, K. Suzuki, S. Yoshida, Characterization and selectivity for methane and carbon dioxide adsorption on the all-silica DD3R zeolite, Microporous and Mesoporous Materials, 98 (2007) 62-69.

[55] Z. Bao, L. Yu, T. Dou, Y. Gong, Q. Zhang, Q. Ren, X. Lu, S. Deng, Adsorption equilibria of CO_2, CH_4, N_2, O_2, and Ar on high silica zeolites, Journal of Chemical & Engineering Data, 56 (2011) 4017-4023.

[56] Q. Liu, T. Pham, M.D. Porosoff, R.F. Lobo, ZK‐5: A CO_2‐Selective Zeolite with High Working Capacity at Ambient Temperature and Pressure, ChemSusChem, 5 (2012) 2237-2242.

[57] M.M. Lozinska, E. Mangano, J.P. Mowat, A.M. Shepherd, R.F. Howe, S.P. Thompson, J.E. Parker, S. Brandani, P.A. Wright, Understanding carbon dioxide adsorption on univalent cation forms of the flexible zeolite Rho at conditions relevant to carbon capture from flue gases, Journal of the American Chemical Society, 134 (2012) 17628-17642.

[58] S.-T. Yang, J. Kim, W.-S. Ahn, CO_2 adsorption over ion-exchanged zeolite beta with alkali and alkaline earth metal ions, Microporous and Mesoporous Materials, 135 (2010) 90-94.

[59] T.H. Nguyen, H. Gong, S.S. Lee, T.-H. Bae, Amine-Appended Hierarchical Ca-A Zeolite for Enhancing CO_2/CH_4 Selectivity of Mixed-Matrix Membranes, ChemPhysChem, 17 (2016) 3165-3169.

[60] D. Serrano, P. Pizarro, Synthesis strategies in the search for hierarchical zeolites, Chemical Society Reviews, 42 (2013) 4004-4035.

[61] K. Na, M. Choi, R. Ryoo, Recent advances in the synthesis of hierarchically nanoporous zeolites, Microporous and Mesoporous Materials, 166 (2013) 3-19.

[62] B. Sulikowski, The fractal dimension in molecular sieves: synthetic faujasite and related solids, The Journal of Physical Chemistry, 97 (1993) 1420-1425.

[63] M. Ogura, S.-y. Shinomiya, J. Tateno, Y. Nara, E. Kikuchi, M. Matsukata, Formation of uniform mesopores in ZSM-5 zeolite through treatment in alkaline solution, Chemistry letters, 29 (2000) 882-883.

[64] A. Huczko, Template-based synthesis of nanomaterials, Applied Physics A, 70 (2000) 365-376.

[65] Z. Li, H. Gong, T. Mu, Y. Luan, Ionic liquid-assisted synthesis of unusual Pd particles with enhanced electrocatalytic performance for ethanol and methanol oxidation, CrystEngComm, 16 (2014) 4038-4044.

[66] A. Janssen, I. Schmidt, C. Jacobsen, A. Koster, K. De Jong, Exploratory study of mesopore templating with carbon during zeolite synthesis, Microporous and mesoporous materials, 65 (2003) 59-75.

[67] I. Schmidt, A. Boisen, E. Gustavsson, K. Ståhl, S. Pehrson, S. Dahl, A. Carlsson, C.J. Jacobsen, Carbon nanotube templated growth of mesoporous zeolite single crystals, Chemistry of Materials, 13 (2001) 4416-4418.

[68] C.J. Jacobsen, C. Madsen, J. Houzvicka, I. Schmidt, A. Carlsson, Mesoporous zeolite single crystals, Journal of the American Chemical Society, 122 (2000) 7116-7117.

[69] S. Basu, A.L. Khan, A. Cano-Odena, C. Liu, I.F. Vankelecom, Membrane-based technologies for biogas separations, Chemical Society Reviews, 39 (2010) 750-768.

[70] B. Ozturk, F. Demirciyeva, Comparison of biogas upgrading performances of different mixed matrix membranes, Chemical engineering journal, 222 (2013) 209-217.

[71] Y. Li, T.S. Chung, S. Kulprathipanja, Novel Ag+ ‐ zeolite/polymer mixed matrix membranes with a high CO_2/CH_4 selectivity, AIChE Journal, 53 (2007) 610-616.

[72] H. Karkhanechi, H. Kazemian, H. Nazockdast, M.R. Mozdianfard, S.M. Bidoki, Fabrication of Homogenous Polymer ‐ Zeolite Nanocomposites as Mixed ‐ Matrix Membranes for Gas Separation, Chemical Engineering & Technology, 35 (2012) 885-892.

[73] Y. Zhang, K.J. Balkus, I.H. Musselman, J.P. Ferraris, Mixed-matrix membranes composed of Matrimid® and mesoporous ZSM-5 nanoparticles, Journal of Membrane Science, 325 (2008) 28-39.

[74] M. Junaidi, C. Leo, S. Kamal, A. Ahmad, T. Chew, Carbon dioxide removal from methane by using polysulfone/SAPO-44 mixed matrix membranes, Fuel processing technology, 112 (2013) 1-6.

[75] M. Junaidi, C. Leo, A. Ahmad, S. Kamal, T. Chew, Carbon dioxide separation using asymmetric polysulfone mixed matrix membranes incorporated with SAPO-34 zeolite, Fuel Processing Technology, 118 (2014) 125-132.

[76] M. Junaidi, C. Khoo, C. Leo, A. Ahmad, The effects of solvents on the modification of SAPO-34 zeolite using 3-aminopropyl trimethoxy silane for the preparation of asymmetric polysulfone mixed matrix membrane in the application of CO 2 separation, Microporous and Mesoporous Materials, 192 (2014) 52-59.

[77] L.Y. Jiang, T.S. Chung, S. Kulprathipanja, Fabrication of mixed matrix hollow fibers with intimate polymer–zeolite interface for gas separation, AIChE journal, 52 (2006) 2898-2908.

[78] H. Hosseinzadeh Beiragh, M. Omidkhah, R. Abedini, T. Khosravi, S. Pakseresht, Synthesis and characterization of poly (ether‐block‐amide) mixed matrix membranes incorporated by nanoporous ZSM‐5 particles for CO_2/CH_4 separation, Asia‐Pacific Journal of Chemical Engineering, (2016).

[79] A.E. Amooghin, M. Omidkhah, A. Kargari, Enhanced CO_2 transport properties of membranes by embedding nano-porous zeolite particles into Matrimid® 5218 matrix, RSC Advances, 5 (2015) 8552-8565.

[80] D. Şen, H. Kalıpçılar, L. Yilmaz, Development of polycarbonate based zeolite 4A filled mixed matrix gas separation membranes, Journal of Membrane Science, 303 (2007) 194-203.

[81] B. Zornoza, B. Seoane, J.M. Zamaro, C. Tél lez, J. Coronas, Combination of MOFs and Zeolites for Mixed‐Matrix Membranes, ChemPhysChem, 12 (2011) 2781-2785.

[82] O.G. Nik, X.Y. Chen, S. Kaliaguine, Amine-functionalized zeolite FAU/EMT-polyimide mixed matrix membranes for CO_2/CH_4 separation, Journal of Membrane Science, 379 (2011) 468-478.

[83] Y.C. Hudiono, T.K. Carlisle, J.E. Bara, Y. Zhang, D.L. Gin, R.D. Noble, A three-component mixed-matrix membrane with enhanced CO_2 separation properties based on zeolites and ionic liquid materials, Journal of Membrane Science, 350 (2010) 117-123.

[84] M. Hussain, A. Koenig, Mixed‐Matrix Membrane for Gas Separation: Polydimethylsiloxane Filled with Zeolite, Chemical Engineering & Technology, 35 (2012) 561-569.

[85] T.H. Bae, J.Q. Liu, J.S. Lee, W.J. Koros, C.W. Jones, S. Nair, Facile High-Yield Solvothermal Deposition of Inorganic Nanostructures on Zeolite Crystals for Mixed Matrix Membrane Fabrication, Journal of the American Chemical Society, 131 (2009) 14662-+.

[86] R.T. Adams, J.S. Lee, T.-H. Bae, J.K. Ward, J.R. Johnson, C.W. Jones, S. Nair, W.J. Koros, CO_2–CH_4 permeation in high zeolite 4A loading mixed matrix membranes, Journal of Membrane Science, 367 (2011) 197-203.

[87] Y. Shen, A.C. Lua, Preparation and characterization of mixed matrix membranes based on PVDF and three inorganic fillers (fumed nonporous silica, zeolite 4A and mesoporous MCM-41) for gas separation, Chemical engineering journal, 192 (2012) 201-210.

[88] B. Zornoza, C. Tébez, J. Coronas, O. Esekhile, W.J. Koros, Mixed matrix membranes based on 6FDA polyimide with silica and zeolite microsphere dispersed phases, AIChE Journal, 61 (2015) 4481-4490.

[89] B. Zornoza, O. Esekhile, W.J. Koros, C. Tébez, J. Coronas, Hollow silicalite-1 sphere-polymer mixed matrix membranes for gas separation, Separation and Purification Technology, 77 (2011) 137-145.

[90] Y. Li, H.-M. Guan, T.-S. Chung, S. Kulprathipanja, Effects of novel silane modification of zeolite surface on polymer chain rigidification and partial pore

blockage in polyethersulfone (PES)–zeolite A mixed matrix membranes, Journal of Membrane Science, 275 (2006) 17-28.

[91] O.G. Nik, B. Nohair, S. Kaliaguine, Aminosilanes grafting on FAU/EMT zeolite: effect on CO_2 adsorptive properties, Microporous and Mesoporous Materials, 143 (2011) 221-229.

[92] E. Karatay, H. Kalıpçılar, L. Yılmaz, Preparation and performance assessment of binary and ternary PES-SAPO 34-HMA based gas separation membranes, Journal of Membrane Science, 364 (2010) 75-81.

[93] H.H. Yong, H.C. Park, Y.S. Kang, J. Won, W.N. Kim, Zeolite-filled polyimide membrane containing 2, 4, 6-triaminopyrimidine, Journal of Membrane Science, 188 (2001) 151-163.

[94] S. Shu, S. Husain, W.J. Koros, A general strategy for adhesion enhancement in polymeric composites by formation of nanostructured particle surfaces, The journal of physical chemistry C, 111 (2007) 652-657.

[95] S. Shu, S. Husain, W.J. Koros, Formation of nanostructured zeolite particle surfaces via a halide/grignard route, Chemistry of materials, 19 (2007) 4000-4006.

[96] T.-H. Bae, J. Liu, J.S. Lee, W.J. Koros, C.W. Jones, S. Nair, Facile high-yield solvothermal deposition of inorganic nanostructures on zeolite crystals for mixed matrix membrane fabrication, Journal of the American Chemical Society, 131 (2009) 14662-14663.

[97] M.E. Lydon, K.A. Unocic, T.-H. Bae, C.W. Jones, S. Nair, Structure–Property Relationships of Inorganically Surface-Modified Zeolite Molecular Sieves for Nanocomposite Membrane Fabrication, The Journal of Physical Chemistry C, 116 (2012) 9636-9645.

[98] Y.C. Hudiono, T.K. Carlisle, A.L. LaFrate, D.L. Gin, R.D. Noble, Novel mixed matrix membranes based on polymerizable room-temperature ionic liquids and SAPO-34 particles to improve CO_2 separation, Journal of Membrane Science, 370 (2011) 141-148.

[99] S. Ma, H.-C. Zhou, Gas storage in porous metal–organic frameworks for clean energy applications, Chemical Communications, 46 (2010) 44-53.

[100] J. Caro, Are MOF membranes better in gas separation than those made of zeolites?, Current Opinion in Chemical Engineering, 1 (2011) 77-83.

[101] L.E. Kreno, K. Leong, O.K. Farha, M. Allendorf, R.P. Van Duyne, J.T. Hupp, Metal–organic framework materials as chemical sensors, Chemical reviews, 112 (2011) 1105-1125.

[102] Y. He, J. Shang, Q. Gu, Q. Zhao, K. Xie, G. Li, R. Singh, P. Xiao, P.A. Webley, Exchange Method Using Acid‐Solvent Synergy for Metal Gu, Q. Zhao, K. Xie, G. Li, R. Si‐MOFs) Based on a Typical Pillar‐Layered Parent Structure, European Journal of Inorganic Chemistry, 2016 (2016) 1466-1469.

[103] N.A. Khan, S.H. Jhung, Synthesis of metal-organic frameworks (MOFs) with microwave or ultrasound: Rapid reaction, phase-selectivity, and size reduction, Coordination Chemistry Reviews, 285 (2015) 11-23.

[104] Y. Yoo, Z. Lai, H.-K. Jeong, Fabrication of MOF-5 membranes using microwave-induced rapid seeding and solvothermal secondary growth, Microporous and Mesoporous Materials, 123 (2009) 100-106.

[105] J. Kim, H.-Y. Cho, W.-S. Ahn, Synthesis and adsorption/catalytic properties of the metal organic framework CuBTC, Catalysis Surveys from Asia, 16 (2012) 106-119.

[106] Z. Ni, R.I. Masel, Rapid production of metal− organic frameworks via microwave-assisted solvothermal synthesis, Journal of the American Chemical Society, 128 (2006) 12394-12395.

[107] B. Zornoza, A. Martinez-Joaristi, P. Serra-Crespo, C. Tellez, J. Coronas, J. Gascon, F. Kapteijn, Functionalized flexible MOFs as fillers in mixed matrix membranes for highly selective separation of CO_2 from CH_4 at elevated pressures, Chemical Communications, 47 (2011) 9522-9524.

[108] N.A. Khan, S.-H. Jhung, Facile Syntheses of Metal-organic Framework $Cu_3(BTC)_2(H_2O)_3$ under Ultrasound, Bulletin of the Korean Chemical Society, 30 (2009) 2921-2926.

[109] J.-S. Choi, W.-J. Son, J. Kim, W.-S. Ahn, Metal–organic framework MOF-5 prepared by microwave heating: factors to be considered, Microporous and Mesoporous Materials, 116 (2008) 727-731.

[110] H. Gong, T.H. Nguyen, R. Wang, T.-H. Bae, Separations of binary mixtures of CO_2/CH_4 and CO_2/N_2 with mixed-matrix membranes containing Zn $(pyrz)_2(SiF_6)$ metal-organic framework, Journal of Membrane Science, 495 (2015) 169-175.

[111] H.-Y. Cho, J. Kim, S.-N. Kim, W.-S. Ahn, High yield 1-L scale synthesis of ZIF-8 via a sonochemical route, Microporous and Mesoporous Materials, 169 (2013) 180-184.

[112] E. Haque, N.A. Khan, C.M. Kim, S.H. Jhung, Syntheses of Metal–Organic Frameworks and Aluminophosphates under Microwave Heating: Quantitative Analysis of Accelerations, Crystal Growth & Design, 11 (2011) 4413-4421.

[113] D.-W. Jung, D.-A. Yang, J. Kim, J. Kim, W.-S. Ahn, Facile synthesis of MOF-177 by a sonochemical method using 1-methyl-2-pyrrolidinone as a solvent, Dalton Transactions, 39 (2010) 2883-2887.

[114] J. Gordon, H. Kazemian, S. Rohani, Rapid and efficient crystallization of MIL-53 (Fe) by ultrasound and microwave irradiation, Microporous and Mesoporous Materials, 162 (2012) 36-43.

[115] T. Chalati, P. Horcajada, R. Gref, P. Couvreur, C. Serre, Optimisation of the synthesis of MOF nanoparticles made of flexible porous iron fumarate MIL-88A, Journal of Materials Chemistry, 21 (2011) 2220-2227.

[116] E. Haque, S.H. Jhung, Synthesis of isostructural metal–organic frameworks, CPO-27s, with ultrasound, microwave, and conventional heating: Effect of synthesis methods and metal ions, Chemical engineering journal, 173 (2011) 866-872.

[117] W. Yuan, A.L. Garay, A. Pichon, R. Clowes, C.D. Wood, A.I. Cooper, S.L. James, Study of the mechanochemical formation and resulting properties

of an archetypal MOF: $Cu_3(BTC)_2$ (BTC= 1, 3, 5-benzenetricarboxylate), CrystEngComm, 12 (2010) 4063-4065.

[118] M. Klimakow, P. Klobes, A.F. Thünemann, K. Rademann, F. Emmerling, Mechanochemical synthesis of metal− organic frameworks: a fast and facile approach toward quantitative yields and high specific surface areas, Chemistry of Materials, 22 (2010) 5216-5221.

[119] P.J. Beldon, L. Fábián, R.S. Stein, A. Thirumurugan, A.K. Cheetham, T. Friščić, Rapid Room - Temperature Synthesis of Zeolitic Imidazolate Frameworks by Using Mechanochemistry, Angewandte Chemie International Edition, 49 (2010) 9640-9643.

[120] W. Yuan, T. Friščić, D. Apperley, S.L. James, High reactivity of metal–organic frameworks under grinding conditions: parallels with organic molecular materials, Angewandte Chemie, 122 (2010) 4008-4011.

[121] U. Mueller, H. Puetter, M. Hesse, H. Wessel, WO 2005/049892, 2005, BASF Aktiengesellschaft, (2007).

[122] M. Eddaoudi, D.F. Sava, J.F. Eubank, K. Adil, V. Guillerm, Zeolite-like metal–organic frameworks (ZMOFs): design, synthesis, and properties, Chemical Society Reviews, 44 (2015) 228-249.

[123] R. Banerjee, A. Phan, B. Wang, C. Knobler, H. Furukawa, M. O'keeffe, O.M. Yaghi, High-throughput synthesis of zeolitic imidazolate frameworks and application to CO_2 capture, Science, 319 (2008) 939-943.

[124] P. Nugent, Y. Belmabkhout, S.D. Burd, A.J. Cairns, R. Luebke, K. Forrest, T. Pham, S. Ma, B. Space, L. Wojtas, Porous materials with optimal adsorption thermodynamics and kinetics for CO_2 separation, Nature, 495 (2013) 80-84.

[125] O. Shekhah, Y. Belmabkhout, Z. Chen, V. Guillerm, A. Cairns, K. Adil, M. Eddaoudi, Made-to-order metal-organic frameworks for trace carbon dioxide removal and air capture, Nature communications, 5 (2014).

[126] P. Pachfule, R. Das, P. Poddar, R. Banerjee, Structural, Magnetic, and Gas Adsorption Study of a Two-Dimensional Tetrazole-Pyrimidine Based Metal− Organic Framework, Crystal Growth & Design, 10 (2010) 2475-2478.

[127] Z. Wang, S.M. Cohen, Postsynthetic modification of metal–organic frameworks, Chemical Society Reviews, 38 (2009) 1315-1329.

[128] X.C. Huang, Y.Y. Lin, J.P. Zhang, X.M. Chen, Ligand ‐ Directed Strategy for Zeolite ‐ Type Metaltrategy for Zeolite.P. Zhang, X.M. Chen, Ligandmetal–organic frameworks, Chemical Society Reviews, 38 (2009) 1315-1329

[129] J.A. Mason, T.M. McDonald, T.-H. Bae, J.E. Bachman, K. Sumida, J.J. Dutton, S.S. Kaye, J.R. Long, Application of a high-throughput analyzer in evaluating solid adsorbents for post-combustion carbon capture via multicomponent adsorption of CO_2, N_2, and H_2O, Journal of the American Chemical Society, 137 (2015) 4787-4803.

[130] A. Banerjee, S. Nandi, P. Nasa, R. Vaidhyanathan, Enhancing the carbon capture capacities of a rigid ultra-microporous MOF through gate-opening at low CO_2 pressures assisted by swiveling oxalate pillars, Chemical Communications, 52 (2016) 1851-1854.

[131] S. Nandi, U. Werner-Zwanziger, R. Vaidhyanathan, A triazine–resorcinol based porous polymer with polar pores and exceptional surface hydrophobicity showing CO_2 uptake under humid conditions, Journal of Materials Chemistry A, 3 (2015) 21116-21122.

[132] S. Nandi, P. De Luna, T.D. Daff, J. Rother, M. Liu, W. Buchanan, A.I. Hawari, T.K. Woo, R. Vaidhyanathan, A single-ligand ultra-microporous MOF for precombustion CO_2 capture and hydrogen purification, Science advances, 1 (2015) e1500421.

[133] P.M. Bhatt, Y. Belmabkhout, A. Cadiau, K. Adil, O. Shekhah, A. Shkurenko, L.J. Barbour, M. Eddaoudi, A Fine-Tuned Fluorinated MOF Addresses the Needs for Trace CO_2 Removal and Air Capture Using

Physisorption, Journal of the American Chemical Society, 138 (2016) 9301-9307.

[134] L. Zhang, K. Jiang, M. Jiang, D. Yue, Y. Wan, H. Xing, Y. Yang, Y. Cui, B. Chen, G. Qian, A highly stable amino-coordinated MOF for unprecedented block off N_2 adsorption and extraordinary CO_2/N_2 separation, Chemical Communications, 52 (2016) 13568-13571.

[135] S. Couck, J.F. Denayer, G.V. Baron, T. Rémy, J. Gascon, F. Kapteijn, An amine-functionalized MIL-53 metal−organic framework with large separation power for CO_2 and CH_4, Journal of the American Chemical Society, 131 (2009) 6326-6327.

[136] G. FãcRey, C. Serre, Large breathing effects in three-dimensional porous hybrid matter: facts, analyses, rules and consequences, Chemical Society Reviews, 38 (2009) 1380-1399.

[137] T. Rodenas, M. van Dalen, E. Garcá‐Pérez, P. Serra‐Crespo, B. Zornoza, F. Kapteijn, J. Gascon, Visualizing MOF Mixed Matrix Membranes at the Nanoscale: Towards Structure‐Performance Relationships in CO_2/CH_4 Separation Over NH2‐MIL‐53 (Al)@ PI, Advanced Functional Materials, 24 (2014) 249-256.

[138] T.-H. Bae, J.S. Lee, W. Qiu, W.J. Koros, C.W. Jones, S. Nair, A High-Performance Gas-Separation Membrane Containing Submicrometer-Sized Metal–Organic Framework Crystals, Angewandte Chemie International Edition, 49 (2010) 9863-9866.

[139] O.G. Nik, X.Y. Chen, S. Kaliaguine, Functionalized metal organic framework-polyimide mixed matrix membranes for CO_2/CH_4 separation, Journal of Membrane Science, 413 (2012) 48-61.

[140] T. Li, Y. Pan, K.-V. Peinemann, Z. Lai, Carbon dioxide selective mixed matrix composite membrane containing ZIF-7 nano-fillers, Journal of membrane science, 425 (2013) 235-242.

[141] I. Erucar, S. Keskin, Screening metal–organic framework-based mixed-matrix membranes for CO_2/CH_4 separations, Industrial & Engineering Chemistry Research, 50 (2011) 12606-12616.

[142] T.-H. Bae, J.R. Long, CO_2/N_2 separations with mixed-matrix membranes containing Mg_2(dobdc) nanocrystals, Energy & Environmental Science, 6 (2013) 3565-3569.

[143] Y. Zhang, I.H. Musselman, J.P. Ferraris, K.J. Balkus, Gas permeability properties of Matrimid® membranes containing the metal-organic framework Cu–BPY–HFS, Journal of Membrane Science, 313 (2008) 170-181.

[144] S. Shahid, K. Nijmeijer, High pressure gas separation performance of mixed-matrix polymer membranes containing mesoporous Fe(BTC), Journal of membrane science, 459 (2014) 33-44.

[145] X. Guo, H. Huang, Y. Ban, Q. Yang, Y. Xiao, Y. Li, W. Yang, C. Zhong, Mixed matrix membranes incorporated with amine-functionalized titanium-based metal-organic framework for CO_2/CH_4 separation, Journal of Membrane Science, 478 (2015) 130-139.

[146] M.W. Anjum, F. Vermoortele, A.L. Khan, B. Bueken, D.E. De Vos, I.F. Vankelecom, Modulated UiO-66-based mixed-matrix membranes for CO_2 separation, ACS applied materials & interfaces, 7 (2015) 25193-25201.

[147] E.V. Perez, K.J. Balkus, J.P. Ferraris, I.H. Musselman, Mixed-matrix membranes containing MOF-5 for gas separations, Journal of Membrane Science, 328 (2009) 165-173.

[148] C. Duan, X. Jie, D. Liu, Y. Cao, Q. Yuan, Post-treatment effect on gas separation property of mixed matrix membranes containing metal organic frameworks, Journal of Membrane Science, 466 (2014) 92-102.

[149] M. Arjmandi, M. Pakizeh, Mixed matrix membranes incorporated with cubic-MOF-5 for improved polyetherimide gas separation membranes: Theory and experiment, Journal of Industrial and Engineering Chemistry, 20 (2014) 3857-3868.

[150] L. Hao, P. Li, T. Yang, T.-S. Chung, Room temperature ionic liquid/ZIF-8 mixed-matrix membranes for natural gas sweetening and post-combustion CO_2 capture, Journal of membrane science, 436 (2013) 221-231.

[151] M.A. Aroon, A.F. Ismail, T. Matsuura, M.M. Montazer-Rahmati, Performance studies of mixed matrix membranes for gas separation: a review, Separation and purification Technology, 75 (2010) 229-242.

[152] T. Rodenas, I. Luz, G. Prieto, B. Seoane, H. Miro, A. Corma, F. Kapteijn, F.X.L. i Xamena, J. Gascon, Metal–organic framework nanosheets in polymer composite materials for gas separation, Nature materials, 14 (2015) 48-55.

[153] Z. Kang, Y. Peng, Y. Qian, D. Yuan, M.A. Addicoat, T. Heine, Z. Hu, L. Tee, Z. Guo, D. Zhao, Mixed matrix membranes (MMMs) comprising exfoliated 2D covalent organic frameworks (COFs) for efficient CO_2 separation, Chem. Mater, 28 (2016) 1277-1285.

[154] Y. Yang, K. Goh, R. Wang, T.-H. Bae, High-performance nanocomposite membranes realized by efficient molecular sieving with CuBDC nanosheets, Chemical Communications, (2017).

[155] Z. Kang, Y. Peng, Z. Hu, Y. Qian, C. Chi, L.Y. Yeo, L. Tee, D. Zhao, Mixed matrix membranes composed of two-dimensional metal–organic framework nanosheets for pre-combustion CO_2 capture: a relationship study of filler morphology versus membrane performance, Journal of Materials Chemistry A, 3 (2015) 20801-20810.

[156] A.E. Amooghin, M. Omidkhah, A. Kargari, The effects of aminosilane grafting on NaY zeolite–Matrimid® 5218 mixed matrix membranes for CO_2/CH_4 separation, Journal of Membrane Science, 490 (2015) 364-379.

[157] X.Y. Chen, O.G. Nik, D. Rodrigue, S. Kaliaguine, Mixed matrix membranes of aminosilanes grafted FAU/EMT zeolite and cross-linked polyimide for CO_2/CH_4 separation, Polymer, 53 (2012) 3269-3280.

[158] J. Liu, T.-H. Bae, W. Qiu, S. Husain, S. Nair, C.W. Jones, R.R. Chance, W.J. Koros, Butane isomer transport properties of 6FDA–DAM and

MFI–6FDA–DAM mixed matrix membranes, Journal of Membrane Science, 343 (2009) 157-163.

[159] T.H. Bae, J.Q. Liu, J.A. Thompson, W.J. Koros, C.W. Jones, S. Nair, Solvothermal deposition and characterization of magnesium hydroxide nanostructures on zeolite crystals, Microporous Mesoporous Mat., 139 (2011) 120-129.

[160] W.A. Khanday, R. Tomar, Conversion of zeolite—A in to various ion-exchanged catalytic forms and their catalytic efficiency for the synthesis of benzimidazole, Catalysis Communications, 43 (2014) 141-145.

[161] C. Henrist, J.-P. Mathieu, C. Vogels, A. Rulmont, R. Cloots, Morphological study of magnesium hydroxide nanoparticles precipitated in dilute aqueous solution, Journal of Crystal Growth, 249 (2003) 321-330.

[162] X. Lv, M. Li, X. Ma, S. Ma, Y. Gao, L. Tang, J. Zhao, Y. Guo, X. Zhao, Z. Wang, In situ synthesis of nanolamellas of hydrophobic magnesium hydroxide, Colloids and Surfaces A: Physicochemical and Engineering Aspects, 296 (2007) 97-103.

[163] C. Yan, D. Xue, L. Zou, X. Yan, W. Wang, Preparation of magnesium hydroxide nanoflowers, Journal of Crystal Growth, 282 (2005) 448-454.

[164] H. Sun, D. Wu, X. Guo, B. Shen, J. Liu, A. Navrotsky, Energetics of Confinement of n-Hexane in Ca–Na Ion Exchanged Zeolite A, The Journal of Physical Chemistry C, 118 (2014) 25590-25596.

[165] K. Sumida, D.L. Rogow, J.A. Mason, T.M. McDonald, E.D. Bloch, Z.R. Herm, T.H. Bae, J.R. Long, Carbon Dioxide Capture in Metal-Organic Frameworks, Chem. Rev., 112 (2012) 724-781.

[166] J.R. Li, J. Sculley, H.C. Zhou, Metal-Organic Frameworks for Separations, Chem. Rev., 112 (2012) 869-932.

[167] B. Seoane, J. Coronas, I. Gascon, M.E. Benavides, O. Karvan, J. Caro, F. Kapteijn, J. Gascon, Metal-organic framework based mixed matrix membranes: a solution for highly efficient CO_2 capture?, Chemical Society Reviews, (2015).

[168] P.S. Goh, A.F. Ismail, S.M. Sanip, B.C. Ng, M. Aziz, Recent advances of inorganic fillers in mixed matrix membrane for gas separation, Separation and Purification Technology, 81 (2011) 243-264.

[169] S. Basu, A.L. Khan, A. Cano-Odena, C. Liu, I.F.J. Vankelecom, Membrane-based technologies for biogas separations, Chemical Society Reviews, 39 (2010) 750-768.

[170] X.Y. Chen, H. Vinh-Thang, D. Rodrigue, S. Kaliaguine, Amine-Functionalized MIL-53 Metal–Organic Framework in Polyimide Mixed Matrix Membranes for CO2/CH4 Separation, Industrial & Engineering Chemistry Research, 51 (2012) 6895-6906.

[171] T.-H. Bae, J.R. Long, CO_2/N_2 separations with mixed-matrix membranes containing Mg2(dobdc) nanocrystals, Energy & Environmental Science, 6 (2013) 3565-3569.

[172] B. Zornoza, A. Martinez-Joaristi, P. Serra-Crespo, C. Tellez, J. Coronas, J. Gascon, F. Kapteijn, Functionalized flexible MOFs as fillers in mixed matrix membranes for highly selective separation of CO_2 from CH_4 at elevated pressures, Chemical Communications, 47 (2011) 9522-9524.

[173] K. Uemura, A. Maeda, T.K. Maji, P. Kanoo, H. Kita, Syntheses, Crystal Structures and Adsorption Properties of Ultramicroporous Coordination Polymers Constructed from Hexafluorosilicate Ions and Pyrazine, European Journal of Inorganic Chemistry, 2009 (2009) 2329-2337.

[174] P. Nugent, Y. Belmabkhout, S.D. Burd, A.J. Cairns, R. Luebke, K. Forrest, T. Pham, S. Ma, B. Space, L. Wojtas, M. Eddaoudi, M.J. Zaworotko, Porous materials with optimal adsorption thermodynamics and kinetics for CO_2 separation, Nature, 495 (2013) 80-84.

[175] H. Lin, E. Van Wagner, R. Raharjo, B.D. Freeman, I. Roman, High-Performance Polymer Membranes for Natural-Gas Sweetening, Advanced Materials, 18 (2006) 39-44.

[176] J. Liu, T.-H. Bae, W. Qiu, S. Husain, S. Nair, C.W. Jones, R.R. Chance, W.J. Koros, Butane isomer transport properties of 6FDA–DAM and

MFI–6FDA–DAM mixed matrix membranes, Journal of Membrane Science, 343 (2009) 157-163.

[177] Q. Song, S.K. Nataraj, M.V. Roussenova, J.C. Tan, D.J. Hughes, W. Li, P. Bourgoin, M.A. Alam, A.K. Cheetham, S.A. Al-Muhtaseb, E. Sivaniah, Zeolitic imidazolate framework (ZIF-8) based polymer nanocomposite membranes for gas separation, Energy & Environmental Science, 5 (2012) 8359-8369.

[178] Y. Li, T.-S. Chung, C. Cao, S. Kulprathipanja, The effects of polymer chain rigidification, zeolite pore size and pore blockage on polyethersulfone (PES)-zeolite A mixed matrix membranes, Journal of Membrane Science, 260 (2005) 45-55.

[179] L. Wang, Y. Cao, M. Zhou, S.J. Zhou, Q. Yuan, Novel copolyimide membranes for gas separation, Journal of Membrane Science, 305 (2007) 338-346.

[180] W.-H. Lin, T.-S. Chung, Gas permeability, diffusivity, solubility, and aging characteristics of 6FDA-durene polyimide membranes, Journal of Membrane Science, 186 (2001) 183-193.

[181] S. Kelman, H. Lin, E.S. Sanders, B.D. Freeman, CO_2/C_2H_6 separation using solubility selective membranes, Journal of Membrane Science, 305 (2007) 57-68.

[182] X. Duthie, S. Kentish, C. Powell, K. Nagai, G. Qiao, G. Stevens, Operating temperature effects on the plasticization of polyimide gas separation membranes, Journal of membrane science, 294 (2007) 40-49.

[183] Y. Liu, R. Wang, T.-S. Chung, Chemical cross-linking modification of polyimide membranes for gas separation, Journal of Membrane Science, 189 (2001) 231-239.

[184] C.E. Powell, X.J. Duthie, S.E. Kentish, G.G. Qiao, G.W. Stevens, Reversible diamine cross-linking of polyimide membranes, Journal of membrane science, 291 (2007) 199-209.

[185] J. Barsema, S. Klijnstra, J. Balster, N.F. van der Vegt, G. Koops, M. Wessling, Intermediate polymer to carbon gas separation membranes based on Matrimid PI, Journal of membrane science, 238 (2004) 93-102.

[186] H. Gong, S.S. Lee, T.-H. Bae, Mixed-matrix membranes containing inorganically surface-modified 5A zeolite for enhanced CO_2/CH_4 separation, Microporous and Mesoporous Materials, 237 (2017) 82-89.

[187] L. Wang, Y. Cao, M. Zhou, Q. Liu, X. Ding, Q. Yuan, Gas transport properties of 6FDA-TMPDA/MOCA copolyimides, European Polymer Journal, 44 (2008) 225-232.

[188] S.J. Datta, C. Khumnoon, Z.H. Lee, W.K. Moon, S. Docao, T.H. Nguyen, I.C. Hwang, D. Moon, P. Oleynikov, O. Terasaki, CO_2 capture from humid flue gases and humid atmosphere using a microporous coppersilicate, Science, 350 (2015) 302-306.

[189] W.-J. Son, J. Kim, J. Kim, W.-S. Ahn, Sonochemical synthesis of MOF-5, Chemical Communications, (2008) 6336-6338.

[190] T.-H. Bae, J. Liu, J.A. Thompson, W.J. Koros, C.W. Jones, S. Nair, Solvothermal deposition and characterization of magnesium hydroxide nanostructures on zeolite crystals, Microporous and Mesoporous Materials, 139 (2011) 120-129.

[191] L.M. Robeson, The upper bound revisited, Journal of Membrane Science, 320 (2008) 390-400.

[192] N. Jusoh, Y.F. Yeong, K.K. Lau, A. M. Shariff, Enhanced gas separation performance using mixed matrix membranes containing zeolite T and 6FDA-durene polyimide, Journal of Membrane Science, 525 (2017) 175-186.

[193] J.K. Ward, W.J. Koros, Crosslinkable mixed matrix membranes with surface modified molecular sieves for natural gas purification: I. Preparation and experimental results, Journal of Membrane Science, 377 (2011) 75-81.

[194] N. Tien-Binh, H. Vinh-Thang, X.Y. Chen, D. Rodrigue, S. Kaliaguine, Polymer functionalization to enhance interface quality of mixed matrix

membranes for high CO2/CH4 gas separation, Journal of Materials Chemistry A, 3 (2015) 15202.

[195] B. Seoane, C. Tellez, J. Coronas, C. Staudt, NH_2-MIL-53(Al) and NH2-MIL-101(Al) in sulfur-containing copolyimide mixed matrix membranes for gas separation, Separation and Purification Technology, (2013).

[196] J.E. Bachman, J.R. Long, Plasticization-resistant Ni_2(dobdc)/polyimide composite membranes for the removal of CO_2 from natural gas, Energy & Environmental Science, 9 (2016) 2031-2036.

[197] M. Askari, T.-S. Chung, Natural gas purification and olefin/paraffin separation using thermal cross-linkable co-polyimide/ZIF-8 mixed matrix membranes, Journal of Membrane Science, (2013).

[198] S. Japip, H. Wang, Y. Xiao, T.S. Chung, Highly permeable zeolitic imidazolate framework (ZIF)-71 nano-particles enhanced polyimide membranes for gas separation, Journal of Membrane Science, 467 (2014) 162-174.

[199] T.-H. Bae, J.S. Lee, W. Qiu, W.J. Koros, C.W. Jones, S. Nair, A high-performance gas-separation membrane containing submicrometer-sized metal-organic framework crystals, Angewandte Chemie (International Ed. In English), 49 (2010) 9863-9866.

[200] M. Calle, Y.M. Lee, Thermally rearranged (TR) poly (ether− benzoxazole) membranes for gas separation, Macromolecules, 44 (2011) 1156-1165.

[201] W. Liu, W. Xie, Acetate-Functional Thermally Rearranged Polyimides Based on 2, 2-Bis (3-amino-4-hydroxyphenyl) hexafluoropropane and Various Dianhydrides for Gas Separations, Industrial & Engineering Chemistry Research, 53 (2013) 871-879.

[202] Y.F. Yeong, H. Wang, K.P. Pramoda, T.-S. Chung, Thermal induced structural rearrangement of cardo-copolybenzoxazole membranes for enhanced gas transport properties, Journal of membrane science, 397 (2012) 51-65.

[203] C.A. Scholes, C.P. Ribeiro, S.E. Kentish, B.D. Freeman, Thermal rearranged poly (benzoxazole-co-imide) membranes for CO_2 separation, Journal of Membrane Science, 450 (2014) 72-80.

[204] B. Comesaña-Gándara, M. Calle, H.J. Jo, A. Hernández, G. Jose, J. de Abajo, A.E. Lozano, Y.M. Lee, Thermally rearranged polybenzoxazoles membranes with biphenyl moieties: Monomer isomeric effect, Journal of Membrane Science, 450 (2014) 369-379.

[205] H. Wang, S. Liu, T.-S. Chung, H. Chen, Y.-C. Jean, K.P. Pramoda, The evolution of poly (hydroxyamide amic acid) to poly(benzoxazole) via stepwise thermal cyclization: Structural changes and gas transport properties, Polymer, 52 (2011) 5127-5138.

[206] M.L. Chua, Y.C. Xiao, T.-S. Chung, Effects of thermally labile saccharide units on the gas separation performance of highly permeable polyimide membranes, Journal of membrane science, 415 (2012) 375-382.

[207] M. Askari, Y. Xiao, P. Li, T.-S. Chung, Natural gas purification and olefin/paraffin separation using cross-linkable 6FDA-Durene/DABA co-polyimides grafted with α, β, and γ-cyclodextrin, Journal of membrane science, 390 (2012) 141-151.

[208] S.H. Han, N. Misdan, S. Kim, C.M. Doherty, A.J. Hill, Y.M. Lee, Thermally rearranged (TR) polybenzoxazole: effects of diverse imidization routes on physical properties and gas transport behaviors, Macromolecules, 43 (2010) 7657-7667.

[209] H.B. Park, S.H. Han, C.H. Jung, Y.M. Lee, A.J. Hill, Thermally rearranged (TR) polymer membranes for CO 2 separation, Journal of Membrane Science, 359 (2010) 11-24.

[210] R. Guo, D.F. Sanders, Z.P. Smith, B.D. Freeman, D.R. Paul, J.E. McGrath, Synthesis and characterization of thermally rearranged(TR) polymers: effect of glass transition temperature of aromatic poly(hydroxyimide) precursors on TR process and gas permeation properties, Journal of Materials Chemistry A, 1 (2013) 6063-6072.

[211] C.H. Jung, J.E. Lee, S.H. Han, H.B. Park, Y.M. Lee, Highly permeable and selective poly(benzoxazole-co-imide) membranes for gas separation, Journal of Membrane Science, 350 (2010) 301-309.

[212] M. Calle, C.M. Doherty, A.J. Hill, Y.M. Lee, Cross-linked thermally rearranged poly(benzoxazole-co-imide) membranes for gas separation, Macromolecules, 46 (2013) 8179-8189.

[213] F. Alghunaimi, B. Ghanem, N. Alaslai, R. Swaidan, E. Litwiller, I. Pinnau, Gas permeation and physical aging properties of iptycene diamine-based microporous polyimides, Journal of Membrane Science, 490 (2015) 321-327.

[214] R. Swaidan, B.S. Ghanem, E. Litwiller, I. Pinnau, Pure-and mixed-gas CO_2/CH_4 separation properties of PIM-1 and an amidoxime-functionalized PIM-1, Journal of Membrane Science, 457 (2014) 95-102.

[215] Y. Zhuang, J.G. Seong, Y.S. Do, W.H. Lee, M.J. Lee, Z. Cui, A.E. Lozano, M.D. Guiver, Y.M. Lee, Soluble, microporous, Tröger's Base copolyimides with tunable membrane performance for gas separation, Chemical Communications, 52 (2016) 3817-3820.

[216] N. Du, M.M. Dal-Cin, G.P. Robertson, M.D. Guiver, Decarboxylation-induced cross-linking of polymers of intrinsic microporosity (PIMs) for membrane gas separation, Macromolecules, 45 (2012) 5134-5139.

[217] J.L. Santiago-García, C. Álvarez, F. Sánchez, G. José, Gas transport properties of new aromatic polyimides based on 3, 8-diphenylpyrene-1, 2, 6, 7-tetracarboxylic dianhydride, Journal of Membrane Science, 476 (2015) 442-448.

[218] R. Swaidan, M. Al-Saeedi, B. Ghanem, E. Litwiller, I. Pinnau, Rational design of intrinsically ultramicroporous polyimides containing bridgehead-substituted triptycene for highly selective and permeable gas separation membranes, Macromolecules, 47 (2014) 5104-5114.

[219] Y. Zhuang, J.G. Seong, Y.S. Do, W.H. Lee, M.J. Lee, M.D. Guiver, Y.M. Lee, High-strength, soluble polyimide membranes incorporating Tröger's Base for gas separation, Journal of Membrane Science, 504 (2016) 55-65.

[220] M. Carta, P. Bernardo, G. Clarizia, J.C. Jansen, N.B. McKeown, Gas Permeability of Hexaphenylbenzene Based Polymers of Intrinsic Microporosity, Macromolecules, 47 (2014) 8320-8327.

[221] W.F. Yong, F. Li, Y. Xiao, P. Li, K. Pramoda, Y. Tong, T. Chung, Molecular engineering of PIM-1/Matrimid blend membranes for gas separation, Journal of membrane science, 407 (2012) 47-57.

[222] X. Ma, B. Ghanem, O. Salines, E. Litwiller, I. Pinnau, Synthesis and effect of physical aging on gas transport properties of a microporous polyimide derived from a novel spirobifluorene-based dianhydride, ACS Macro Letters, 4 (2015) 231-235.

[223] X. Ma, O. Salinas, E. Litwiller, I. Pinnau, Novel spirobifluorene-and dibromospirobifluorene-based polyimides of intrinsic microporosity for gas separation applications, Macromolecules, 46 (2013) 9618-9624.

[224] Z. Wang, D. Wang, J. Jin, Microporous polyimides with rationally designed chain structure achieving high performance for gas separation, Macromolecules, 47 (2014) 7477-7483.

[225] Z.G. Wang, X. Liu, D. Wang, J. Jin, Tröger's base-based copolymers with intrinsic microporosity for CO_2 separation and effect of Tröger's base on separation performance, Polymer Chemistry, 5 (2014) 2793-2800.

[226] C.R. Mason, L. Maynard-Atem, N.M. Al-Harbi, P.M. Budd, P. Bernardo, F. Bazzarelli, G. Clarizia, J.C. Jansen, Polymer of intrinsic microporosity incorporating thioamide functionality: preparation and gas transport properties, Macromolecules, 44 (2011) 6471-6479.

[227] X. Ma, R. Swaidan, Y. Belmabkhout, Y. Zhu, E. Litwiller, M. Jouiad, I. Pinnau, Y. Han, Synthesis and gas transport properties of hydroxyl-functionalized polyimides with intrinsic microporosity, Macromolecules, 45 (2012) 3841-3849.

[228] C. Casado-Coterillo, M. del Mar López-Guerrero, Á. Irabien, Synthesis and characterisation of ETS-10/acetate-based ionic liquid/chitosan mixed matrix membranes for CO_2/N_2 permeation, Membranes, 4 (2014) 287-301.

[229] V. Martin-Gil, A. López, P. Hrabanek, R. Mallada, I. Vankelecom, V. Fila, Study of different titanosilicate (TS-1 and ETS-10) as fillers for Mixed Matrix Membranes for CO 2/CH 4 gas separation applications, Journal of Membrane Science, 523 (2017) 24-35.

[230] S. Sorribas, B. Comesaña-Gándara, A.E. Lozano, B. Zornoza, C. Téllez, J. Coronas, Insight into ETS-10 synthesis for the preparation of mixed matrix membranes for CO_2/CH_4 gas separation, RSC Advances, 5 (2015) 102392-102398.

[231] X. Cao, Z. Qiao, Z. Wang, S. Zhao, P. Li, J. Wang, S. Wang, Enhanced performance of mixed matrix membrane by incorporating a highly compatible covalent organic framework into poly (vinylamine) for hydrogen purification, International Journal of Hydrogen Energy, 41 (2016) 9167-9174.

[232] M. Shan, B. Seoane, E. Rozhko, A. Dikhtiarenko, G. Clet, F. Kapteijn, J. Gascon, Azine‐Linked Covalent Organic Framework (COF)‐Based Mixed‐Matrix Membranes for CO_2/CH_4 Separation, Chemistry-A European Journal, 22 (2016) 14467-14470.

[233] Y. Yang, C.Y. Chuah, H. Gong, T.-H. Bae, Robust microporous organic copolymers containing triphenylamine for high pressure CO_2 capture application, Journal of CO2 Utilization, 19 (2017) 214-220.

List of Publications

1. **Heqing Gong**, Tien Hoa Nguyen, Rong Wang, Tae-Hyun Bae*, Separations of Binary Mixtures of CO_2/CH_4 and CO_2/N_2 with Mixed-Matrix Membranes Containing $Zn(pyrz)_2(SiF_6)$ Metal-Organic Framework, *J. Membrane Science.* **2015**, *495,* 169-175

2. Tien Hoa Nguyen[1], **Heqing Gong[1]**, Siew Siang Lee, Tae-Hyun Bae*, Amine-appended hierarchical Ca-A zeolite for enhancing CO_2/CH_4 selectivity of mixed-matrix membranes, *ChemPhysChem,* **2016**, *17,* 3165-3169

   [1]These authors contributed equally to this work.

3. **Heqing Gong[1]**, Siew Siang Lee[1], Tae-Hyun Bae*, Mixed-matrix membranes containing inorganically surface-modified 5A zeolite for enhanced CO_2/CH_4 separation, *Microporous and Mesoporous Materials,* **2017,** *237,* 82-89

   [1]These authors contributed equally to this work

4. Yanqin Yang, Chong Yang Chuah, **Heqing Gong**, Tae-Hyun Bae*, Robust microporous organic copolymers containing triphenylamine for high pressure CO_2 capture application, *J. CO_2. Util.*, **2017**, *19,* 214-220

5. **Heqing Gong**, Chong Yang Chuah, Yanqin Yang, Tae-Hyun Bae*, High performance composite membranes comprising $Zn(pyrz)_2(SiF_6)$ nanocrystals for CO_2/CH_4 separation, *J. Ind.Eng.Chem.*,**2017**, in press

6. Chong Yang Chuah[1], Kunli Goh[1], Yanqin Yang, **Heqing Gong**, Wen Li, Michael D Guiver, Rong Wang, Tae-Hyun Bae*, Emerging Materials for Membranes in Biogas Separation, *submitted*

[1]These authors contributed equally to this work.